Laser Desorption Postionization Mass Spectrometric Analysis of

Multispecies Coculture Biofilms

BY
CHHAVI BHARDWAJ
B.Sc.(Honors), University of Delhi, 2003
M.Sc., University of Delhi, 2005
M.S., University of Illinois at Chicago, 2009

THESIS
Submitted as partial fulfillment of the requirements
for the degree of Doctor of Philosophy in Chemistry
in the Graduate College of the
University of Illinois at Chicago, 2014

Chicago, Illinois

Defense Committee:

Prof. Luke Hanley, Chair and Advisor

Prof. Timothy A. Keiderling

Prof. Scott A. Shippy

Prof. Lawrence W. Miller

Dr. Mrignayani Kotecha, Bioengineering

I dedicate this thesis to my parents Vijay Krishan and Sudha Bhardwaj

for their unconditional love and support

and

To the memory of my beloved *Amma*

ACKNOWLEDGEMENTS

I would like to express my deep appreciation and gratitude to several individuals for their help and encouragement through my doctoral work. My sincere gratitude to my advisor Prof. Luke Hanley for his patience and guidance. I would also like to thank the members of my defense committee for their time and valuable suggestions.

I am grateful to Dr. Jerry Moore for both his technical assistance, due to which the completion of my first project was possible, and for his support and encouragement. I thank my colleagues from the Hanley group, both past and present, especially Yang Cui, for all his technical help and valuable suggestions and also Gerald Gasper for his help with machining and instrument design. I thank Prof. Yoshitaka Ishii for his mentorship during the initial years of my graduate study. To Robert Widing for a pleasant teaching experience and for all the delicious pizza. To Sachin Tyagi for being a great friend. I would also like to acknowledge the support from the staff at the chemistry department, especially, Patricia Ratajczyk, Frank Tobias, Rhonda Staudohar and Silvia Solis.

I am thankful to my parents and my siblings Surbhi, Ankit and Ankush for their love support and unwavering faith in me. Finally, I thank Anjan for making it all worthwhile. It was him and his positivity that kept me going through this journey.

CB

TABLE OF CONTENTS

TABLE OF CONTENTS (continued)

TABLE OF CONTENTS (continued)

LIST OF TABLES

TABLE PAGE

LIST OF FIGURES

FIGURE PAGE

LIST OF ABBREVIATIONS

AP	Atmospheric Pressure
APCI	Atmospheric Pressure Chemical Ionization
APPI	Atmospheric Pressure Photoionization
DESI	Desorption Electrospray Ionization
EI	Electron Ionization
ESI	Electrospray Ionization
EV	Electron Volt
GC	Gas Chromatography
HCA	Hierarchical Cluster Analysis
IR	Infrared
LAESI	Laser Ablation Electrospray Ionization
LC	Liquid Chromatography
LCMS	Liquid Chromatography Mass Spectrometry
LD	Laser Desorption
LDI	Laser Desorption Ionization
LDPI-MS	Laser Desorption Postionization Mass Spectrometry
MALDI	Matrix Assisted Laser Desorption Ionization
MS	Mass Spectrometry
MVA	Multivariate Analysis
Nd:YAG	Neodymium Doped Yttrium Aluminum Garnet
Nd:YLF	Neodymium Doped Lithium Yttrium Fluoride
OD	Optical Density
PC	Principal Component
PCA	Principal Component Analysis
S/N	Signal to Noise Ratio
SIMS	Secondary Ion Mass Spectrometry
SPI	Single Photon Ionization
ToF	Time of Flight
UV	Ultra Violet
VUV	Vacuum Ultra Violet

SUMMARY

Biofilms are complex, three dimensional communities of microorganisms, embedded in a self-produced polymeric matrix and attached to a surface. Biofilms impact many aspects of human life in environmental, industrial and medical settings and are often a challenge to control due to limited understanding of their structure and function. Moreover, microbial cells in biofilms have different genetic expression and properties than their planktonic counterparts and are significantly more resistant to antimicrobial agents. Cells from a disrupted biofilm, when regrown planktonicly usually become susceptible to antibiotics again, and therefore, it is imperative to study biofilms in intact form for a comprehensive understanding.

In nature, biofilms often exist as a consortia of more than one species of either bacteria or bacteria together with fungi. These co-existing species commonly benefit from functional differentiation and metabolite exchange through cross feeding among members (syntrophy), making the system more robust and efficient against environmental perturbations. Examining such interactions will therefore immensely enhance the understanding of biofilm systems.

Keeping these objectives in mind, two synthetic consortia models were used for the thesis work presented here. These models consisted of two interacting members each, 1) *Escherichia coli* bacteria strains referred as citrine and tomato and 2) *Saccharomyces cerevisiae* yeast and *E. coli* tomato strain. These consortia were engineered to possess naturally occurring specialized metabolic roles for each member. One member grows on carbohydrate anaerobically and produces byproducts which in turn are consumed by the other member which grows aerobically. Therefore, the former acts as the system's primary producer and the latter behaves as the system's consumer, through syntrophic metabolite exchange.

The ability of mass spectrometric (MS) methods to study biological systems in intact form was utilized in this thesis work. Therefore, coculture biofilms of the aforementioned microbes were studied using laser desorption postionization mass spectrometry (LDPI-MS) and secondary ion mass spectrometry (SIMS) directly from their intact surfaces.

LDPI-MS utilizes two separate light sources for desorption and photoionization of analytes from a solid surface. Briefly, the first pulsed ultraviolet laser desorbs analyte molecules into gaseous neutrals, which are then ionized by the second light source with photon energy in the vacuum ultraviolet range. The ionization occurs due to single photon ionization therefore the photon energy of the ionizing light source must be higher than the ionization energy of the target molecule. Many organic molecules have ionization energies in the range of 7.5 - 10.5 eV. Therefore, a 10.5 eV ionization source was designed and built to complement the previously existing commercial laser source of 7.87 eV. Majority of the work reported here was thus performed using these two laser ionization sources with photon energies of 7.87 eV and 10.5 eV.

Next, the two ionization sources were utilized to image coculture biofilm samples. MS Imaging was utilized to probe chemical distributions between the two members. Mass spectral images for the intact biofilms were obtained directly from the polycarbonate substrate with no sample pretreament. The study indicated that 7.87 eV and 10.5 eV photon energy provided an optimal balance of selectivity and sensitivity. Using 7.87 eV photon energy only a small fraction of endogenous compounds were ionized, whereas a 10.5 eV ionization source was sufficient to ionize a wide range of compound classes from the biofilm.

The effect of varying photon energies was further explored by analyzing yeast- *E. coli* biofilm consortia using tunable vacuum ultraviolet synchrotron radiation in the range of 7.8 eV to

10.5 eV. Higher photon energy increased the number of observed peaks and overall signal intensity. Interestingly, 10.5 eV was found to be an optimal photon energy to study biofilm samples, since higher photon energies (which were explored but data not shown here) resulted in significantly increased fragmentation, thereby making the overall spectra very complicated. Synchrotron LDPI-MS analysis was performed on biofilms which were blotted on stainless steel substrate. Blotting was done to remove the polycarbonate membranes which hindered the analysis due to excessive charging. Blotted samples were additionally analyzed using laser LDPI-MS.

Although, both laser and synchrotron LDPI-MS analysis resulted in many mass spectral peaks corresponding to endogenous compounds, these peaks could not be identified due to lack of high resolution and tandem MS capabilities of the instrument. Multivariate analysis techniques were applied to obtain further information about small molecule metabolites which are embedded in the crowded low mass region of the MS. Principal component analysis (PCA) was performed to reduce the dimensionality of the large MS dataset and extract relevant information on the metabolites. PCA of the LDPI-MS data of coculture biofilms, resulted in three distinct groups which corresponded to the two microbial species and the region where they grow together. The observation was significant as the two microbial species were closely related *E. coli* strains and did not show visible mass spectral difference. Further analysis provided the peaks responsible for the separation of the three regions. Most peaks corresponded to low mass metabolites and compounds involved in the syntrophic exchange between microbial species.

Finally, SIMS analysis was carried out on intact biofilm samples in both positive and negative ion modes. Unlike LDPI-MS where *E. coli* (citrine and tomato) cocultures did not show significant peak differences for the two strains, SIMS analysis resulted in significant spectral peak

differences. Moreover, positive SIMS resulted in more peaks for citrine whereas the negative ion mode favored tomato. Mixed region in both cases showed features from both strains. Overall, SIMS analysis provided valuable information complementary to the LDPI-MS for interdependent coculture biofilm systems.

1. INTRODUCTION

1.1 Biofilms: Definition and Significance

Biofilms are structured microbial communities encapsulated in a self-produced extracellular polymeric matrix and are often organized as multispecies consortia composed of metabolically differentiated members interacting via exchanged metabolites.[1-3] Figure 1 shows a scanning electron microscopy (SEM) image of an *Escherichia coli* biofilm. The biofilm phenotype is common to many microbes and can occur on nearly any moist biotic or abiotic surface. Biofilms are ubiquitous and impact humans in many natural, medical and industrial settings. Microbial colonization and biofilm formation on medical devices, such as catheters or implants, often result in robust and persistent infections. Additionally, infectious biofilms have been reported in dental, dermatological and urinary tract settings.[4] Biofouling and biofilm induced corrosion represent costly, negative effects within many industrial settings including ship hulls, pipelines and heat exchangers.[2]

Biofilms are inherently tolerant of antimicrobial treatments.[1, 2] Several mechanisms have been proposed to understand this tolerance including, metabolic dormancy, mass transfer limitations, phenotypic heterogeneity associated with chemical gradients and coordinated gene regulation via exchange of quorum sensing and other molecules.[5, 6]

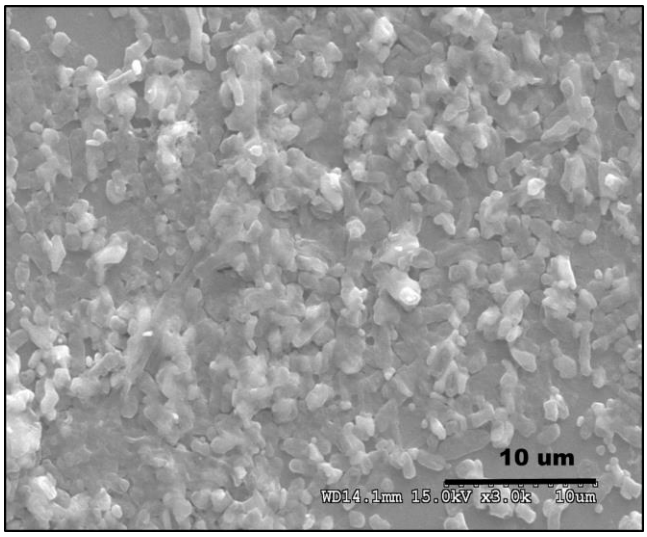

Figure 1 Scanning Electron Microscopic (SEM) image for *Escherichia coli* (K-12) biofilm.

1.2 Biofilms with Interacting Members: Ideal Model System

Naturally occurring biofilms, which are optimized by evolutionary cycles over long periods, are almost exclusively organized as mixed communities, comprising multiple species of either bacteria alone or bacteria together with fungi (multispecies). Traditionally, however microbial biofilm studies often focus on single species biofilms (monoculture). Although, such studies have provided valuable insight in understanding microbial biofilms, monoculture biofilms often fail to mimic naturally occurring environmental interactions of participating members, such as: division of labor, functional differentiation and/or altered physiology/morphology.[7] In order to obtain a more comprehensive understanding of the metabolism, structure and function of microbial biofilms, it is imperative to study a multispecies biofilm that mimics some of the natural microbial interactions.

Escherichia coli and *Saccharomyces cerevisiae* are arguably the best-studied prokaryotic and eukaryotic microorganisms, respectively, and serve as ideal model systems for developing techniques to examine biofilm interactions. The current study employs two distinct binary (two member) model systems, synthetically designed to mimic a naturally occurring producer-consumer ecological motif which revolves around exchanges of metabolites between microorganisms.[8] The synthetic consortia were developed by a collaborator Prof. Ross Carlson and his group members at the Center for Biofilm Engineering at Montana State University, Bozeman, MT.

Figure 2 shows a schematic of the two synthetically engineered binary consortia which were used for the research work presented here. Both consortia (I and II in Figure 2) have a glucose-oxidizing member, which is an *Escherichia coli* deletion mutant strain ("citrine" strain, described in Chapter 2) in the prokaryote-prokaryote binary model.[7] or the baker's yeast *Saccharomyces cerevisiae* in case of a prokaryote-eukaryote system: both these species act as the primary producer for their respective consortium and use glucose for their energy source. Both of these producer species cross feed their metabolic byproducts such as acetate or ethanol to a glucose-negative *Escherichia coli* consumer strain ("tomato" strain, described in Chapter 2) which acts as the system's scavenger. Interaction of two *E. coli* strains in the prokaryote-prokaryote model results in an enhanced overall biomass productivity.[8] Similarly, interaction of *E. coli* tomato strain with yeast in prokaryote-eukaryote model results in an increased cell growth for *E. coli* closer to yeast, thereby resulting in a growth gradient for the bacteria. Consequently, these models ideally mimic natural synergistic relationships often observed in biofilms.

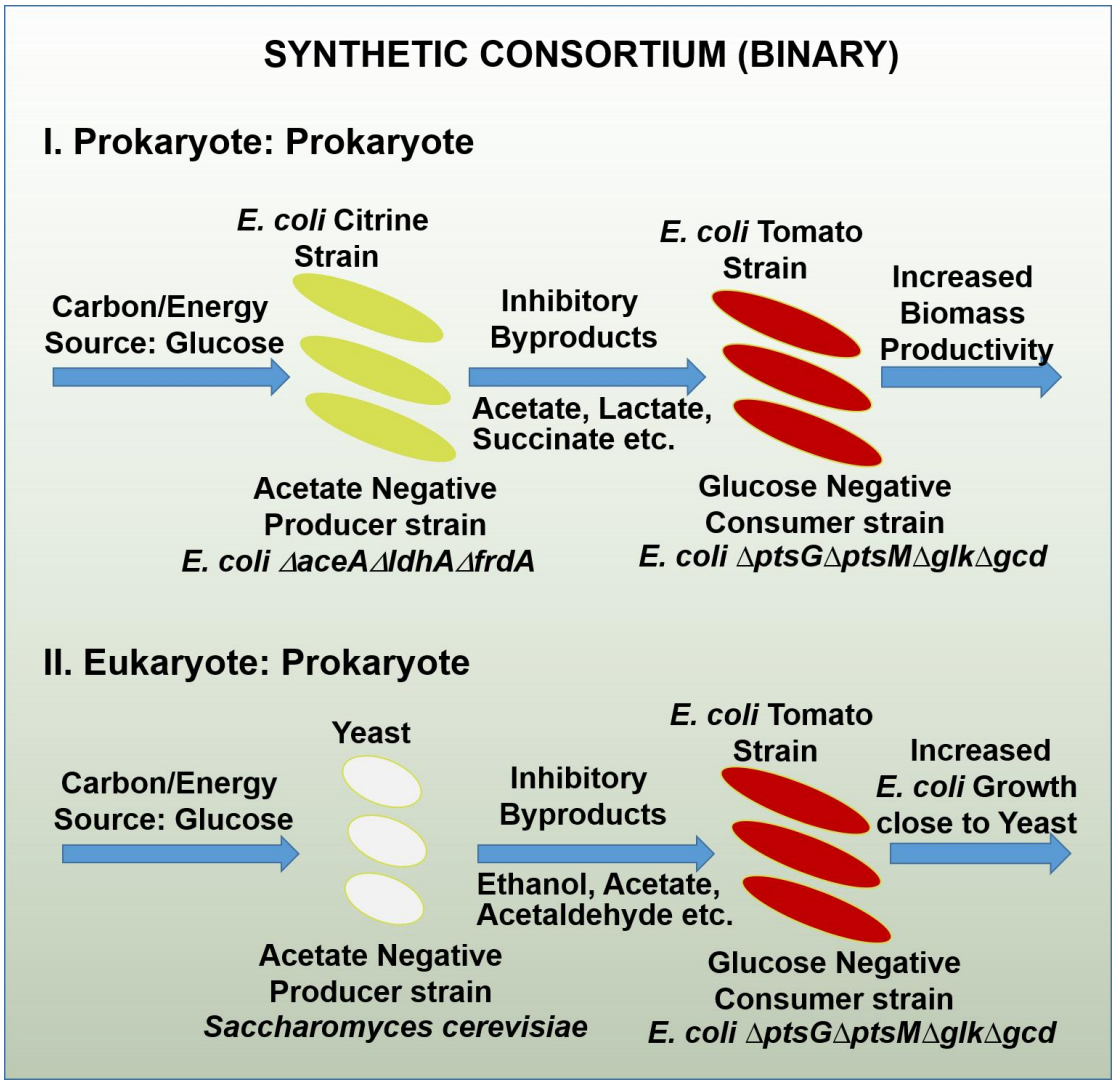

Figure 2 Schematic showing synthetic consortia of microbial biofilms with interacting members. Figure inspired from Ref. [7].

1.3 Mass Spectrometry for the Study of Microbial Biofilms

Many analytical techniques have been applied to characterize the natural products/metabolites found in living organisms such as plants and microbial communities. Mass spectrometry (MS) is one of the more extensively used techniques for the characterization of small molecule natural products due to its potential for rapid analysis, high throughput, and accuracy in identification of a wide variety of sample types.[9-13] The ability to volatilize and ionize molecular species is central to their analysis and a few methods have traditionally dominated natural products analysis by MS. The choice of technique to volatilize and ionize is ideally governed by the chemical and physical properties of the target molecule and the biological substrate in which it is found. However, more traditional methods often utilize extraction and purification strategies that are not always ideally suited for specific analyses. MS imaging strategies are rapidly developing to probe intact, native biological samples, thereby preserving spatial distributions of molecular species.[14-20]

This section attempts a brief overview of some of the more popular and/or promising ion sources that are increasingly applied to natural products MS, but which are also applicable to other fields of analysis including materials science. Ion sources are grouped into common modes of ionization of neutral species, ranging from electron ionization to electrospray ionization. Ion sources are categorized by how they volatilize neutrals, using strategies ranging from simple evaporation to nebulization to laser desorption. The most common types of precursor ions that are formed are given for each class of ion source. Precursor, molecular, or pseudomolecular ions include the less stable, odd electron radical cations ($M^{\bullet +}$) of an analyte (M); the more stable, even electron protonated species (MH^+), including multiply protonated species (MH_n^{n+}); those associated with alkali metal ions (most commonly NaM^+ or KM^+) or other metals (i.e., AgM^+);

adduct ions (i.e., MNH_4^+) or cluster ions (i.e., $MH(H_2O)_n^+$); and negative ions formed by electron attachment (M^-), deprotonation ($(M-H)^-$), or clustering. The extent to which an ion source imparts internal energy to the precursor ions, where "soft" and "hard" ionization correspond to low and high internal energy, respectively, is also considered as it qualitatively predicts the extent of precursor ion fragmentation.[21]

The pressure range at which the ions are formed is highly relevant: ion sources under high vacuum of $<10^{-5}$ mBar do not permit ion-neutral gas phase collisions. By contrast, sources operating at atmospheric pressure (AP) allow many gas phase collisions, facilitating ion cooling, ion-molecule reactions, and/or removal of adducts via collision induced dissociation. AP sources also permit intact samples to be analyzed under ambient conditions, [20] while vacuum sources induce sample dehyrdration prior to and during analysis.

The various ion sources can be further categorized based on their suitability of sample pretreatment and separation such as sample clean up, extraction, and chemical derivatization. Some ion sources are particularly well suited to MS imaging analyses of intact biological samples such as microbial communities.[14, 15, 17-20, 22, 23].

1.3.1 Ionization of Gaseous Neutrals: Electron Ionization vs. Single Photon Ionization

Electron ionization (EI) and single photon ionization both result in ionization of desorbed neutrals to form radical cations. Figure 3 shows a schematic comparing these two ion sources. EI is historically the ion source most widely used in organic mass spectrometry.[24] EI involves simple evaporation or mild heating of a sample to form gaseous neutrals which are then ionized by collisions with 70 eV kinetic energy electrons to produce radical cations, $M^{\bullet+}$. EI data is highly reproducible between different instruments, which has allowed the collection of what are probably

the most extensive, highest quality mass spectral libraries [25] whose use facilitates identification of known compounds and helps determination of unknowns. Those analytes most suited for EI analysis are relatively volatile and thermally stable. EI is usually coupled to GC for chromatographic separation, necessitating sample pretreatment and extraction of natural products from their native source.

EI is a hard ionization technique whose mass spectra are often so dominated by fragment ion peaks that the precursor ion is often either low intensity or not present. EI analysis suffers the further disadvantage of not being well suited to the study of thermolabile molecules such as alkaloids or those with molecular weights above ~500 Da. However, fragmentation can be reduced by lowering the kinetic energy of the ionizing electrons,[24] supersonic cooling of the neutrals prior to ionization,[26] or more commonly, by chemical derivatization with trimethyl silane or other compounds that facilitate analyte volatilization.

Single photon ionization (SPI) also generates radical cations from gaseous neutrals, but it uses ~10 eV vacuum ultraviolet (VUV) radiation rather than electrons for ionization, as shown in Figure 3.[27, 28] SPI is a much softer ionization technique than EI and usually produces intense molecular ion signal. VUV photons can be generated by a laser, a rare gas discharge lamp, or a synchrotron light source. SPI generally occurs when the desorbed analyte neutrals have ionization energies below the energy of irradiating photons. Most organic species have ionization energies between 7 - 11 eV, so a VUV photon of ~10 eV energy is often sufficient to ionize a large fraction of molecular analytes while excluding ionization of water, carbon dioxide and other uninteresting, but abundant species with high ionization energies. SPI thereby greatly simplifies mass spectra and decreases background/chemical noise for improved sensitivity, especially compared to EI. Furthermore, clusters of pure analyte, analyte/solvent, or analyte/matrix have lower ionization

energies than the isolated molecules, permitting SPI of such clustered species at slightly lower VUV photon energies.[29] SPI in vacuum can additionally dissociate clusters to both protonated and non-protonated ions,[29] although ~10 eV VUV photons are probably not sufficiently energetic to desolvate large, multiply charged droplets commonly formed in some ion sources (see below).

A wide variety of analyses have been performed by SPI,[27, 28] such as detection of the aromatic vapors from individual coffee beans.[30] SPI yields depend on the photoionization cross section of the analyte, which only vary by an order of magnitude for different organic species compared to a variation of several orders of magnitude for EI.[27] This makes SPI potentially more quantifiable compared to EI and many other ionization methods.[31]

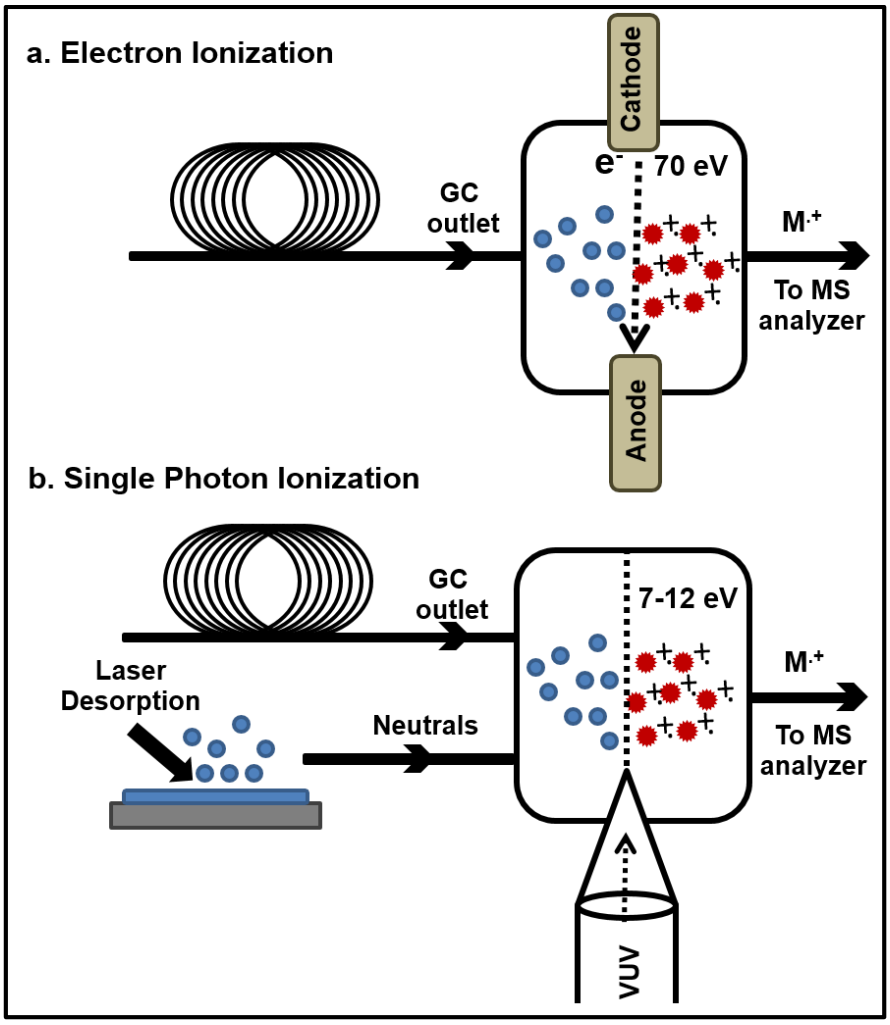

Figure 3 Schematic of electron ionization and single photon ionization MS methods: (a) electron ionization (EI) and (b) single photon ionization (SPI) sources. The figure also shows the dominant radical cation precursor produced by the ionization process.

The extent of fragmentation for SPI depends upon how species are volatilized and thermalized (i.e., transfer line temperature when coupled to GC), since internally hot neutrals will dissociate more than cold neutrals upon SPI.[32] The energy of the VUV photons used for SPI

also affects the fragmentation of the analyte, but only to a lesser degree when the VUV photon energy is within a few eV of the ionization energy threshold.

SPI has the ability to selectively ionize target analytes using different VUV photon energies, as reported for the analysis of aerosols,[33] combustion products,[34] and chemical stimulants.[35] Although a wide range of target analytes and samples can be studied using SPI, selectivity can be introduced by the use of low photon energy VUV sources such as the fluorine excimer laser. Chemical derivatization of high ionization energy analytes with a low ionization energy chromophore will create a complex whose ionization energy approaches that of the chromophore, thereby allowing selective detection of the complex from a mixture by SPI using a low photon energy source.[15]

The most significant disadvantage of SPI is that commercial instruments are only beginning to be introduced, leading to a relative low utilization of the method compared to other more popular ion sources. Furthermore, SPI is performed under vacuum and adaptation to intermediate or atmospheric pressure fundamentally alters the ionization event (see below). Finally, there are effectively no mass spectral libraries available to assist in compound identification with SPI, unlike EI.

1.3.2 Chemical, Plasma, and Related Ionization Methods

Chemical ionization was developed as the first soft ionization alternate to EI,[36] but is now available on relatively few commercial instruments. Chemical ionization proceeds most commonly via proton transfer to or from reagent ions formed by EI via thermodynamically favorable gas phase ion-neutral collisions that occur at elevated gas pressures. Proton affinities for reagent and analyte predict proton transfer as well the amount of excess energy available for

subsequent molecular dissociation. Analytes are introduced in chemical ionization by evaporation or rapid heating of a solid probe, again allowing facile coupling to GC.

The significance of chemical ionization lay not so much in its relatively infrequent current utilization, but rather because it serves as a mechanistic template for some of the more popular chemical, plasma and related ionization techniques discussed in this section and shown in Figure 4. Proton transfer reactions play a key role in ionization of analytes under elevated pressure conditions, as described below. For example, proton transfer reaction MS is a subset of chemical ionization in which the reagent ions are protonated water clusters (which themselves play an important role in many chemical ionization-like sources).[37] Proton transfer reaction MS has potential for application to the analysis of volatile natural products given its expanding usage in gas and aerosol sampling.

Atmospheric pressure chemical ionization (APCI, see Figure 4) is the most popular of the chemical ionization-type sources and is available on the majority of mass spectrometers coupled to LC. Like chemical ionization, APCI generally forms singly charged ions via proton transfer which in the positive and negative modes are protonated MH^+ and deprotonated $(M-H)^-$, respectively, formed by gas phase ion-molecule reactions with the reagent ions.[38] Analyte ions can also form in APCI via adduction of reactant gas, solvent, and/or clusters thereof as well as by other mechanisms (see below). Reagent ions in APCI are formed by a direct current corona discharge emanating from a needle located adjacent to the solvent/analyte aerosol formed in a nebulizer. APCI is best suited for the analysis of polar to relatively non-polar compounds with mass up to 1500 Da.

It has been argued that many of the other AP-based ion sources can be considered variants of APCI.[38] Atmospheric pressure photoionization (APPI) is mechanistically similar to chemical

ionization and APCI, but is initiated by SPI induced by continuous VUV discharge lamps.[39-42] Efficient absorption of VUV by air implies that the initial photoionization event in APPI occurs either via the more abundant solvent or dopant species which initiate an eventual proton transfer to the analyte. Dopants are often added in large quantities compared to the analyte since they are thought to enhance ionization overall, but recent work has argued that water and/or other solvent clusters can play an important role in proton transfer.[43] While direct VUV SPI of the analyte (similar to what occurs in vacuum) is possible in APPI, it typically occurs with low efficiency.[44] APPI in the negative mode produces molecular radical anions (in addition to deprotonated species) by electron capture for analytes with positive electron affinity or by charge transfer between excited gas anions produced by electron capture by atmospheric gases such as O_2 and analyte molecules. APPI is generally more suited to study nonpolar compounds compared to APCI.[39]

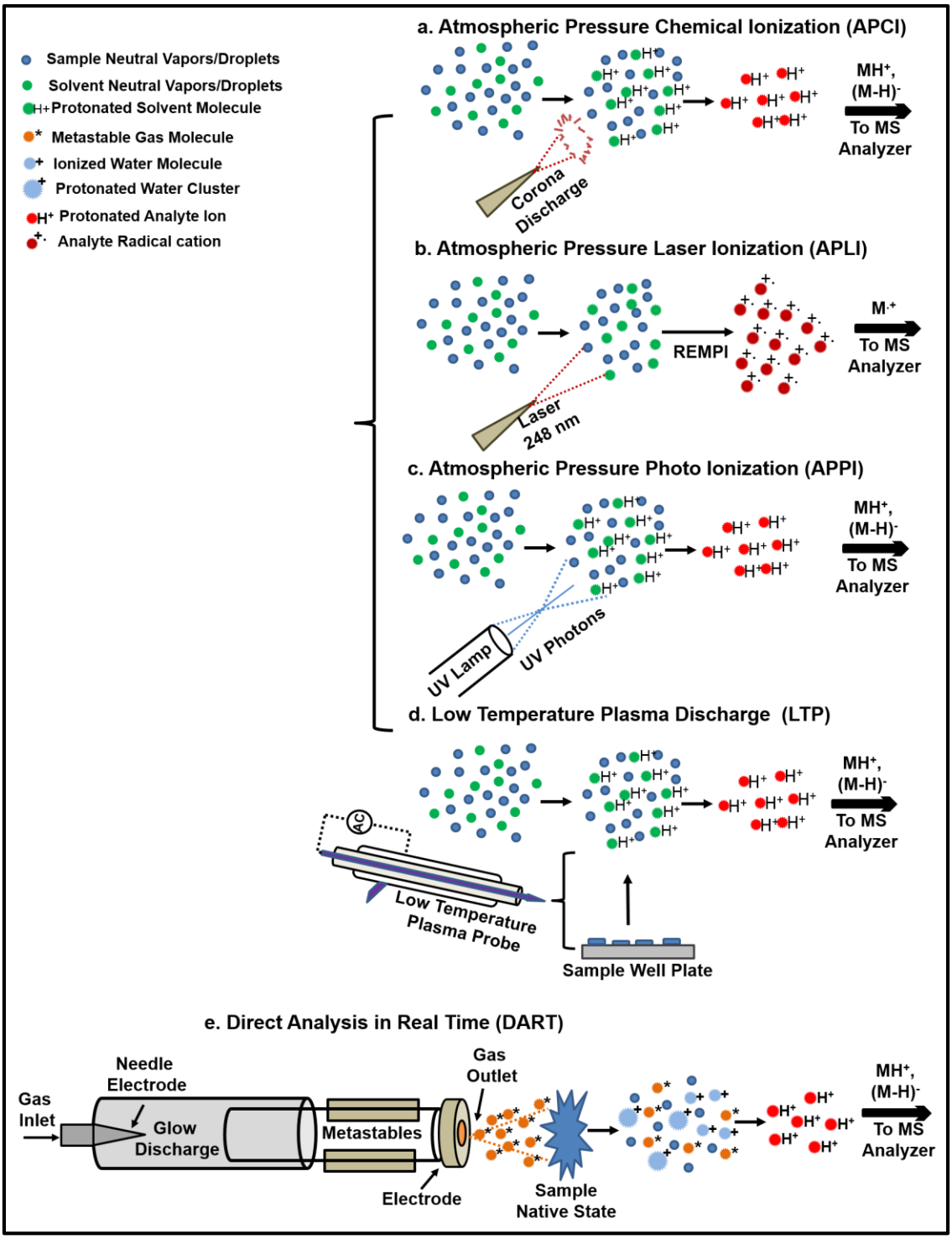

Figure 4 Schematic of various chemical ionization-like MS sources: (a) atmospheric pressure chemical ionization (APCI), (b) atmospheric pressure laser ionization (APLI), (c) atmospheric pressure photoionization (APPI), (d) low temperature plasma (LTP), (e) paper spray and (f) direct analysis in real time (DART). The dominant ions produced by each source are also shown.

Both APPI and APCI are highly sensitive to the experimental conditions and properties of solvents, additives, dopants, and buffer components present in the sample that can strongly influence the selectivity and sensitivity to specific analytes. APCI, APPI, and the other chemical ionization-like methods all suffer from a high background of "chemical noise" due to efficient ionization of gases, solvents and impurities. Thus, these chemical ionization-like methods also require sample cleanup or extraction of the target analyte from complex matrices when coupled to LC.

Micro-APPI is one of the earlier variants of APPI which renders the method compatible with microfluidic separation systems.[41] Desorption APPI (DAPPI) relies on a nebulizer microchip to deliver a heated jet of vaporized solvent for desorption, permitting efficient ionization of nonpolar and neutral compounds on surfaces such as pharmaceuticals in tablet form.[45] Capillary APPI (cAPPI) and capillary photoionization (CPI) are variants of APPI specifically designed for coupling to chromatographic interfaces in which APPI occurs within the confined volume of a capillary.[46, 47] Both capillary APPI and CPI display improved sensitivity compared to APPI by improved ion transmission in the MS and reduction in unfavorable ion-molecule reactions. Capillary APPI is well suited to the analysis of volatile compounds while CPI can detect both volatile and nonvolatile compounds regardless of polarity since it provides additional sample heating. Atmospheric pressure laser ionization (APLI) replaces the VUV discharge lamp in APPI with a nanosecond pulsed laser operating at 248 or 266 nm, making the initiating ionization event a resonant multiphoton process.[44]

The original APCI source is driven by a corona discharge and the strategy of using plasmas to initiate ionization at AP has been widely expanded into new ion sources. Direct analysis in real time (DART) utilizes a He or N_2 plasma glow discharge at AP to induce positive ion formation

via interaction of neutrals with electronically excited (metastable) atoms or molecules in a process known as Penning ionization, as shown in Figure 4.[48, 49] However, many of the disadvantages of other chemical ionization-like methods remain since ionization in DART can also proceed via many (or all) of the aforementioned secondary ion-molecule reactions.[48] Often, the metastable species efficiently ionize atmospheric moisture to form protonated water clusters, which then facilitate proton transfer to the analyte. Abundant non-protonated molecular ions have also been observed in DART analyses, often for nonpolar species such as alkanes. Intact molecular ions are favored under certain experimental conditions in the DART source, which can also be tuned to enhance fragmentation. DART can analyze a wide variety of solid, liquid and gaseous samples with little pretreatment, including the analysis of drugs in their native form.[50, 51]

Another AP plasma based ion source that is well suited for the analysis of nonpolar analytes is low temperature plasma (LTP) discharge which utilizes a non-equilibrium plasma for desorption/ionization.[52] LTP employs a high frequency alternating current between specially designed electrodes to produce a dielectric-barrier discharge in helium, as shown in Figure 4. Penning ionization is also evoked in LTP, specifically to form N_2^+ that undergoes subsequent ion-molecule reactions to form analyte ions. Potential desorption mechanisms in LTP (and DART) of solid samples include thermal desorption, sputtering, and surface reactions. LTP is useful for studying low mass compounds over a relatively wide polarity range compared to APCI.

It should already be clear from the above discussion that many of the ion sources in this section have common mechanistic features. Furthermore, the atmospheric pressure plasmas used in APCI, DART, LTP, and related methods will generate electrons, radicals, larger particles, UV photons, and VUV photons in addition to atomic and molecular ions of both polarities.[53, 54] The role of radicals has been considered,[44, 48] but the role of VUV and the other energetic

particles has not been fully appreciated in all of the chemical ionization-like methods. Understanding how APCI and other AP sources function requires sophisticated computer simulations that takes into account the density and interaction of these energetic particles as well as their hydrodynamic and electrostatic flow from the source into the mass spectrometer.[38, 55] Furthermore, radicals, ions, and/or VUV photons with surfaces can modify sample surfaces during MS analysis.[53, 54, 56] Thus, caution must be taken when claims are made that the aforementioned ion sources are non-destructive of solid samples.

1.3.3 Electrospray Ionization-Based Methods (ESI)

Figure 5 shows a schematic of electrospray ionization (ESI), perhaps the most common ion source currently in use.[38] ESI involves nebulization of a liquid feed, but differs from APCI in that the ionization occurs from liquid droplets rather than in the gas phase. ESI applies a strong electric field to the sample solution passing through a capillary and the field induces charge accumulation on the liquid surface at the end of the capillary. This charging produces a Taylor cone which breaks down to release highly charged droplets that are dispersed in space as micron and sub-micron sized droplets by flowing gas.[38, 57, 58] These droplets are then desolvated by passing through a curtain of heated inert gas which, via collisions and Coulombic explosion, leads to the formation of ions. ESI produces a wide range of ions varying from protonated and deprotonated ions in positive and negative mode, respectively, to multiply charged ions for large molecules, such as $(M+zH)^{+z}$ or $(M-zH)^{-z}$ and pseudomolecular ions such as NaM^+, KM^+, NH_4M^+ and/or MCl^-. ESI is a soft ionization technique with very little fragmentation or dissociation observed in the mass spectra. Ions are produced at AP and samples are often required to be pretreated and extracted into the liquid phase for inclusion in the liquid eluent of an LC feed. ESI

can analyze a wide range of analytes, but is most effective for polar samples. ESI has the distinct advantage of forming multiply charged ions, enabling the study of large molecules at relatively low m/z values. However, this leads to the observation that a given compound can and often does display ions in multiple charge states, requiring a simple mathematical deconvolution to convert the raw data back to mass spectra of singly charged masses vs. intensities.

Desorption electrospray ionization (DESI) induces analyte desorption by directing the electrosprayed charged droplets to the sample surface, most simply by inserting a bend in an ESI source at which point sits a solid sample.[11, 20, 49, 59] Studies of the desorption/ionization mechanism for DESI continues to evolve, with recent investigations suggesting that DESI occurs through wetting of the sample surface by the spray plume, extraction of the analyte into the wet surface film, momentum transfer from impacting particles and gas to form progeny charged droplets, and transport of the said droplets towards the AP interface of the MS analyzer. DESI produces ions similar to those produced by ESI and has similarly high mass limit of ~100 kDa. Amino acids, alkaloids, steroids, other drugs, peptides, proteins, and a wide range of other analytes have been analyzed by DESI, which also permits imaging analysis of intact biological samples.[20, 22]

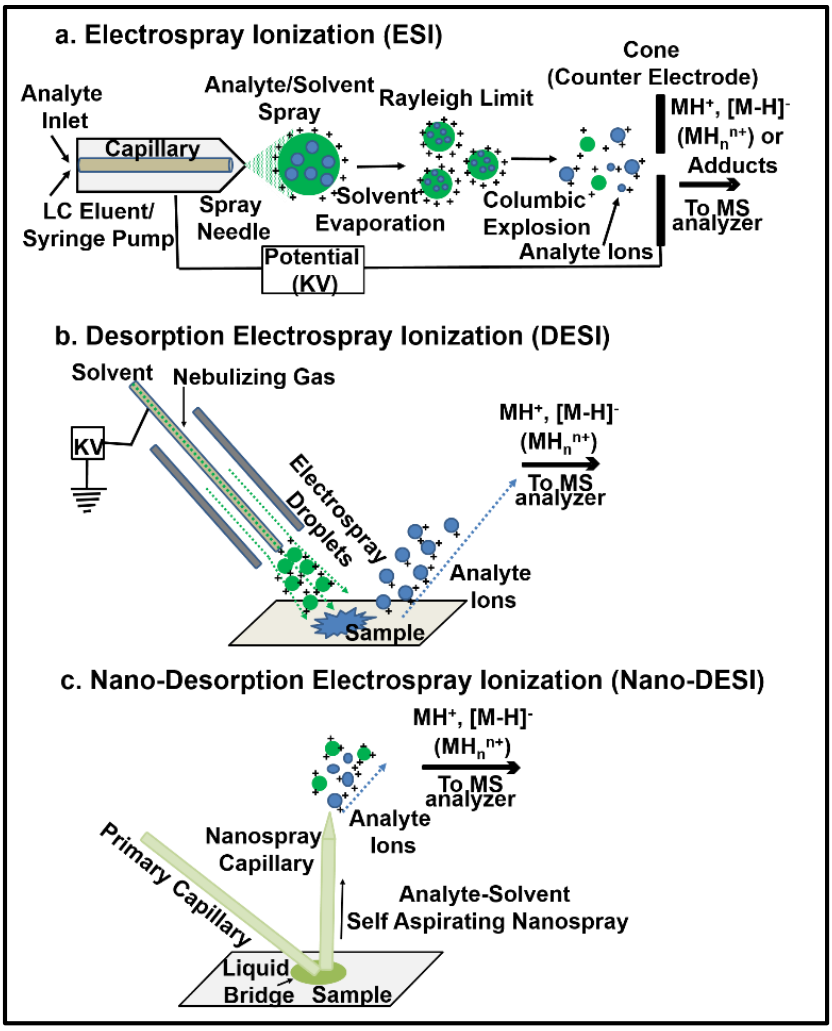

Figure 5 Schematic of electrospray ionization based MS methods: (a) electrospray ionization (ESI), (b) desorption electrospray ionization (DESI), and (c) nanoDESI. The dominant protonated and deprotonated ions produced by each source are also shown.

One variant of DESI is nanoDESI, in which analyte is desorbed into a solvent bridge formed between two capillaries and the analysis surface (Figure 5).[60] One capillary supplies solvent to the sample and the second capillary transports the dissolved analyte to the mass

spectrometer, allowing variation of the size of the sampled area. Another ESI variant is liquid DESI,[49] in which the sample solution is sheeted on a surface and then the normal DESI spray is performed. Finally, a proximal heated probe has been demonstrated to induce spatially confined thermal desorption from a sample surface for introduction in an ESI source.[61]

Paper spray is an AP-plasma discharge method in which a solvated sample is transported by wicking in a porous material such as paper cut to a sharp point that facilitates a high voltage direct current plasma discharge.[20] Paper spray is more difficult to characterize because it has characteristics of both the chemical ionization-like methods and ESI. Whole blood, dried blood, and tissue samples have been analyzed for hormones, drugs, and lipids by paper spray with minimum sample preparation.

1.3.4 Laser Desorption (LD)-Based Methods

LD-based ion sources are widely used for MS analyses of natural products, both for pretreated samples as well as for MS imaging of samples in native form.[14-16, 18, 62] These methods mostly employ nanosecond pulse length lasers in the ultraviolet (260 – 380 nm) and less commonly, in the mid-infrared (~3000 nm). The laser wavelength must be strongly absorbed by the solid sample, analyte, and/or added strong light absorbing matrix to induce efficient desorption.[62] The mid-IR wavelength has the advantage that it is resonant with the water naturally present in native biological samples, allowing efficient desorption without the addition of matrix. Ultrashort pulse lasers also avoid the need for a strong light absorber (see below). Ions can form directly in laser desorption ionization from a solid target. Alternatively, most of the ion sources discussed above can be used for postionization of neutrals that have been laser desorbed into the gas phase.

1.3.4.1 Matrix assisted and other methods of direct laser desorption ionization (LDI)

Matrix-assisted laser desorption ionization (MALDI) is by far the most popular of the LDI methods. Samples are mixed with an organic matrix and are then irradiated with intense laser pulses, leading predominantly to singly charged protonated (or deprotonated) species. The mechanism of desorption ionization in MALDI is an explosive event that is a combination of molecular desorption, particle ejection, proton transfer, gas phase collisions, photoionization, charged droplet/cluster decay, and/or other phenomena.[63-67] MALDI is a soft ionization method where singly charged molecular ions are readily observed and multiply charged ions similar to those formed by ESI can be detected under certain conditions.[67] A matrix that absorbs most of the incident laser energy and a high matrix to analyte ratio are both typically required. MALDI was originally performed only on samples under high vacuum conditions, but is now also routinely performed at intermediate[68] and atmospheric pressures.[69, 70] MALDI performed with UV lasers dominates due to lower laser costs and generally higher ion yields. However, mid-IR lasers allow MALDI without the addition of matrix compounds via excitation of water.[71, 72] Both wavelength regions are widely used for imaging intact samples.[14, 16, 18, 23] The wide range of commercial instruments and sample preparation strategies have facilitated many natural products analyses with MALDI.

LDI can also be enhanced by the close association of metal or semiconductor coatings, nanoparticles or nanostructures with a sample.[73-81] The mechanism of desorption, ionization, and fragmentation is associated with the unique optical, electronic, and thermal properties that arise in such nanostructures. Phenomena such as enhancement of the excitation field in the proximity of the nanostructured surface, various confinement effects based on the dimensions of

the nanostructures, plasmon resonances, in-plume reactions, and adsorbate-solvent and adsorbate-surface interactions all likely affect the ion formation.[81] Altering the surface chemistry of the nanostructures can promote selective capture of certain molecules and improve sensitivity.[75, 76, 81] The extent of ion decomposition and the level of fragmentation can be controlled by adjusting the laser fluence, incidence angle, or polarization. Pharmaceutical, metabolite, tissue imaging, biofilms, single cell and other potential sources of natural products have been analyzed by nanostructure-based LDI, with limits arising from the fashion in which the nanostructures are prepared and introduced to the sample.

Laser spray ionization (LSI), and related methods[67, 82] also utilize laser desorption of a matrix-analyte mixture in a fashion similar to MALDI except that unique matrix compounds and ion source conditions are used to detect multiply charged ions similar to those produced by ESI. LSI and related ion sources operate in both positive and negative ion modes, with ions produced under vacuum or at intermediate pressures.

Moving beyond the nanosecond pulse length lasers employed above, ultra short pulse lasers display additional advantages for LDI. Laser pulses at 800 nm wavelength and sub-100 fs pulse lengths have been used for fs-LDI of purified samples and intact biological material via a non-resonant desorption event that avoids the need to add a matrix compound.[83-86] Femtosecond laser ablation can remove sample from a solid while doing minimal damage to the remaining material, a remarkable effect that has motivated fs laser applications in laser surgery and micromachining of intact biological samples.[87-90] For example, ablation with 800 nm, ~75 fs laser pulses can remove material from bacterial biofilms and bovine eye tissue with minimum chemical modification to the underlying sample, indicating that depth profiling should be feasible with this method.[91, 92] An LDI instrument with 800 nm, <100 fs laser pulses has been recently

described.[86, 93] Combined with the increasing availability of reliable and lower cost fs pulse length lasers, these capabilities are opening up new possibilities for laser desorption that have yet to be explored for natural products analyses. However, fs lasers are apparently being considered by at least one instrument manufacturer for AP ionization.[94]

1.3.4.2 LD combined with postionization of neutrals

Laser desorption of neutrals has been coupled with most of the ionization sources described above. For example, LD has been coupled with EI[27], but the strategy is much more effective when supersonic cooling is incorporated into the instrument.[26, 95] Laser desorption postionization (LDPI) (described in detail in the next section) utilizes a nanosecond UV (ns) or femtosecond (fs) laser for desorption followed by SPI with a VUV light source [15, 27, 62, 96] or resonant multiphoton ionization with a ns UV laser.[62, 97, 98] Pulsed LD of neutrals can also be achieved with 1.064 μm or 10.6 μm wavelength IR lasers.[27, 62, 96-99]

Several imaging ion sources are based on mid-IR laser desorption at AP, in which the water in a biological sample replaces added matrix, leading to recoil-induced material expulsion to deliver intact sample particulates into a gaseous plume for postionization.[71] Mid-IR laser ablation is well suited for the analysis of intact biological samples, but desorption efficiency depends on the homogeneity of the water content in the sample. Laser ablation electrospray ionization (LAESI) uses a mid-IR laser beam to produce the gaseous plume that then interacts with highly charged electrospray droplets emitted from an ESI source to produce ESI-like ions (see above).[18, 100, 101] LAESI is commercially available and is well suited to the analysis of natural product distributions within intact plant samples[100, 101] and microbial biofilms.[18] Laser ablation atmospheric pressure photoionization (LAAPPI) is similar to LAESI except that the

ablation plume is first desolvated by an orthogonal hot solvent jet, then ionized by an APPI source.[102] LAAPPI efficiently ionizes neutral and nonpolar compounds from the analysis of intact biological samples, making it complimentary to LAESI, which itself is better suited to the analysis of polar compounds.

Mid-IR laser ablation metastable-induced chemical ionization (IR-LAMICI) produces sample neutrals that interact with a reactive, ambient temperature metastable plume to induce chemical ionization in the gas phase.[103] The precursor ions generated by IR-LAMICI are protonated or deprotonated species in the positive and negative ion modes, respectively. This ion source also provides an AP-plasma-based platform for small molecule imaging, with analysis of algal tissues for natural products and imaging of pharmaceutical tablets demonstrated using IR-LAMICI.

Ultra short pulse laser ablation of neutrals has been used instead of mid-IR laser ablation for coupling to ESI in a method referred to as laser electrospray ionization (LESI).[104, 105] LESI has at least one advantage over LAESI in that LESI's non-resonant ablation efficiency will not depend upon water content (see above).

The laser desorption methods described above generally expose a sample to pulsed laser radiation on the same side from which desorption occurs. Alternatively, the laser light can shine through a transparent substrate for optical absorption and desorption from the opposite surface.[106] Back laser irradiation of an opaque, thin foil can create a shock wave resulting in laser-induced acoustic desorption (LIAD) of neutral molecules from the opposite surface.[107] Postionization is required in LIAD and has been demonstrated using both SPI[107] and chemical ionization.[108, 109]

1.3.5 Secondary Ion Mass Spectrometry (SIMS)

SIMS is perhaps the original MS imaging method: a sample surface is bombarded with a focused beam of high energy primary ions which causes sputtering of the sample surface resulting in the ejection of positive and negative "secondary" ions.[19, 110] The desorption/ionization event in SIMS is a highly energetic process that often leads to extensive fragmentation. However, the extent of fragmentation tends to be lower for static versus dynamic SIMS, the distinction between the two defined by ~10^{13} ions/cm^2 total flux of primary ions impacting a given sample area. SIMS analyzes samples under vacuum and the method is not readily coupled to chromatography. However, SIMS is capable of the highest spatial resolution possible with any MS technique: ion beams can be focused to <20 nm enabling subcellular resolution, albeit at the cost of enhanced fragmentation.[17] SIMS is also the only MS imaging method that has been fully developed for depth profiling.[19, 110]

SIMS was originally performed with atomic primary ion beams, but C_{60}, Bi_3, and other cluster ions beams have been shown to produce more secondary ion signal that is representative of intact molecular species while imparting less damage to the remaining sample.[14, 19, 62, 110] SIMS imaging of individual biological cells has been reported using these cluster ion sources.[17, 111, 112] Ionization efficiency can be aided in some cases by evaporation of a metal overlayer[113] or addition of an ionic liquid matrix to the sample surface.[114] Recent work is moving to yet more massive $Au_{\sim 400}^{n+}$,[115] Ar_n^{n+},[116, 117] and water cluster ion beams that permit increasing soft ionization and/or improved depth profiling (often in dual beam configurations). Finally, postionization methods such as EI, SPI and resonant multiphoton ionization have been combined with SIMS to enhance ion yields in a method known as secondary neutral mass spectrometry.[62, 118-120]

1.4 Laser Desorption Postionization Mass Spectrometry (LDPI-MS)

Figure 6 shows a schematic for the laser desorption postionization mass spectrometry setup which was used for the majority of the research work presented here. LDPI-MS utilizes a UV pulsed laser ablation of the sample for desorption of analyte molecules into gaseous neutrals. The desorbed plume is then irradiated by an orthogonal ionization source, which here is either a VUV laser at 7.87 eV or 10.5 eV beam generated by tripling the third harmonic of the fundamental Nd: YAG laser beam (1064 nm), a generation scheme described in detail in Chapter 2. Additionally, tunable synchrotron radiation has been used as an ionization source as reported in later chapters.

LDPI-MS employs single photon ionization of the analyte which are directed to the time of flight (ToF) mass analyzer for detection using a series of ion optics which are pulsed to obtain optimum ion collection. LDPI-MS is a high vacuum technique, wherein desorption and ionization steps occur under vacuum. Sample can be studied in its native state, however, vacuum compatibility of the sample is required.

A wide range of samples on native surfaces some of which were rough, thick and insulating surfaces have been studied: such as intact eye lens tissues.[92] Antibiotics treated bacterial biofilms [121-123] and intact tooth samples. LDPI-MS allows for selective ionization of varied classes of compounds by varying the irradiating ionization photons. However, LDPI suffers a lack of commercially available ion source as well as the limitation of access to tunable VUV sources such as a synchrotron facility.

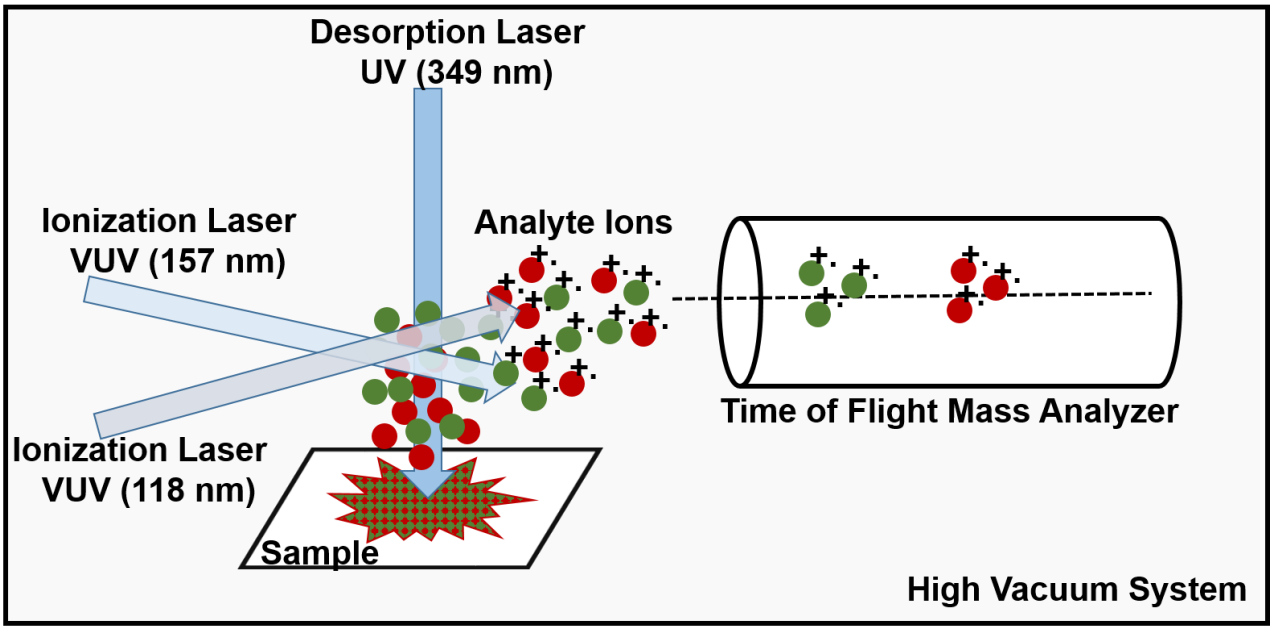

Figure 6 Schematic of laser desorption postionization mass spectrometry.

1.5 Thesis Research Objective

The primary objective of the thesis work presented here was to develop and apply LDPI-MS methods to study endogenous species and metabolites in multispecies microbial biofilms. Consequently, the work in this thesis is presented in the order of development of the method, optimization of the technique followed by its implementation and applications. Below is a brief description of the work presented in each chapter:

Chapter 2 describes the experimental details of the work. It describes the MS instrumentation used for the study, design and construction of the 10.5 eV ionization source, sample preparation protocols, biofilm growth procedures, imaging parameters, data acquisition

and data processing protocols and the relevant control studies which were performed throughout the work are presented in this thesis.

Chapter 3 describes the successful implementation of the 10.5 eV ionization source for imaging coculture biofilms. LDPI-MS imaging is demonstrated with this 10.5 eV source for analysis and imaging of small endogenous molecules within intact biofilms. LDPI-MS was able to collect ion images from intact, electrically insulating biofilms at ~100 μm spatial resolution. The chapter also draws a comparison between MS data/images obtained using two ionization sources at photon energy 7.87 eV and 10.5 eV.

Chapter 4 describes the mass spectrometric study of microbial biofilms using tunable VUV synchrotron radiation. The chapter explores the effect of varying ionization photon energy on the MS data, the comparison of synchrotron vs. laser ionization sources and also describes the effect of sample preparation on the quality of the spectra with respect to synchrotron vs laser LDPI-MS.

Chapter 5 describes the use of principal components analysis (PCA) for the MS data to differentiate species and strains in multispecies/multistrain biofilms. The chapter describes the protocol used and the results obtained by PCA treatment of LDPI-MS data at the two photon energies of: 7.87 eV and 10.5 eV. The two VUV photon energies gave different spreads via PCA and provide complementary information for the metabolic profile of the biofilm systems.

Chapter 6 describes the secondary ion mass spectrometric (SIMS) analysis performed on biofilm samples. The chapter shows SIMS analysis in both positive and negative mode and draws a brief comparison of the information which can be obtained using SIMS vs. that using LDPI-MS.

Chapter 7 describes the conclusions drawn from these studies. The chapter also touches upon some potential techniques for quantitative and/or qualitative analysis of endogenous species

from biological matrices, use of commercial instruments and lists the advantages as well as limitation of the technique.

2. EXPERIMENTAL METHODS

2.1 Instrumentation

LDPI-MS analysis was carried out on customized instruments utilizing either pulsed laser VUV or quasi-continuous synchrotron radiation as postionization sources. The LDPI-MS setup with 7.87 eV and 10.5 eV laser ionization sources was located at the University of Illinois at Chicago (referred to as laser LDPI-MS hereon). The second instrument was located at the Advanced Light Source in Lawrence Berkeley National Laboratory, Berkeley, CA and utilized 7.87-10.5 eV tunable synchrotron radiation for postionization of the desorbed neutrals (referred to as synchrotron LDPI-MS hereon).

2.1.1 Laser LDPI-MS

A prototype of the laser LDPI-MS at the University of Illinois at Chicago has been described in detail elsewhere.[15] Briefly, A 349 nm Nd:YLF laser (Spectra-Physics Explorer) was used for desorption at 10 or 100 Hz repetition rate which depended on the VUV ionization laser. The desorption laser beam was used at peak power density of ~300 MW/cm^2 with a ~50 μm diameter beam on the sample. Laser postionization was carried out at two fixed photon energies: 7.87 and 10.5 eV. A 157.6 nm fluorine laser (Optex Pro, Lambda Physik, Ft Lauderdale, FL) operating at 100 Hz was used for 7.87 eV postionization with a cross sectional area of 2 × 1 mm^2 and an energy of ~100 μJ/pulse. 10.5 eV laser postionization was performed with a 118 nm beam generated by tripling the third harmonic of a Nd:YAG laser operating at 10 Hz (355 nm, ~20 mJ,

5 ns, Tempest, New Wave Research, Fremont, CA) in a Xe gas cell at 6.5 torr pressure (described in later section). The resulting photoions were pulse extracted through a large bore Einzel lens that allowed efficient collection and transport of the large energy and spatial distribution from the ionized volume. The ions were then analyzed using a reflectron ToF which is similar to that described previously.[15] Software used for data acquisition was also partially described elsewhere with respect to its use on a different instrument.[93]

The schematic diagram in Figure 7 displays the ion source region of the LDPI-MS instrument including the relative positions of the sample plate, lasers, and ion optics. Samples were mounted on an ultrahigh vacuum compatible precision translation stage (LS-120, Micos USA, Irvine, CA). A digital camera (Nikon D300) with macro lens (Nikon ED AF Macro Nikkor 200 mm 1:4 D) with a tilting adapter, for increasing the depth of view, was used to monitor the sample inside the vacuum chamber. The time delay used between desorption and ionization lasers was in the range of 18 - 23 μs.

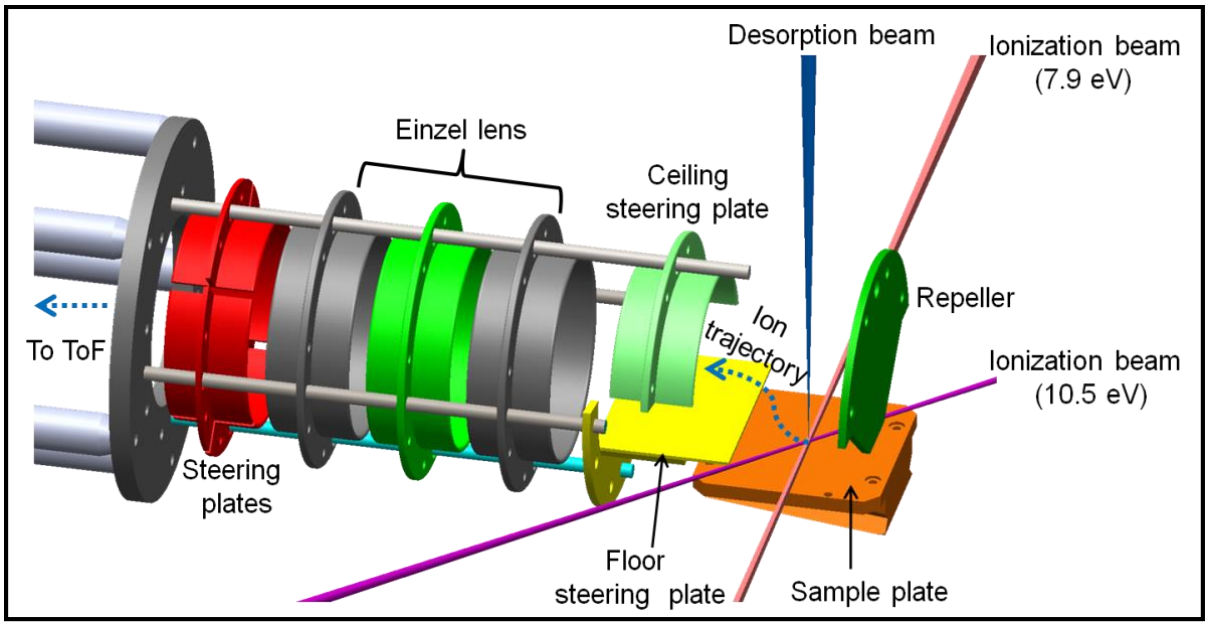

Figure 7 Schematic of the ion optics of the laser LDPI-MS instrument: showing the sample plate, desorption and ionization laser beams (solid lines), and the trajectory of the ions from the sample plate to the detector (broken arrow).

2.1.2 Synchrotron LDPI-MS and SIMS

Details of the synchrotron LDPI-MS instrument have also been reported previously.[29, 124] In brief, the synchrotron LDPI-MS was consisted of a commercial SIMS instrument (TOF.SIMS 5, ION-TOF Inc., Munster, Germany) modified by the addition of a 349 nm Nd:YLF pulsed desorption laser (Spectra-Physics Explorer, Newport Corporation, Irvine, CA). This laser was operated at 2500 Hz repetition rate with a spot size of ~30 μm diameter and laser desorption peak power density of 1 to 10 MW/cm^2. Tunable VUV synchrotron radiation in the range of 7.87 - 10.5 eV photon energy was additionally introduced into this instrument for single photon ionization of laser desorbed neutrals. The sample stage on the synchrotron LDPI-MS was moved

to analyze a ~3 mm^2 area for each biofilm sample with 10 laser shots per spot before moving to a fresh spot for repeated analysis. ~1.2×10^5 laser shots were used for collecting each displayed synchrotron mass spectrum.

Secondary ion mass spectrometry (SIMS) analysis was additionally carried out at the using the above mentioned commercial SIMS instrument and 25 keV Bi_3^+ primary ions.

2.1.3 Generation of 10.5 eV

Figure 8 shows a schematic of the 10.5 eV (118 nm) source generation along with the ion source region of the LDPI-MS setup. 10.5 eV radiation was generated by tripling the third harmonic of a Nd:YAG laser (~20 mJ, 5 ns, Tempest 10 Hz 355 nm, New Wave Research, Fremont, CA) in a Xe gas cell at 6.5 torr pressure, similar to methods described previously. [27, 62, 125-127] The 355 nm radiation from the Nd:YAG laser was focused through a 200 mm focal length quartz lens (L1) to a custom-made, stainless steel Xe gas cell with high vacuum pumping, gas delivery, precision gauging and integrated input and output optics mounts. The input window was antireflective coated quartz (for 355 nm normal incidence) while the output window was a VUV grade LiF lens (L2) with 400 mm VUV focal length (±2% at 120 nm, custom made, Almaz Optics Inc., Marlton, NJ). Two steering mirrors (M1 and M2, highly reflective at 355 nm, 45° incidence) were used to direct the converging UV beam into the cell, and a quartz output window on the LDPI vacuum system mounted opposite the Xe gas cell allowed dumping of the 355 nm beam outside of vacuum, eliminating wall-generated ions and electrons while assisting alignment. This cell was evacuated to $<10^{-4}$ torr with a turbomolecular pump and initially baked out, then filled with Xe gas to a pressure of 6.5 torr as measured by a capacitance manometer. Tripling of the 355 nm beam was most efficient at this pressure, as gauged by acetone photoionization signal

when the sample chamber and ion source region were back filled with a constant pressure of acetone. The ionization energy for acetone is 9.7 eV and its high vapor pressure makes it an ideal candidate for testing the generation of 118 nm radiation. Figure 9 shows a mass spectrum obtained by photoionization of acetone vapors to confirm the generation of a 118 nm beam which corresponds to 10. 5 eV photon energy.

The custom built source described here is compact, reliable, and easy to use. 10.5 eV photons are generated reproducibly without further optimization if the 355 nm Nd:YAG laser is firing efficiently. The optical setup is simple and easy to align, allowing for direct measurement of the incoming 355 nm beam power. Prior estimates for conversion efficiency [127] indicate that the 10.5 eV output is in the low μJ range. High vacuum pumping and an efficient gas delivery design make the baking out and purging of the cell both rapid and efficient. Furthermore, the source design simplifies the performance of control experiments used to rule out ablation by desorption beam and multiphoton ionization from the residual 355 nm beam.

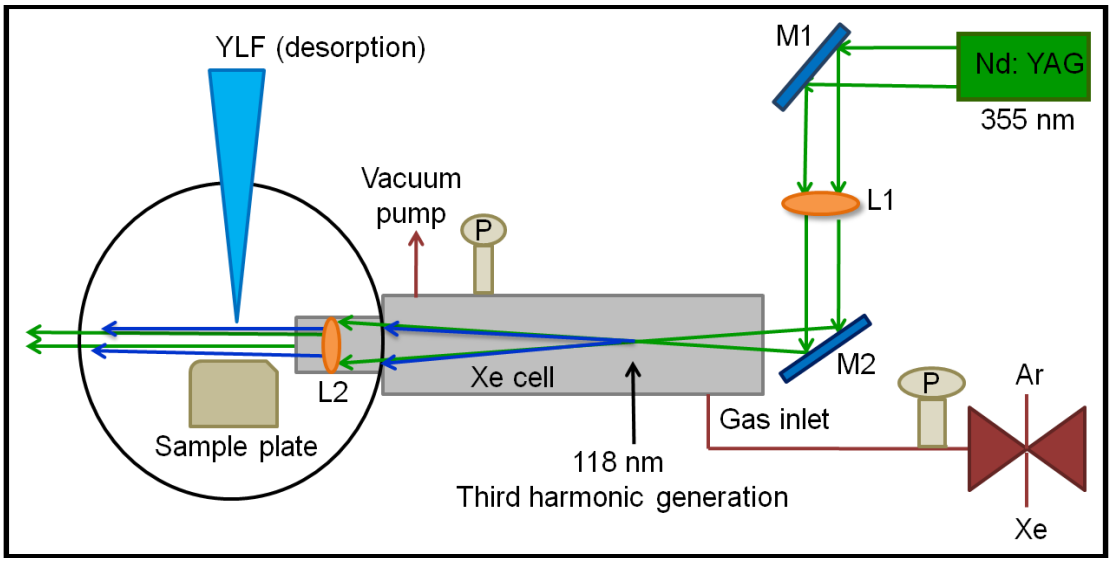

Figure 8 Schematic of the 10.5 eV (118 nm) third harmonic generation source and ion source region of the laser LDPI-MS. L1, L2, M1, and M2 denotes lens 1, lens 2, mirror 1 and mirror 2, respectively.

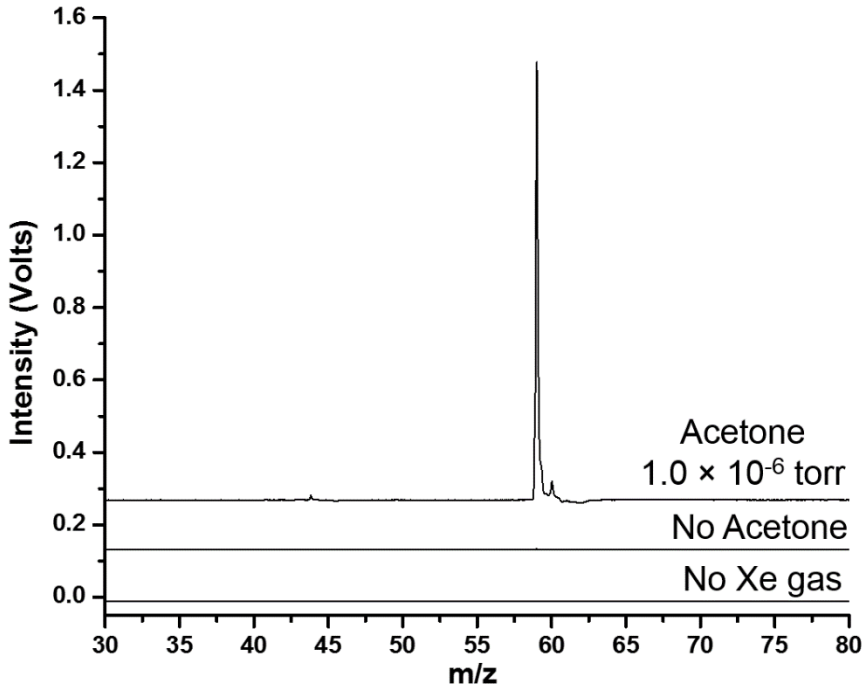

Figure 9 Mass spectrum obtained by photoionization of acetone vapors. Acetone signal is used to confirm 118 nm generation.

2.1.4 Data acquisition and processing

Most MS studies in this thesis were performed using the laser LDPI-MS instrument, wherein the data was acquired by a 12 bit, 125MS/s plug-in data acquisition card with 128 MS memory (CompuScope 8229, Dynamic Signals LLC, Lockport, IL) using customized software for instrument control (LabView 2011, National instruments, Austin, TX). The data acquisition rate was determined by the 10 Hz repetition rate of the Nd:YAG laser for 10.5 eV LDPI-MS and by fluorine laser repetition rate of 100 Hz in case of 7.87 eV LDPI-MS. Data was collected continuously while the desorption laser scanned over the sample surface at a speed of 0.05 mm/s. All of the data shown is the result of at least four replicates. Each figure shown is an average of at minimum 10,000 laser shots (unless reported otherwise), with the laser scanning area ~1 mm^2 during that collection time. Data was summed and plotted using commercial software (Origin 8.5) without any further processing. All spectra were mass calibrated against standards.

2.1.5 MS Calibration

Mass calibration was performed using a variety of compounds however, the most efficient calibrants were determined to be sexithiophene (mol. wt. 494 Da, Sigma-Aldrich), [6,6] diphenyl C_{62} bis(butyric acid methyl ester) (mol. wt. 1100 Da, Sigma-Aldrich) and a C_{60-70} mixture (mol. wt. 720 Da and 840 Da) which covered the low to mid to high mass range. Calibration curves were obtained based on the known peaks from the calibrants. Exact masses were assigned to these peaks and correlation plots were obtained between the mass and time which were then fitted into a second-order curve. Coefficients of the resulting second-order equation were entered into the software to obtain mass based on time, for the unknown ions.

2.1.6 Control Experiments

A series of controls were performed to unambiguously correlate MS signal with species from the samples of interest. For example, a desorption-only control was performed by blocking the photoionization laser beam while the desorption laser beam was used to collect background signal due to direct ionization. Controls performed by pumping out the Xe gas cell ruled out multiphoton ionization background due to the residual 355 nm YAG beam. The background signal from the membrane used to grow biofilms were also obtained: Polycarbonate membranes, used for growing biofilms, were incubated on agar plates without bacteria for the same time as the biofilm samples under identical conditions and were then measured as other samples. Peaks from samples were determined after carefully excluding the peaks from the above control measurements.

2.1.7 MS Imaging Data Acquisition and Processing

MS images were collected using an x-y translational stage, where the stage meander establishing the sampling path was controlled by software. Meander speed and step width could be varied according to the image size and were determined by the required acquisition time. For the images presented here, the meander speed was ~0.3 mm/s with a step width of 100 μm for 10.5 eV MS and a step width of 50 μm for 7.87 eV MS, yielding an interpolated spatial resolution of ~100 μm and ~50 μm respectively. Images were processed and analyzed using free software (Biomap, www.maldi-msi.org).

2.2 Sample Preparation

2.2.1 Microbial Species Studied

Work presented in this thesis was done on two binary consortia involving (A) prokaryote-prokaryote interaction and (B) eukaryote-prokaryote interaction. Two *Escherichia coli* K-12 (MG1655) strains were used for the former case and for the latter case *Saccharomyces cerevisiae* yeast and an *E. coli* K-12 strain were grown together as coculture biofilms. These coculture biofilm systems mimic naturally occurring binary consortia relationship template of primary producer supported by a secondary consumer [7]. Figure 10 shows the photographic images of the two consortia.

For prokaryote-prokaryote system a glucose consuming deletion strain (*E. coli* MG1655 *ΔaceAΔldhAΔfrdA,pRSET-mcitrine;* termed here as 'citrine'), acts as the system's primary producer secreting organic acids as byproducts. A glucose-negative metabolically engineered strain (*E. coli* MG1655 Δ*ptsG*Δ*ptsM*Δ*glk*Δ*gcd, pRSET-tdtomato;* termed here as 'tomato') acts as the organic acid scavenger making it system's secondary consumer. These strains constitutively express plasmids bearing their respective fluorescent reporter proteins (more information can be found in [8]) therefore, enabling visual differentiation when grown together as coculture biofilms. For eukaryote-prokaroyte system baker's yeast *Saccharomyces cerevisiae* acts as the primary producer secreting byproducts such as ethanol, acetate or acetaldehyde which are consumed by system's secondary consumer: *E. coli* tomato strain (see above)

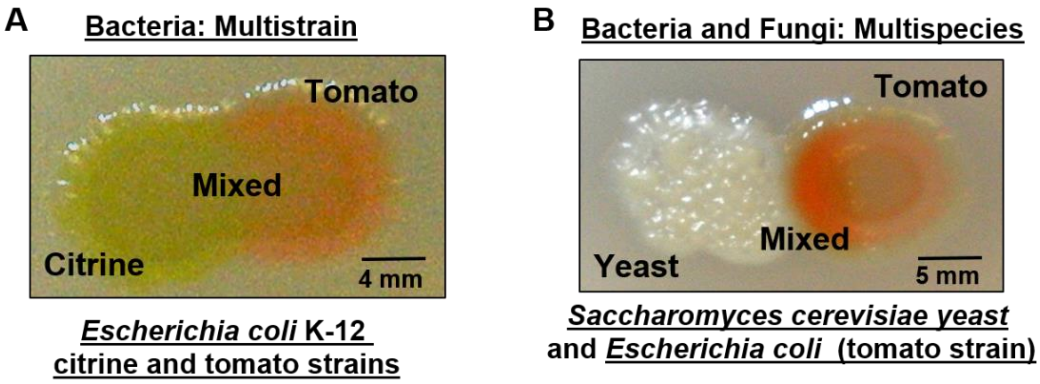

Figure 10 Photographic images of the two model biofilm systems used for the thesis work

2.2.2 Monoculture vs. Coculture

The term monoculture refers to a biofilm sample with only one species or strain. The term coculture refers here to a binary culture of two genetically distinct microorganisms that have been grown together on the same substrate. The coculture biofilms grown here were inoculated initially a few mm apart by two monocultures, then allowed to grow towards each other until they visually overlapped. LDPI-MS and SIMS analyses of coculture samples were performed on three distinct regions: two spots comprised predominantly of one type of microbe ("pure" region at the outer edges of the coculture sample) and at the center of the sample where the two species visually overlapped ("mixed" region). All biofilms used for the study were grown for an identical time period of 96 hours and the microbes were in the stationary growth phase. Monoculture and coculture biofilms were grown under identical experimental conditions, to eliminate any variation due to different growth phases.

2.2.3 Growth medium

All biofilms used in the reported experiments were grown in M9 media (6 g/L Na_2HPO_4, 3 g/L KH_2PO_4, 1 g/L NH_4Cl, 0.5 g/L NaCl, 1ml/L of 1M $MgSO_4 \cdot 6H_2O$) and 10 ml/L of trace metal stock solution (0.55 g/L $CaCl_2$, 0.1 g/L $MnCl_2 \cdot 4H_2O$, 0.17 g/L $ZnCl_2$, 0.043 g/L $CoCl_2 \cdot 6H_2O$, 0.06 g/L $Na_2MoO_4 \cdot 2H_2O$, 0.06 g/L $Fe(NH_4)_2$ $(SO_4)2 \cdot 6H_2O$, 0.2 g/L $FeCl_3 \cdot 6H_2O$) [7, 128]. Carbon sources for the microbes were: 10 g/L glucose for the primary producer i.e.; *E. coli* citrine strain and *S. cerevisiae* and 2 g/L sodium acetate for the scavenger strain i.e.; *E. coli* tomato strain. All stock solutions were either autoclaved or filter sterilized. M9 agar plates (typically 15 g agar/L) contained 100 μg/mL ampicillin.

2.2.4 Biofilm growth and sample preparation

Biofilms were grown on polycarbonate membranes (GE PCTE filter membranes, 09-732-18, Fisher Scientific) placed on agar medium. These membranes permitted nutrient access to the microbes via diffusion while providing suitable support for biofilm growth and subsequent MS analysis. Overnight cultures for micobes were prepared by inoculating experimental liquid media from either a fresh plate culture or frozen stocks. Tomato was grown in M9 minimal media with 2 g/L sodium acetate and 100 μg/ml ampicillin and citrine/yeast was grown in M9 minimal media with 10 g/L glucose and 100 μg/ml ampicillin. 5-20% v/v Luria-Bertani (LB) liquid medium was added to the M9 based growth media to ensure high culture densities ($OD_{600nm} \sim 0.1$). The cultures were grown overnight for ~12 hours at 37°C. Membranes were aseptically transferred onto separate agar plates. Typically, three membranes per plate were used and each membrane was inoculated with diluted culture in exponential phase. For monoculture growth, 50 μL of culture was used, while 50 μL of each strain [129] was used for coculture growth. Inoculated membranes

were allowed a short drying period in a laminar hood prior to incubation. The biofilms were grown for ~96 to 120 hrs at 37°C. During this growth period, the membranes were aseptically transferred to fresh plates every 24 hrs. The final growth period varied depending on the desired thickness of the resulting biofilm.

As mentioned above biofilms were grown on insulating polycarbonate membranes, the membranes were then adhered to a stainless steel plate with copper tape for introduction into vacuum for MS analysis. Biofilms were also blotted onto stainless steel plates: the blots were then introduced into vacuum.

3. LASER DESORPTION VUV POSTIONIZATION MS IMAGING OF COCULTURE BIOFILMS

[Chhavi Bhardwaj, Jerry F. Moore, Yang Cui, Gerald L. Gasper, Hans C. Bernstein, Ross P. Carlson & Luke Hanley. Laser desorption VUV postionization MS imaging of a cocultured biofilm. Analytical Bioanalytical Chemistry (2013) 405 (22), 6969-6977 DOI:10.1007/s00216-012-6454-0]- Reproduced with kind permission from Springer Science and Business Media. See Appendix A for permission.

3.1 Introduction

Mass spectrometry (MS) based analyses of biofilms typically rely upon homogenization and extraction, but an improved understanding of biofilm metabolic mechanisms and antibiotic resistance can be gained via analysis of intact biofilms. Various methods in laser desorption have been applied to MS imaging of intact biofilms, including laser desorption postionization (LDPI) [15], matrix assisted laser desorption ionization (MALDI) [16, 23] and laser ablation electrospray ionization (LAESI) [18]. Even ultra short pulse lasers show potential for MS imaging of biological samples.[92] MALDI-MS imaging has many advantages for protein and peptide imaging, but it suffers from low ion to neutral ratios, location-specific ion suppression, and the need to add matrix. LAESI is advantageous for analysis of metabolites and does not require matrix addition, but desorption yield variations with water content require careful manipulation of analysis protocols.[18, 100, 130] Atmospheric pressure-based methods such as LAESI can also suffer from postionization ion-molecule reactions that lead to the formation of new ions that complicate spectral interpretation.[44]

LDPI-MS imaging has several potential advantages including matrix-free analysis, detection of the neutral desorbed fraction and relative insensitivity to ion suppression.[15] LDPI uses vacuum ultraviolet (VUV) radiation to induce a relatively ‘soft’ single photon ionization of

laser desorbed neutrals.[27] These characteristics combine to make LDPI-MS a complementary method to MALDI-MS, LAESI-MS, or other established strategies for MS imaging.

Prior studies of antibiotic-treated bacterial biofilms using a 7.87 eV photon energy VUV source found that antibiotics could be selectively detected from a large background of other desorbed species.[15, 121] However, biologically relevant molecules often have ionization energies higher than 7.87 eV, [27, 29] requiring a higher photon energy source for their analysis. Prior LDPI-MS work with 8 - 24 eV VUV synchrotron radiation showed that higher photon energies dramatically improve sensitivity.[122, 131] For example, 12.5 eV photons produced significant precursor ion signal, but fragment and other low mass ion signal was also enhanced at this relatively high photon energy. A 10.5 eV photon energy appeared to provide an optimal balance between improved sensitivity and minimal fragmentation for biofilm-antibiotic samples.[122] These findings encouraged the current work where a pulsed 10.5 eV VUV source [27, 62, 125, 126] was tested. The design and construction of the 10.5 eV ionization source is described in detail in Chapter 2.

This chapter describes the successful implementation of 10.5 eV ionization source for laser LDPI-MS analysis of biofilms. 10.5 eV and 7.87 eV LDPI-MS imaging are demonstrated here for analysis and imaging of small endogenous molecules within intact biofilms. The study uses a model biofilm consortia comprised of a synthetic coculture engineered for syntrophic metabolite exchange.[7] The two *E. coli* (K-12) strains: citrine and tomato are well characterized for function and constitutively express two different fluorescent reporter genes to facilitate visual strain differentiation and analysis of metabolite localization. This synthetic biofilm consortium is ideal for development of LDPI-MS imaging for the exploration of fundamental biofilm behavior.

3.2 Experimental Section

3.2.1 MS Instrumentation

Laser LDPI-MS instrument which is described in Chapter 2 was used for the study. The energy used for desorption was around 25 - 35 μJ, with the beam spot diameter of ~20-30 μm. Ionization of the desorbed neutrals was achieved using two different photon energies: 7.87 eV and 10.5 eV. The details of the two ionization sources, acquisition parameters and processing methods are described in Chapter 2.

3.2.2 Biofilm Samples

Escherichia coli K-12 strains: citrine and tomato were used for the present study. The growth procedure and conditions are described in detail in Chapter 2. The two strains were grown as coculture as well as individual monoculture biofilms on polycarbonate membranes and were adhered to stainless steel sample plate for LDPI-MS analysis and imaging. This growth procedure enabled a robust growth of the biofilm with clear boundary for each microbe thereby making the localized MS imaging and visual examination of each interacting microbes, feasible in a coculture biofilms. Prior LDPI-MS studies examined biofilms grown using drip flow reactors, [122] but coculture biofilms grown by drip flow tend to lack clear boundaries between different micobes making analysis of pure cultures impossible without additional parallel experiments. Therefore, drip flow growth procedure was avoided for the work presented in this thesis.

3.3 Results and Discussion

3.3.1 10.5 eV LDPI-MS of *E. coli* Coculture Biofilm

Figure 11 (i) shows 10.5 eV LDPI-MS from the citrine (c), tomato (t) and mixed (m) regions of coculture *E. coli* biofilm, similar to that displayed in the inset photograph. Tomato and citrine strains were grown adjacent to each other and were allowed to grow towards each other with a resulting overlap region, which is referred as 'mixed' region, on a single polycarbonate membrane sitting on an agar plate. The mass spectra shown in Figure 11 were collected directly from each of the three noted (see inset photograph) regions of the same membrane after it was removed from the agar and placed in vacuum. Thus, biofilms were analyzed in their intact form on membranes without cell lysing, enzymatic treatment, or addition of any desorption-enhancing matrix.

The citrine, tomato, and mixed regions showed mostly similar peaks in their respective MS, albeit at differing intensities. Citrine showed overall higher MS signal intensity compared to tomato due to more robust growth on the glucose containing medium. A difference spectrum of the two monoculture regions grown under identical conditions and analyzed using identical experimental parameters on the same sample plate, was generated to facilitate comparison: Figure 11(ii) shows the difference of the citrine MS after subtracting out the tomato MS (following normalization of both spectra to their respective peaks at m/z 370). The difference spectrum is mainly positive, indicating a higher overall signal for citrine compared to tomato. Several species above m/z 300 (especially those peaks marked with m/z values) were more dominant in citrine biofilms, although the m/z 258.2 peak was enhanced in tomato biofilms.

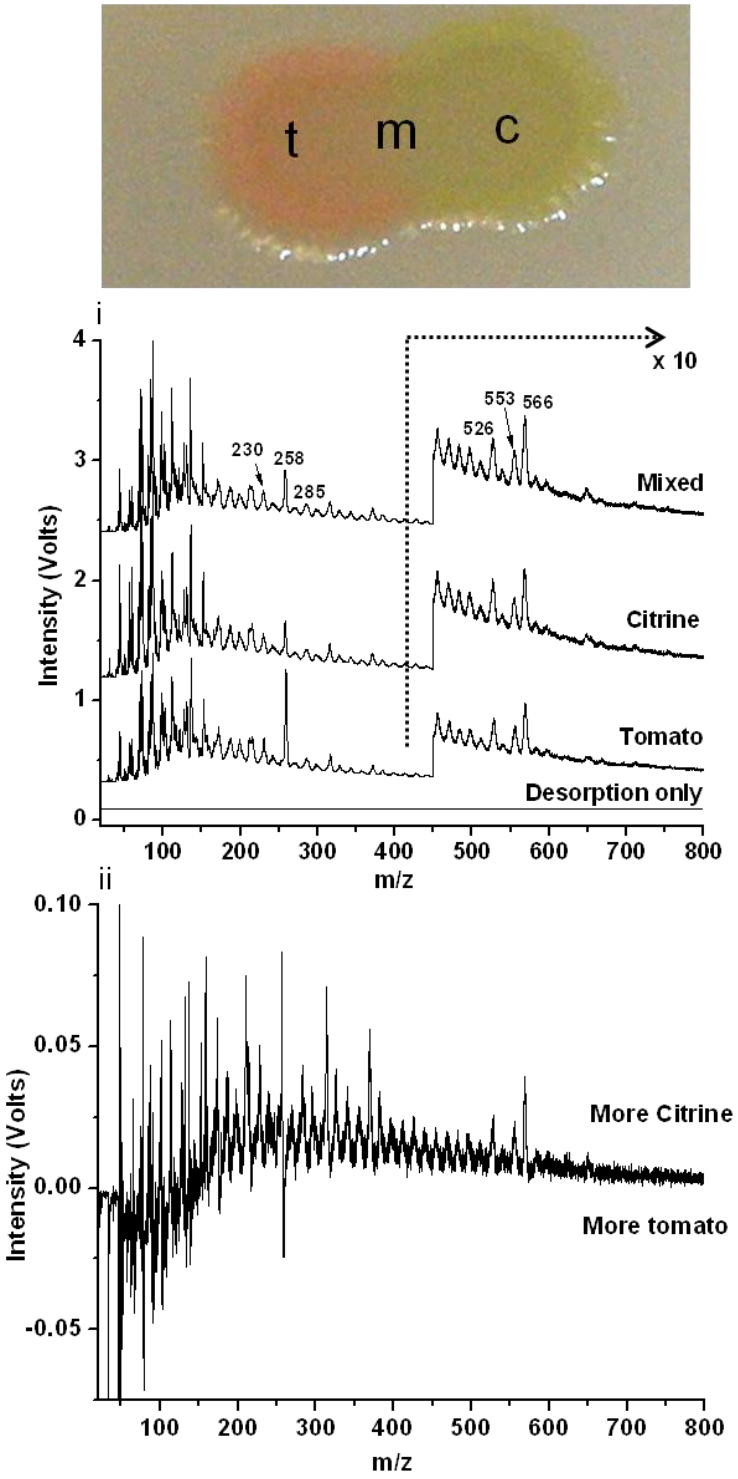

Figure 11 10.5 eV LDPI-MS of coculture *E. coli* biofilm. The photograph at top shows the citrine strain region of the biofilm (c), tomato strain region (t), and mixed region where they overlap (m). (ii): The difference spectrum of tomato subtracted from citrine

The generally higher signal for the citrine biofilm was consistent with the appearance of byproducts preferentially expressed by this strain. For example, enhancement of the peak at m/z 90 might arise from pyruvic and/or lactic acid, two previously observed citrine byproducts. Furthermore, other species and/or fragments thereof might also appear near m/z 90. While LDPI-MS can image microbial byproducts on intact biofilms (see below), correlation of ion signal with specific byproducts requires further verification. Absence of tandem MS capability on the aforementioned LDPI-MS instrument limited our ability to assign compounds to the observed MS peaks with certainty.

Nonetheless, tentative assignments were attempted based on previously reported studies. For example, peaks at m/z 315.7±0.5, 525.8±0.1, 552.9±0.2, and 566.1±0.2 were tentatively assigned to fragments of phospholipids, based on previously reported laser desorption, fast atom bombardment [132] and electrospray ionization [133] studies of *E. coli*. Specifically, m/z 525.8 and 552.9 are thought to correspond to protonated fragments formed by loss of a phosphoethanolamine group from phosphatidylethanolamines with 18:0 and 16:0 fatty acid constituents, respectively. Precursor ion peaks for these phosphatidylethanolamines were not observed and were assumed to be masked by background signal from the membrane. Gas chromatography coupled with electron ionization MS identified fatty acids present in *E. coli* membranes [134] and peaks corresponding to the molecular ion for several of the fatty acids were observed here. For example, the peak at m/z 284.8 ± 0.3 and others in the m/z 50 - 220 range match the stearic acid precursor ion and its fragment pattern (http://lipidlibrary.aocs.org). No assignments were made for the peaks at m/z 229.7 ± 0.6, 258.2 ± 0.5, 369.8 ± 0.1, and 382.1 ± 0.3.

Control measurements found no significant signal from either laser desorption only (see Figure 11 (i) or postionization only, data not shown), indicating an absence of direct ionization

(i.e., MALDI-like events) and single photon ionization of volatile species, respectively. While the LDPI-MS of the membrane alone did show a few peaks, those peaks appearing from biofilms at similar masses were excluded from further consideration. Laser-induced photoelectron ionization was also ruled out experimentally.

A similar study was performed using 7.87 eV LDPI-MS for direct comparison of the two photon energies used as ionization sources. The next section discusses the analysis using 7.87 eV LDPI-MS.

3.3.2 7.87 eV LDPI-MS of *E. coli* Coculture Biofilms

Figure 12 (i) shows the 7.87 eV LDPI-MS of the similar three regions of a coculture *E. coli* biofilm, as described above except collected at a lower VUV photon energy. 7.87 eV LDPI-MS showed fewer peaks compared to 10.5 eV LDPI-MS, particularly in the higher mass range and no peaks for >m/z 366 were observed from the sample. The overall 7.87 eV signal intensity was about three times higher than that from 10.5 eV, which can be explained by the fact that the 7.87 eV laser had ~10^5× higher photon flux. It is clear that most of the laser desorbed species possess higher ionization energy which do not undergo 7.87 eV single photon ionization. However, the similarity in signal levels for two photon energies but a lack of higher mass peaks at 7.87 eV indicates that other effects are also affecting a low 7.87 eV signal, possibly including poor focus of the 7.87 eV beam and/or detector saturation.

On comparing experimental results with the controls, peaks in the mass range m/z 120 to 370 as listed in Table I were assigned to the biofilm and all peaks except for the peak at m/z 229.7 were observed only for 7.87 eV photon energy. The absence of these peaks at 10.5 eV MS is likely

due to more fragmentation at the higher photon energy. 7.87 eV MS showed many high intensity low mass peaks for m/z < 100. As was observed for 10.5 eV source, citrine displayed higher signal at 7.87 eV than tomato in the mass range below m/z 100.

Figure 12 (ii) shows the difference spectrum of the citrine MS after subtracting out the tomato MS at 7.87 eV (following normalization of both spectra to their respective peaks at m/z 366). The difference spectra shows mainly positive peaks in the lower mass range (m/z 10-125), however peaks at m/z 156.4, 167.9, 229.7, and 366.3 were negative indicating that these peaks were more dominant in tomato.

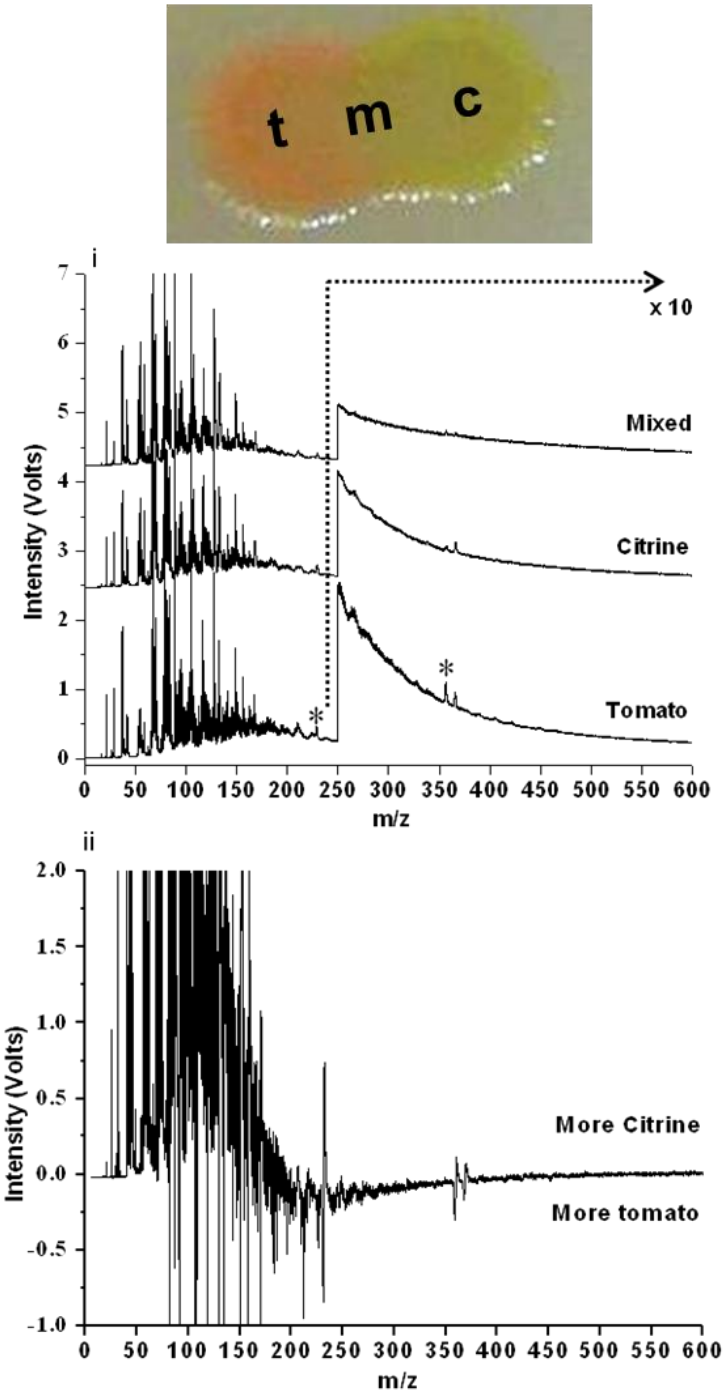

Figure 12 (i) 7.87 eV LDPI-MS of coculture *E. coli* biofilm. (ii) Difference spectrum between citrine and tomato (c – t), following normalization at m/z 366. Peaks with asterisk (*) are more dominant in citrine.

3.3.3 Comparison: 7.87 eV vs. 10.5 eV LDPI-MS

Selective ionization abilities of LDPI-MS using two different VUV sources was demonstrated here. 10.5 eV LDPI-MS showed more high mass peaks (m/z > 250) compared to that of 7.87 eV, presumably because the higher photon energy could ionize more species inherent to the biofilms. Saturated fatty acids with aliphatic carbon chains and phospholipids were excellent candidates, with ionization potentials higher than 7.87 eV, [135] which ionized with 10.5 eV and not with 7.87 eV. MS peaks arising from biofilms were carefully selected after excluding any peaks from the control experiments. These peaks were tabulated in Table I and compounds were tentatively assigned to these peaks based on previously reported studies. All significant peaks along with their tentative assignments are listed in Table I. All of the listed peaks were observed for both strains (citrine and tomato).

Table 1 List of peaks (>m/z 100) observed in the biofilm samples using LDPI-MS. Two different VUV photo energy sources were used: 7.87 eV and 10.5 eV. See text for tentative assignments. t and c refer to tomato and citrine, respectively.

Mass (m/z)	**7.87 eV**	**10.5 eV**	**Tentative assignments**
111.7 ± 0.1		t,c	Not assigned (NA)
128.3 ± 0.2	t,c		NA
152.1 ± 0.4		t,c	NA
156.4 ± 0.2	t,c		NA
167.9 ± 0.2	t, c		NA
229.7 ± 0.6	t, c	t,c	Myristic acid
258.2 ± 0.5		t, c	Palmitic acid
284.8 ± 0.3		t, c	Stearic acid
315.7 ± 0.5		t, c	Phospholipid fragment
366.3 ± 0.2	t, c		NA
369.8 ± 0.1		t, c	NA
382.1 ± 0.3		t, c	NA
525.8 ± 0.1		t, c	Phospholipid fragment
552.9 ± 0.2		t, c	Phospholipid fragment
566.1 ± 0.2		t, c	Phospholipid fragment

It is noteworthy that the low mass region (m/z < 150) for both 10.5 eV and 7.87 eV spectra have a high density of peaks. These peaks could be due to endogenous compounds or fragments of larger precursor molecules. More experiments and tandem mass spectrometric analysis is required to evaluate these peaks and such studies were not performed for the presented work. These peaks were mostly separated by unit mass intervals and are not listed in Table I. The following section discusses the low mass region for the two photon energies and the possible compounds correlating to these peaks.

3.3.4 Low Mass Metabolite LDPI-MS Analysis

Figure 13 shows the mass spectra of tomato monoculture for mass range m/z 20 to 160 at both 7.87 and 10.5 eV. The figure is used to show the high density of peaks which is observed for masses below m/z 150. Similar results were obtained for citrine monoculture as well coculture samples (data not shown). These peaks could be small molecules like aromatics, fused ring species or tertiary amines in case of 7.87 eV and fatty acid fragments, amines or amino acids at 10.5 eV. The spectra in Figure 13 were normalized to the respective maximum intensity peak for the two photon energies to demonstrate a comparison. Overall 7.87 eV LDPI-MS showed higher signal in this region compared to 10.5 eV which could be attributed to much higher photon flux (~10^5×) in case of 7.87 eV ionization. Moreover, 10.5 eV photon energy may result in more fragmentation which decreases the precursor ion intensity. Peaks with an asterisk (*) in Figure 13 were either unique to the photon energy or were significantly higher in intensity for one photon energy than the other. For example, the peaks at m/z 88.1 and 90.1 were tentatively assigned to pyruvic and lactic acid, respectively, both known *E. coli* biofilm metabolites. However, the large number of

possible endogenous species prevents definitive assignment of the low mass region of the spectra. The use of organic matrices for MALDI-MS analysis of bacterial biofilms often results in loss of information for low mass regions m/z < 300, Figure 13 here demonstrates that LDPI-MS, a matrix-less technique, could be used to obtain information on low mass species inherent to the biofilm samples.

Figure 13 also shows that the ~1000 mass resolution is possible with this LDPI-MS instrument from these relatively thick, high dielectric constant membranes. The mass resolution was improved in Figure 13 (compared to Figure 11 and 12) by optimizing the Einzel lens, steering and reflectron voltages which also improved low mass signal at the expense of higher mass signal. By contrast, the spectra in Figure 11 and 12 were recorded at lower resolution to obtain better signal to noise for the higher mass peaks.

Preliminary results found that addition of a matrix compound to biofilms only improved the 7.87 eV LDPI-MS signal to noise by a factor of 3 to 10, but the appearance of matrix ion peaks offset that advantage by obscuring adjacent masses from analysis.[123]

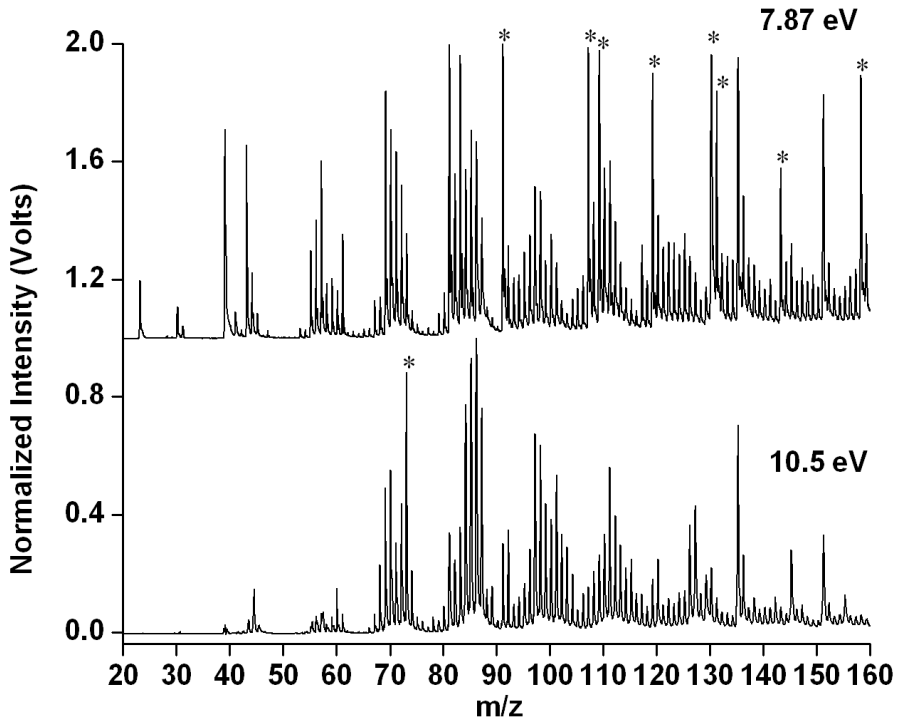

Figure 13 7.87 eV and 10.5 eV LDPI-MS for *E. coli* (tomato strain) monoculture biofilm for mass range m/z 20 to 160. The asterisk (*) indicates peaks which are either unique or differ in intenstity significantly at one photon energy.

3.3.5 Limitation of Metabolite Identification using LDPI-MS

Use of this and similar low resolution, single analyzer instruments for LDPI-MS analysis of intact bacterial biofilms or other biological samples presents challenges in species identification similar to those encountered with secondary ion mass spectrometry. [136] The mass accuracy was calculated to be 340 ppm for 10.5 eV and ~300 ppm for 7.87 eV (Figure 13) and there are over 10^3 known species whose singly charged precursor ions would appear at m/z 150, with more species possible at higher masses.[137] The use of metabolomic databases for limited classes of species

will dramatically reduce the number of candidate species at a given mass. Nevertheless, other strategies are still needed to assist compound identification with this particular type of LDPI-MS instrument. Post-acquisition data processing can be employed to improve effective mass accuracy, reducing the number of likely candidate species.[136] Culturing in media enriched in ^{15}N and/or ^{13}C stable isotopes will induce mass shifts facilitating compound identification [138]. Chemical derivatization followed by 7.87 eV single photon ionization can selectively detect certain classes of species.[15] Finally, solid-phase microextraction can be applied to purify the sample prior to collecting mass spectra, [139] potentially employing blotting techniques to preserve spatial distributions.

Perhaps the most straightforward improvement in the LDPI-MS technique would be the addition of ion optics and an analyzer capable of tandem MS and/or high resolution measurements. For example, there have been many instruments in which laser desorption was combined with postionization then coupled to a radio frequency ion trap [62, 140] or quadrupole-time-of-flight MS. [18, 100, 130]

3.3.6 MS Imaging

3.3.6.1 MS Imaging using 10.5 eV LDPI-MS

Figure 14 shows the LDPI-MS image of an intact coculture bacterial biofilm using 10.5 eV postionization. The software allows an image to be created from any range of masses: this image was constructed from a m/z 0.6 window around the m/z 258.2 peak, which showed a higher signal from the tomato strain. Similar images could have been constructed which showed a brighter image

for the citrine strain due to the higher abundance of other peaks. The peak was selected to show maximum contrast between the two strains.

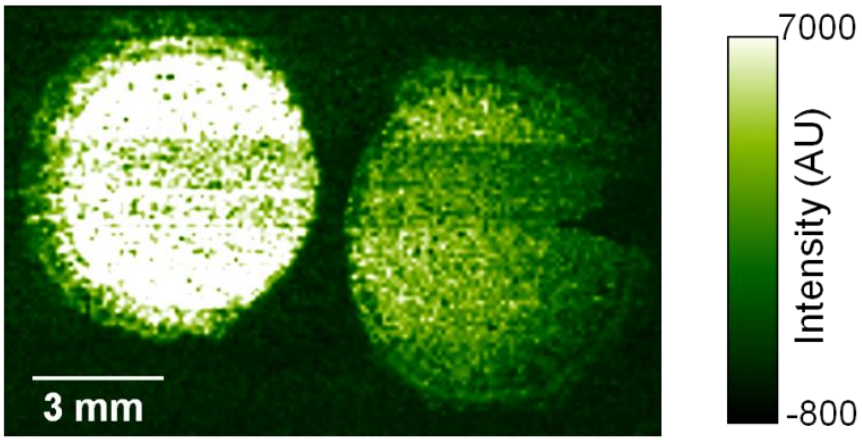

Figure 14 10.5 eV LDPI-MS image of coculture *E. coli* biofilm. Tomato (left) and citrine (right). Image was plotted using ion signal at m/z 258.2 ± 0.3.

The spatial resolution of the instrument was vibration-limited to ~20 µm. However, the spatial resolution of the image was degraded to collect the data in Figure 14 by use of a large meander step size of ~100 µm, employed to allow the entire biofilm area to be imaged in ~90 min. This relatively long image acquisition time was due to the slow, 10 Hz repetition rate of the Nd:YAG laser used to pump the 10.5 eV source. However, this laser can be upgraded to a 30 Hz repetition rate and similar lasers are available at repetition rates up to 2 KHz, dramatically speeding up data acquisition time.

3.3.6.2 MS imaging using 7.87 eV LDPI-MS

Figure 15 shows the LDPI-MS image of an intact coculture bacterial biofilm using 7.87 eV postionization. The image was constructed from an m/z 0.6 window around the m/z 43 peak. The spatial resolution of the image was 50 µm which was again dependent on the repetition rate (100 Hz) of the 7.87 eV laser source. The MS image was obtained at a low mass peak i.e.; m/z 43 because images at higher mass did not show much contrast between the two strains.

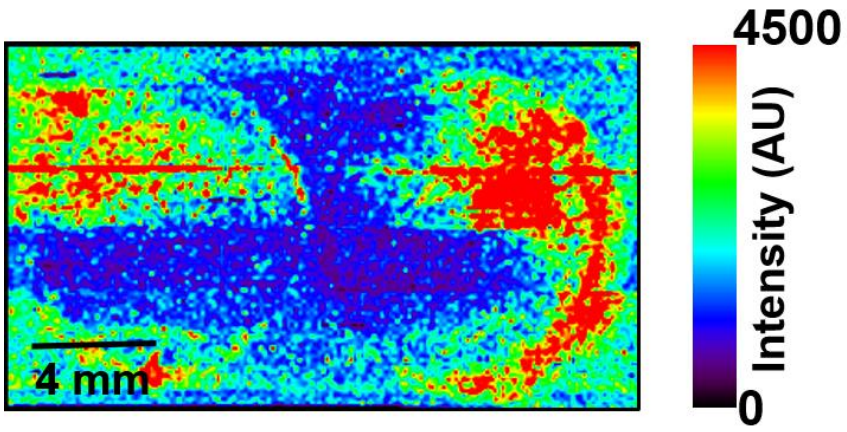

Figure 15 7.87 eV LDPI-MS image for *E. coli* coculture biofilm. The image was obtained by selecting peak at m/z 43.

Overall, the samples were analyzed directly on membranes without any sample preparation or addition of matrix. The images above demonstrate the capability of the instrument to image a thick insulating, biological sample in its native form. 10.5 eV MS image shows significant contrast

between the closely related *E. coli* strains in a biofilm which can be utilized to study spatial localization of a wide range of analytes in a multi microbe biofilm system. Moreover, 7.87 eV MS imaging can be used to locate a subset of analyte in a biofilm and thus can provide complementary information during analysis.

3.4 Conclusion

LDPI-MS imaging was successfully demonstrated with 7.87 eV and 10.5 eV photon energy sources for analysis and imaging of small endogenous molecules within intact biofilms. Biofilm consortia comprised of two synthetic *Escherichia coli* K-12 strains engineered for syntrophic metabolite exchange were grown as cocultures mimicking the naturally occurring interactions. The samples were grown on membranes, then used for LDPI-MS analysis and imaging. Both *E. coli* strains displayed many similar peaks in LDPI-MS up to m/z 650, although some observed differences in peak intensities were consistent with the appearance of byproducts preferentially expressed by one strain. The relatively low mass resolution and accuracy of this specific LDPI-MS instrument prevented definitive assignment of species to peaks, but strategies were discussed to overcome this shortcoming.

Finally, 7.87 eV and 10.5 eV LDPI-MS was able to collect ion images from intact, electrically insulating biofilms at ~50 μm and ~100 μm spatial resolution respectively. Spatial resolution of ~20 μm was possible with the instrument, although a relatively long acquisition time resulted from the relatively lower repetition rate of the single photon ionization sources limited achieving higher spatial resolution. Nonetheless, the ability of LDPI-MS to collect images off of electrically insulating films shows promise for a wider variety of sample types than many other MS imaging strategies which often require thin and conducting samples for successful analysis.

4. LASER DESORPTION POSTIONIZATION MASS SPECTROMETIC STUDY OF MULTISPECIES COCULTURE BIOFILMS USING TUNABLE VUV SYNCHROTRON SOURCE.

4.1 Introduction

The ability of LDPI-MS to detect intact precursor ions of molecular species depends upon the extent of energy transfer during the separate laser desorption and single photon ionization (SPI) steps. In order for a desorbed molecule to ionize, the photon energy of the ionizing source must be higher than the ionization energy of the molecule.[15] Varying the photon energy thereby allows some selectivity in the analysis process.[27, 62] For complex biological systems such as microbial biofilms: different classes of metabolite compounds can be analyzed by varying the photon energy of the ionization source in LDPI-MS analysis. Prior LDPI-MS work showed that the higher VUV photon energies in the range of 7.8 - 12.5 eV improved sensitivity and produce intense molecular ion signal, but led to formation of fragment ions and background gas ions.[29, 122]

The present study utilized 7.87 to 10.5 eV VUV photon energies from tunable synchrotron and 7.87 and 10.5 eV laser sources for LDPI-MS analysis of biofilms comprised of binary cultures containing *Escherichia coli* and *Saccharomyces cerevisiae.* The current study was performed as an exploration of the photon energy effect on the mass spectra of biofilms and for drawing comparison of the two ionization sources: laser vs. synchrotron radiation. The *E. coli*-yeast multispecies biofilm system was used due to the appearance of distinct mass spectra for the two interacting species.

4.2 Experimental Details

4.2.1 MS Instrumentation

Mass spectral analysis presented in this chapter was carried out at the Chemical Dynamics Beamline at the Advanced Light Source (Lawrence Berkeley National Laboratory, Berkeley, CA), wherein, tunable VUV synchrotron radiation in the energy range 7.87 eV - 10.5 eV was utilized for the LDPI-MS analysis of biofilm samples. Details of the instrument as well as acquisition parameters are described in Chapter 2. The instrument will be referred to as synchrotron LDPI-MS hereon. Additional MS analysis of these biofilm samples was carried out at the LDPI-MS instrument at the University of Illinois at Chicago. The instrument is described in Chapter 2 and will be referred to as laser LDPI-MS.

4.2.2 Biofilm Samples

Escherichia coli K-12 bacteria and *Saccharomyces cerevisiae* yeast cocultures as well as monoculture biofilms were used for the study. When grown together as cocultures *E. coli* tomato strain shows a growth gradient more cell growth (bright red) closer to yeast and gradual decrease in cell growth on moving away from the yeast interface.(See Figure 10) Biofilms were grown using the procedure described in Chapter 2. Samples for analysis were prepared by two methods: 1) Mature biofilm intact on polycarbonate membrane substrate was adhered to a stainless steel sample plate using a double sided copper tape, to be analyzed directly from the membrane, referred to as membrane biofilms hereon, 2) Mature biofilms were blotted on the sample plate directly and the membranes were removed from the sample prior to MS analysis, hereon referred to as blotted samples.

Earlier trials at the synchrotron facility had showed that the polycarbonate membrane caused excessive charging and hindered the detection of the target ions. Blotting methods were therefore used to avoid unwanted analysis of the insulating membrane. Synchrotron LDPI-MS analysis was carried out using only blotted biofilm samples. Because samples were blotted prior to analysis, some spatial integrality was lost during sample preparation. Nevertheless, yeast and *E. coli* were very distinct in appearance making the analysis and visual examination feasible.

It is worth noting that significantly higher laser desorption energy was required to analyze intact membrane biofilms compared to the blotted biofilms (see Chapter 2 for the desorption energies used for each sample type). This might have resulted from the thickness of the membrane biofilms and the effective absence of an immediately adjacent metal substrate which otherwise can undergo rapid heating to assist desorption.[62, 141]

4.3 Results and Discussion

4.3.1 Effect of VUV Photon Energy on LDPI-MS Analysis of Biofilms

Blots of yeast and *E. coli* monoculture biofilms were analyzed by synchrotron LDPI-MS using 7.87, 8.5, 9.5 and 10.5 eV VUV photon energies with the results shown in Figure 16 and 17 respectively. The synchrotron LDPI-MS of microbial monocultures showed that increasing photon energy resulted in more peaks in the mass spectra and higher overall signal intensity. 10.5 eV showed more peaks for molecular species as well as more fragments compared to the lower photon energies. However, fragmentation increased significantly at photon energies between 10.5 and 15 eV data as was shown previously.[131] Overall, 10.5 eV photon energy displayed an optimal balance between sensitivity and fragmentation, in agreement with prior experiments.[29, 122, 131]

The data traces labeled “Desorption Laser Only” and “Synchrotron Only” in Figure 16 and 17 demonstrate the absence of any background signal arising from direct ionization via the desorption laser or VUV postionization of background or sublimed gaseous neutrals, respectively. Prior control experiments with the 10.5 eV laser LDPI-MS established the presence of single photon ionization and ruled out both direct ions from laser desorption and photoelectron ionization effects due to the residual 355 nm beam used to generate VUV radiation.[142] Photoelectron ionization was previously ruled out in synchrotron LDPI-MS.[29] The similarity of the spectra of 7.87 eV synchrotron and laser LDPI-MS ruled out photoelectron ionization in the latter case.

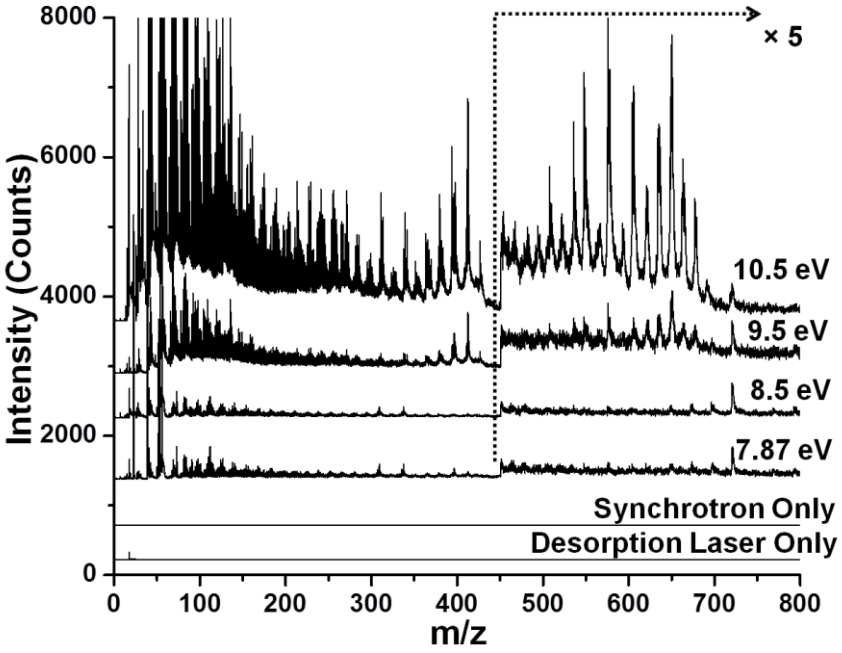

Figure 16 7.87 - 10.5 eV synchrotron LDPI-MS of blotted yeast monoculture biofilms. The bottom two traces show the controls performed with only synchrotron photoionization or desorption laser.

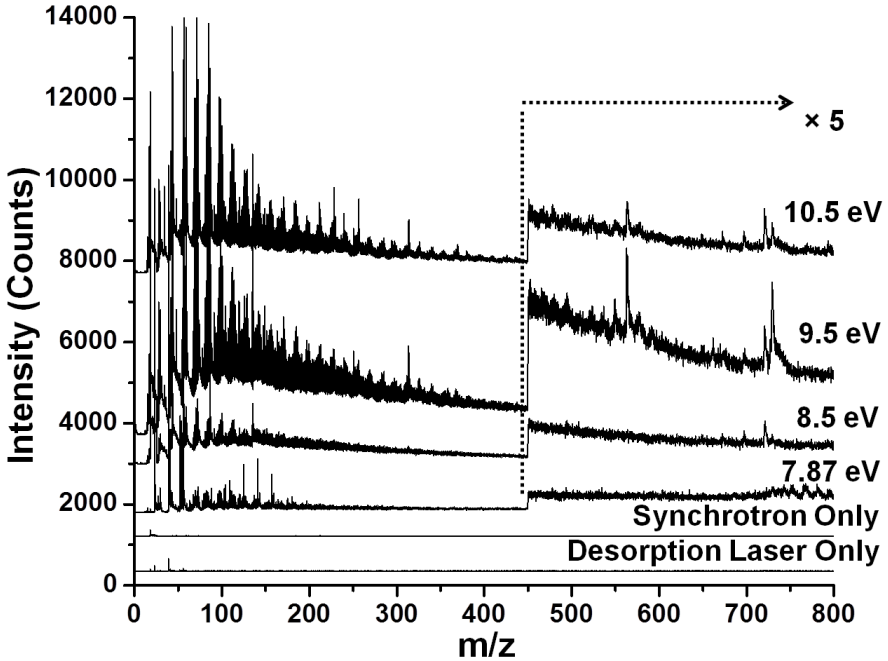

Figure 17 7.87 to 10.5 eV synchrotron LDPI-MS of *E. coli* (tomato) strain blotted monoculture biofilm. Bottom two traces show the controls performed to check for any background signal.

The mass spectral peaks observed for *E. coli* and yeast monocultures were tabulated in Table II, with the VUV photon energies at which they were first observed by synchrotron LDPI-MS. These peaks were selected manually by careful visual examination. Listed peaks were observed reproducibly for at least three replicate mass spectra. MS peaks first appearing at 7.87 eV are shown in the left column of Table II while additional peaks appearing at 9.5 and 10.5 eV photon energies are listed in the middle and right column, respectively. Peaks observed at lower photon energies always appeared at higher photon energies as well, albeit at higher intensities. However, a separate column is not shown for 8.5 eV photon energy, since no new peaks were observed visually beyond those already present at 7.87 eV.

Due to the lack of tandem MS capabilities at the synchrotron LDPI-MS instrument, mass spectral peaks could not be assigned with certainty to any metabolite. However, several metabolites were tentatively assigned to the observed MS peaks, which are listed in Table II, based on the ability of 7.87 eV photon energy to selectively ionize species containing tertiary amines and fused ring structures. These tentative assignments were made by referring to *E. coli*[143] and yeast[144] metabolite databases. *E. coli* peaks at m/z 102, 104, 114, 138, 140, 143, 145, 157, and 366 were assigned to betaine aldehyde, choline, 2-mercapto-1 methylimidazole, urocanic acid, L-histidinal, crotonobetaine, gamma-butyrobetaine, imidazolelactic acid, and phosphoribosyl formamidocarboxamide, respectively. Yeast peaks at m/z 157, 240, 243, 244, 252, 267, 284, and 720 were assigned to N-acetyl-D-proline, anserine, cytidine, uridine, 2'-deoxyinosine, adenosine, xanthosine, and phosphoribosyl-ATP, respectively.

Table 2 List of mass peaks (m/z) first observed at 7.87, 9.5, and 10.5 eV photon energies by synchrotron LDPI-MS of blots of *E. coli* bacteria and *S. cerevisiae* yeast monocultures.

Species	7.87 eV (m/z)	9.5 eV (m/z)	10.5 eV (m/z)
***Escherichia coli* (Bacteria)**	39-45, 53-58, 65-75, 77-87	35	
	95-105, 108-115, 120-130, 135-145, 157, 159, 165, 175, 180, 181,197	153	
	267	212-216, 240, 251	228, 256
	366	315, 326, 338, 371	
	590	550, 565, 578	
	605, 625, 635		665
	732, 745, 763, 780, 793	730, 750, 775	
***Saccharomyces cerevisiae* (Yeast)**	38-45, 53-60, 67-75, 82-88		32, 34, 48
	90-105, 105-115, 135-143	145-150	128, 156, 168-172, 184-194, 198-205
	235-245, 250-260, 264-270, 276-284	213-216, 227-230, 272	
	397	394, 398, 400	395, 396
	413	412, 415, 426	494
	576	508, 536, 564-568, 592-596	510-514, 522, 552
	696-700		
	720-724		
	816-818, 840-845		

Additionally, *E. coli* peaks at m/z 625, 635, 732 and 763 and yeast peaks at m/z 723, 724, 840, and 843 correspond with the molecules in the glycerophospholipids class, an abundant constituent of the microbial cell membrane. These molecules do not have tertiary amines or fused ring moeities in their structure, leading to the speculation that they may have desorbed as clusters which facilitates their VUV postionization.[29]

Additional classes of molecules will be photoionized at 9.5 and 10.5 eV photon energies, increasing the possibility of the precursor ions of different endogenous species appearing at the same nominal m/z values. Nonetheless, tentative assignments were made for some 9.5 and 10.5 eV peaks in Table II. *E.coli* peaks at m/z 153, 228, 240, 256, and 338 could be attributed to to 3-sulfinoalanine, myristic acid, L-cystine, palmitic acid, and N5-carboxyaminoimidazole ribonucleotide, respectively. Peaks at m/z 665, 750 and 775 were assigned to the molecules of glycerophospholipids. Similarly, yeast peaks at m/z 146, 149, 189, 190, 192, 200, 213, and 214 were assigned to L-glutamine, D-methionine, N-acetyl-L-glutamic acid, oxalosuccinic acid, citric acid, lauric acid, 4-phopho-L-aspartic acid, and 3-methylbutyl octanoate, respectively. Peaks at m/z 565, 567 and 593 were assigned to glycerolipids and peaks at m/z 426, 494 and 522 were assigned to glycerophospholipids. Regardless of photon energy, high resolution or tandem MS analysis is required to unequivocally associate any of the aforementioned peaks with specific endogenous species in the biofilm.

4.3.2 Analysis of Biofilms: Synchrotron vs Laser LDPI-MS

Prior synchrotron LDPI-MS studies[29, 122] led to the recent development of a refined laboratory VUV photoionization source that operates at 10.5 eV[142] to complement the 7.87 eV

fluorine excimer laser source.[15] These two laboratory laser VUV sources were used to collect 7.87 and 10.5 eV laser LDPI-MS data from yeast and *E. coli* monocultures.

10.5 eV laser LDPI-MS data for blotted monoculture biofilms (yeast or *E. coli*) was collected and compared with the similar spectra collected by 10.5 eV synchrotron LDPI-MS in Figure 18. Each spectrum in the figure is normalized to correct for differences in data acquisition strategies between the two instruments. The synchrotron LDPI-MS data of the blotted samples showed overall higher S/N compared to that from laser LDPI-MS. Additionally, synchrotron LDPI-MS showed more peaks in the mass range of m/z 500-800 in case of *E. coli* monoculture. The higher S/N can be attributed to higher photon flux of synchrotron source.

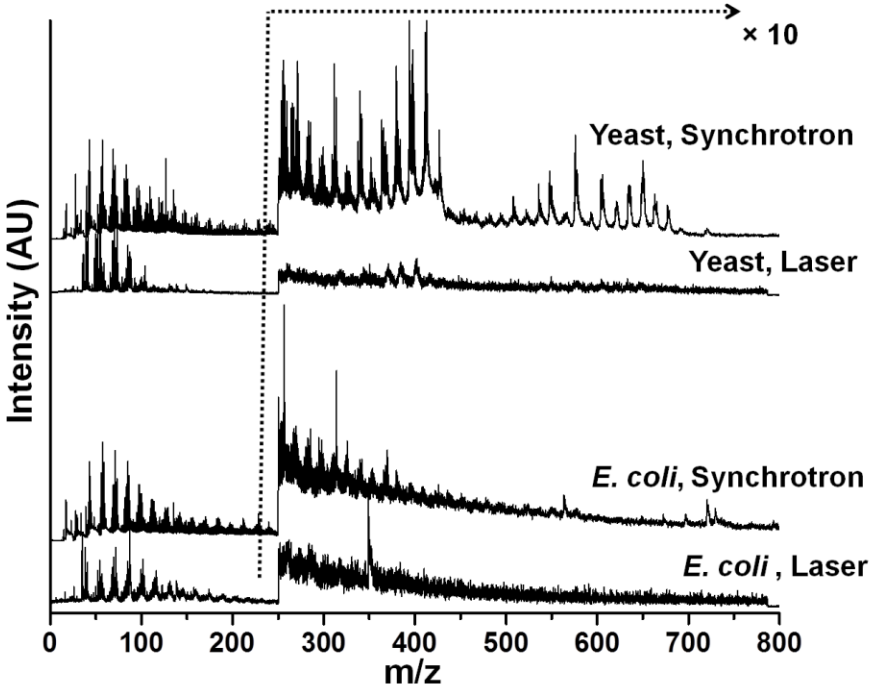

Figure 18 10.5 eV laser and synchrotron LDPI-MS of blotted monoculture biofilms using two different instruments. *E. coli* (tomato strain) and yeast biofilms. Each spectrum in the figure is normalized.

4.3.3 Analysis of Biofilms: Intact on Membrane vs. Blotted Samples

It is technically convenient to grow biofilms on polymer membranes, but these insulating membranes can complicate analysis by MS imaging strategies. Membrane biofilm analyses were attempted on the synchrotron LDPI-MS instrument, but reproducible MS signal was elusive due to what appeared to be excessive sample charging of these electrically insulating membranes. However, intact membrane biofilms could be analyzed directly in vacuum by laser LDPI-MS, as discussed below.

Figure 19 shows 10.5 eV laser LDPI mass spectra of blotted and intact biofilm samples from yeast monocultures. There was ~8 fold higher S/N for the intact membrane samples compared to the blotted biofilms. Although the same peaks were observed for both samples, overall peak intensity was higher for membrane samples. Additionally, peaks at m/z 600 - 700 were not discernible in the blotted sample due to low S/N.

Intact membrane biofilms were not observed to delaminate in vacuum and maintained their structural integrity. However, the blotted biofilms occasionally suffered from delamination in vacuum which adversely impacted the synchrotron LDPI-MS. Ablation signal was not observed in laser LDPI-MS since the pulsed VUV beam passed farther above the sample, missing the delaminated pieces of biofilm. In any case, ablation would occur to a lesser extent by the pulsed VUV laser beam whose duty cycle was 10^{-6} at 7.87 eV and 10^{-7} at 10.5 eV (vs. near unity for the quasi-continuous synchrotron radiation).

Direct comparison was also made for membrane biofilms analyzed with laser LDPI-MS vs. blotted biofilms analyzed with synchrotron LDPI-MS: the different spectra showed similar peaks, albeit with differences in S/N and absolute signal intensity. The synchrotron MS data showed more peaks in the low mass (< m/z 300) region.

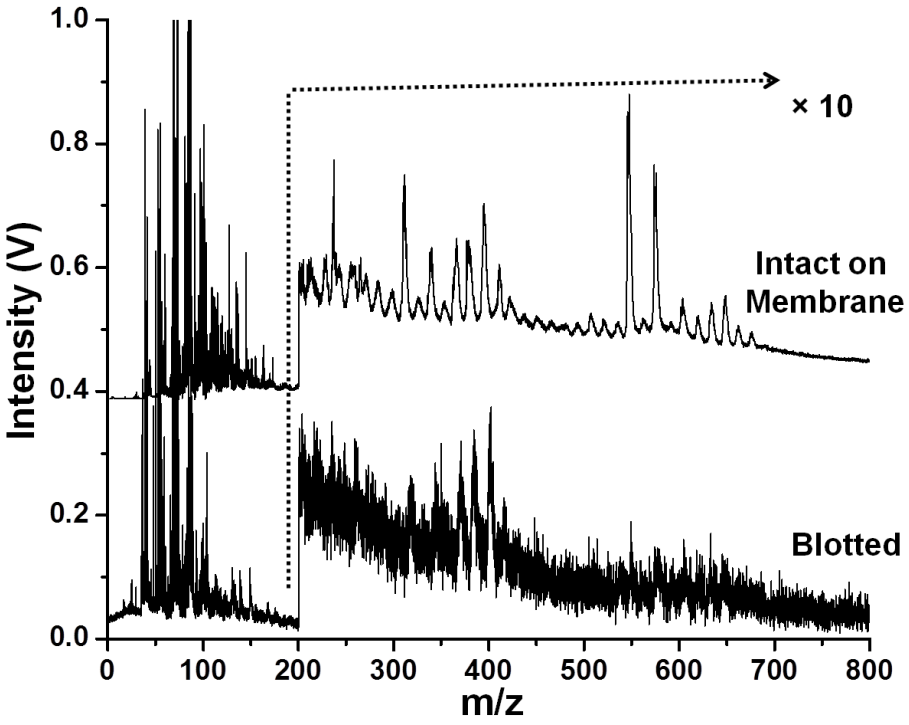

Figure 19 10.5 eV laser LDPI-MS of yeast monoculture biofilms using two different sample preparation techniques. Spectra are normalized.

4.3.4 Synchrotron LDPI-MS of Coculture Biofilm

LDPI-MS for coculture biofilms was performed next, wherein three regions of the coculture biofilm samples were used to collect mass spectra under identical experimental conditions. Figure 20 shows the 10.5 eV synchrotron LDPI-MS for an *E. coli* and *S. cerevisiae* yeast coculture biofilms. The trace labeled mixed in Figure 20 refers to the region where the two species overlap. Mass spectra for the two species in the coculture sample were similar to that of the respective monocultures and the mass spectra for the mixed region showed peaks for both of the participating species. As noted above, the continuous synchrotron radiation readily ablated

delaminating pieces since the VUV beam passed very close to the top of the sample, leading to signal spikes near m/z 270 in the MS.

Similar analysis was carried out using 7.87 eV and 10.5 eV laser LDPI-MS on membrane biofilms as is described in the following section.

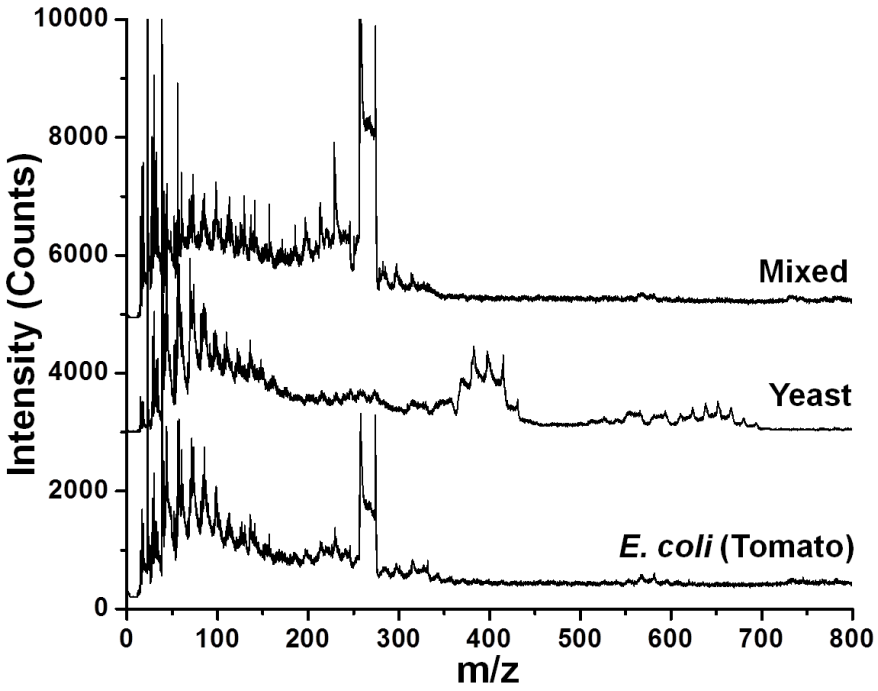

Figure 20 10.5 eV synchrotron LDPI-MS of different regions of a blotted coculture biofilm. The distinct *E. coli* (tomato strain) and yeast regions as well as the "Mixed" overlapping region were examined.

4.3.5 Laser LDPI-MS of Coculture Biofilm

E. coli and yeast monoculture as well as coculture biofilms were studied using both the 7.87 and 10.5 eV laser photoionization sources. Figure 21 and 22 show the 10.5 eV and 7.87 eV laser LDPI-MS of coculture *E. coli* (tomato strain) and yeast multispecies biofilms respectively. As above, LDPI-MS in both cases were recorded at three distinct regions of *E. coli* and yeast coculture biofilms. The "pure" *E. coli* and yeast regions of the biofilms generated spectra that generally appeared similar to those from the corresponding monocultures. The trace labeled "Mixed" in Figure 20 and 21 refer to the region where the two species overlap. The "pure" regions of *E. coli* and yeast could be readily distinguished by visual examination of the intact membrane biofilms. The mass spectra for the mixed region showed peaks from both of the species. Although, there was a slight increase in tomato MS signal intensity in the mixed region which could be attributed to the growth gradient of tomato strain in proximity to yeast. More experiments are required to determine the correlation conclusively and such study is not performed here.

10.5 eV laser LDPI-MS showed more peaks in the high mass region ($m/z > 400$) compared to 7.87 eV data, indicating more molecular species were ionized at the higher photon energy. Overall, thick, intact biofilm samples grown on insulating membranes were successfully analyzed using laser LDPI-MS. Polycarbonate membranes provided a surface for robust growth of coculture biofilms and could produce visually obvious boundaries between different species or strains.

On comparing the two instruments for coculture biofilm analysis it was observed that the spatial localization of the metabolites was more efficiently studied using laser LDPI-MS set up compared to the synchrotron LDPI-MS. This could be due to the larger spot size of the desorption beam at the Advanced Light Source and relatively larger area of analysis which made assigning a region to a specific microbe ambiguous.

Additionally, due to the differences in the ion optics design, laser LDPI-MS allowed for the analysis of biofilms directly from the substrate. In contrast, biofilms needed to be blotted onto a stainless steel plate for synchrotron LDPI-MS analysis, which caused loss of spatial integrity and sometimes sample itself.

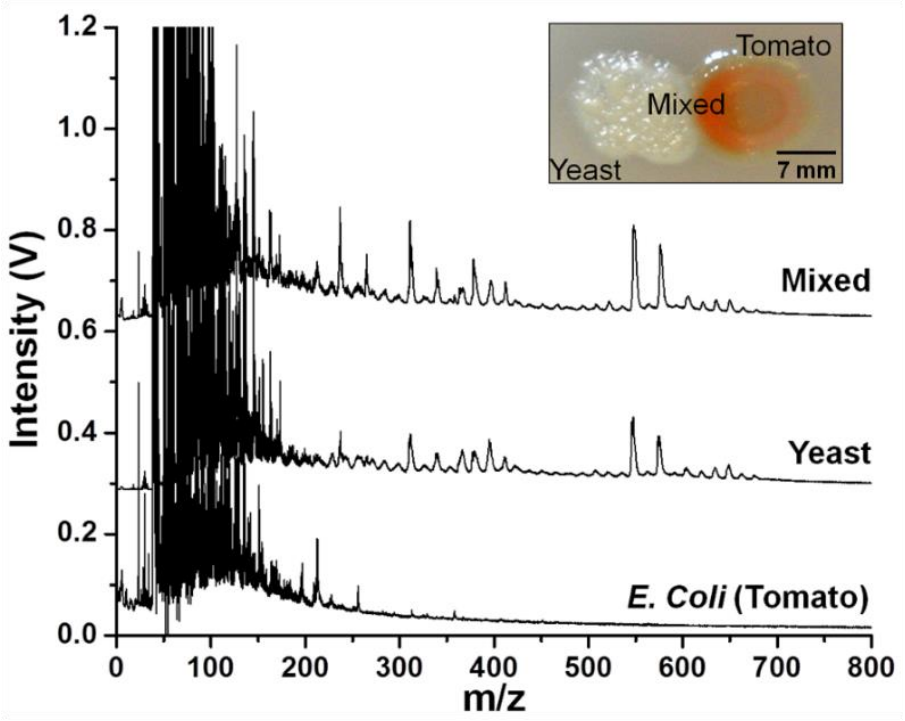

Figure 21 10.5 eV laser LDPI-MS of coculture membrane biofilm consisted of *E. coli* (tomato strain) and yeast. "Mixed" indicates the region of overlap between the two species while other spectra correspond to "pure" regions of biofilms, as labeled in the inset photo of a typical coculture biofilm.

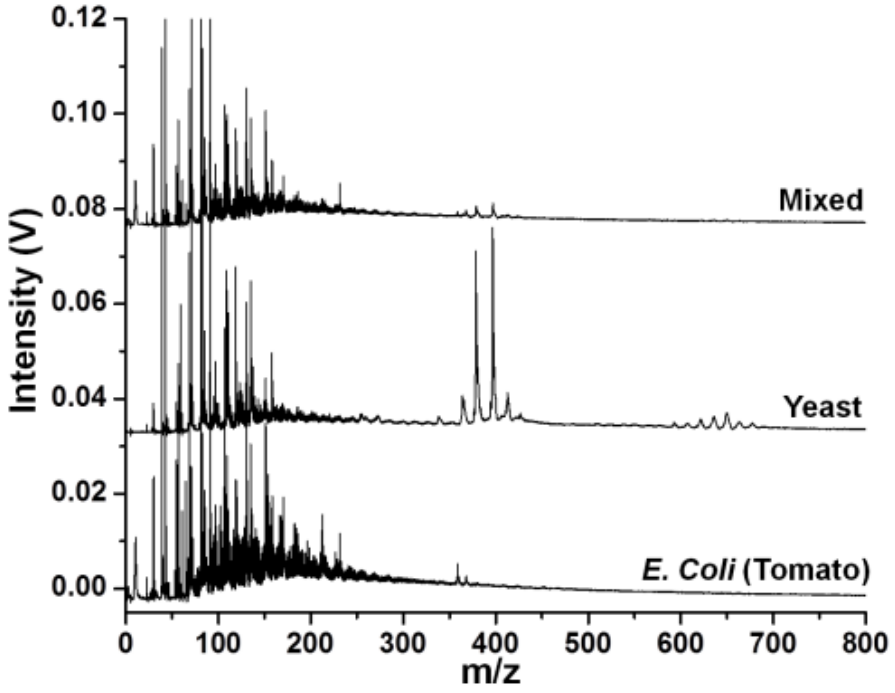

Figure 22 7.87 eV laser LDPI-MS of three regions of *E. coli* (tomato strain) and yeast coculture membrane biofilm, including the "Mixed" overlapping region.

4.4 Conclusion

Both the synchrotron and laser LDPI-MS indicated that different classes of molecules can be targeted with different photon energies. New peaks appeared with increasing photon energy (see table 2) as expected since many organic compounds have ionization energies in the 9 - 10 eV range and single photon ionization requires VUV photon energies in excess of a molecule's ionization energy.[15, 145]

Synchrotron LDPI-MS was able to successfully analyze blots of biofilms, which can also be analyzed by other MS imaging methods,[16] but could not analyze intact membrane biofilms.

Laser LDPI-MS of intact membrane biofilms showed overall higher signal intensity than from blotted samples. This could be due to the difference in desorption efficiency for the two samples. By contrast, blotting of the biofilm resulted in loss of structural integrity and loss of sample that decreased the overall signal intensity. Furthermore, the efficiency of chemical transfer during blotting, including differential transfer, cannot be ruled out as a contributing factor.

5. DIFFERENTIATION OF MICROBIAL SPECIES AND STRAINS IN COCULTURE BIOFILMS BY MULTIVARIATE ANALYSIS OF LASER DESORPTION POSTIONIZATION MASS SPECTRA

[Chhavi Bhardwaj, Yang Cui, Theresa Hofstetter, Suet Liu, Hans C. Bernstein, Ross P. Carlson, Musahid Ahmed & Luke Hanley. Differentiation of Microbial Species and Strains in Coculture Biofilms by Multivariate Analysis of Laser Desorption Postionization Mass Spectra. Analyst (2013) 138 (22), 6844-6851 DOI: 10.1039/C3AN01389H]- Reproduced by permission of The Royal Society of Chemistry. See Appendix A.

5.1 Introduction

Biofilms often exist as consortia of multiple interacting species.[146, 147] Consortial biofilms can exhibit complex interspecies relationships and dependencies that are the subject of many ongoing investigations.[8, 148] Controlling problematic medical or beneficial environmental multispecies biofilms is challenging due to limited knowledge of the critical interactions occurring between the microorganisms organized within micro scale structures. Spatially differentiating strains or species in a mixed culture biofilm can provide useful information, such as localization of available metabolic potential as well as provide insight into the competitive nature of the metabolic interactions.[149, 150]

SIMS and MALDI-MS have been widely used for such analysis of biofilms and other intact biological samples.[16-19, 23] SIMS has the advantage of high spatial resolution. However, molecular information for many species is often lost to fragmentation in SIMS, which readily detects low mass (m/z <500) and atomic ions. MALDI-MS is less chemically destructive than SIMS and is often used to detect molecular ions of species up to several kDa mass. However, MALDI-MS has lower spatial resolution than SIMS and requires extensive sample preparation

such as the addition of matrix, which can obscure species in the low mass range. Both SIMS and MALDI-MS typically require thin, electrically conductive samples. Finally, ion suppression and local fluctuations in ionization efficiency can complicate quantification in these and other methods in MS imaging.[19]

Some of these limitations of SIMS and MALDI-MS for the analysis of biofilms and other biological samples can be overcome using LDPI-MS. As LDPI-MS, which is also referred to as two laser mass spectrometry (L2MS),[96] does not require the addition of a matrix compound to enhance desorption and is not sensitive to ion suppression since it detects desorbed neutrals and shows some advantages for quantification.[151] Furthermore, LDPI-MS can readily analyze thick, electrically insulating samples.[142]

MS analysis of biological systems often result in large data sets which need further analysis to extract useful information about the analyzed system. Multivariate analysis (MVA) can facilitate the processing of large data sets from the chemical analysis of biofilms and other intact biological samples. Principal component analysis (PCA) is the most commonly used and widely reported of the various MVA methods. PCA decomposes data with correlated measurements into a new set of uncorrelated (i.e., orthogonal) variables called principal components.[152] PCA is ideal for interrogating large data sets such as mass spectra,[101, 153, 154] because it reduces variable dimensionality with a minimal loss of information. For these reasons, PCA is often used for classification and/or grouping of experimental results to extract useful information. Several studies have differentiated strains of microorganisms by PCA of secondary ion mass spectra (SIMS)[154, 155] and matrix assisted laser desorption ionization mass spectra (MALDI-MS).[156, 157] MVA techniques were thus applied here to extract information about small molecule metabolites which was buried in the crowded low mass region of the MS.

The present study utilized 7.87 and 10.5 eV VUV photon energy laser sources for LDPI-MS to analyze biofilms comprised of binary cultures of interacting microorganisms. PCA was applied to the MS data to reduce the data dimensionality for better separation of species in *E. coli*-*S. cerevisiae* biofilms and of individual *E. coli* strains in a biofilm comprised of two interacting gene deletion strains: citrine and tomato. Clear spatial separation of both species as well as both *E. coli* strains, based on their distinct metabolic states, was demonstrated by PCA of LDPI-MS of intact biofilms.

5.2 Experimental

5.2.1 MS Instrumentation

Laser LDPI-MS instrument as described in Chapter 2 was used for the study. 7.87 eV and 10.5 eV VUV ionization sources were used to study multi species as well as multi strain coculture biofilms. The details of the two ionization sources, acquisition parameters and processing methods are described in Chapter 2.

5.2.2 Biofilm samples

The study involved two biofilm systems: 1) Eukaryote-prokaryote multi species coculture involving *Escherichia coli* K-12 bacteria and *Saccharomyces cerevisiae* yeast grown together on a substrate. 2) Prokaryote-prokaryote multi strain coculture consisted of *Escherichia coli* K-12 strains: tomato and citrine grown as coculture biofilms. Details of the biofilm growth procedure and sample preparation are described in Chapter 2. Each microbe was grown as individual monoculture biofilm as well. All biofilms used for the study were grown for an identical time

period of 96 hours. Monoculture and coculture biofilms were grown under identical experimental conditions, to eliminate any variation due to different growth phases.

5.2.3 Data acquisition

LDPI-MS analysis of coculture samples was performed on three distinct regions under identical experimental conditions: two spots comprised predominantly of one type of microbe ("pure" region at the outer edges of the coculture sample) and at the center of the sample where the two species visually overlapped ("mixed" region).The laser LDPI-MS utilized a sample stage that was continuously moving at a speed of 0.05 mm/s while the desorption laser scanned over the sample for a total area of analysis of 1 mm^2. Mass spectra were averaged over the entire analyzed area such that ~4×10^4 laser shots were used to collect each displayed laser LDPI mass spectrum.

5.2.4 Data Preprocessing and PCA

A custom program was designed in-house for converting full mass spectra to integer m/z peak values similar to those used for electron impact MS database searching.[25] No peak selections were made. Rather, the entire raw mass spectrum was aligned to integer m/z values, then zeroes were inserted as intensity values for peaks where no ion signal was observed above the assigned signal threshold of ~35 mV. Ion intensities were normalized prior to PCA by setting the most intense peak to unity, thereby minimizing potential fluctuations due to instrumental factors such as modulating detector efficiencies. Finally, ion intensities at each integer m/z 50-700 value for each sample were exported to a spreadsheet. A nonlinear iterative partial least squares algorithm ("princomp" function, MATLAB, The MathWorks Inc., Natick, MA) was used to

perform PCA[133, 158] on the n × p data matrix where n represents the number of experiment trials for each strain and p represents the ion intensities written to the aforementioned spreadsheet for each integer m/z value. PCA was performed after mean centering of the columns of the data matrix. Each data set used in the analysis was replicated at least three times and a minimum of 15 spectra of each microbe type was used to compose the original data matrix.

5.3 Results and Discussion

5.3.1 Multispecies biofilms: *E.coli* and Yeast

LDPI-MS of multispecies biofilms consisting of *E. coli* (tomato) strain and yeast were studied using 10.5 eV and 7.87 eV laser photoionization sources (see Chapter 4 for more multispecies MS analysis). A multispecies system was chosen in order to develop and optimize the MVA algorithm prior to its application to multistrain *E. coli* biofilms wherein the interacting strains citrine and tomato do not show much MS peak differences. Figure 23 shows the 10.5 eV laser LDPI-MS of *E. coli* (tomato strain) and yeast multispecies biofilms. The "pure" regions of *E. coli* and yeast could be readily distinguished by visual examination of the intact membrane biofilms and as expected the mass spectra of the two species showed a significant difference, which was an ideal system to develop the PCA protocol for LDPI-MS study of coculture biofilms.

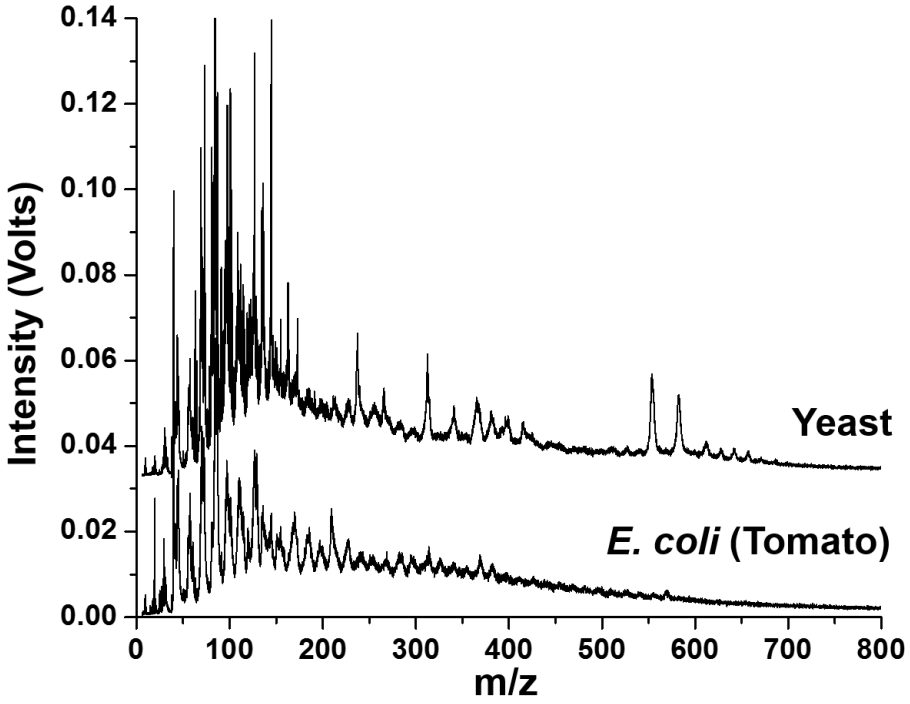

Figure 23 10.5 eV laser LDPI-MS of *E. coli* (tomato strain) and yeast membrane biofilm.

5.3.2 PCA of LDPI-MS for species differentiation

The results above and work presented in Chapter 3 demonstrated the capability of LDPI-MS to study monoculture biofilms as well as multispecies/multistrain coculture biofilms in their intact form directly on an insulating substrate. The mass spectral data however, did not show much difference between the analyzed microbes especially in case of *E. coli* strain coculture biofilms (See Figure 10 & 11 in Chapter 3). Additionally, the low mass region (m/z < 250) which is of great interest for metabolite study was too crowded to visually observe any obvious differences among strains. PCA was therefore used as a statistical tool to reduce the data size without significant information loss and for better visualization of the data. The approach was optimized by first

applying PCA to the clearly distinct MS data of *E. coli* and yeast in a coculture biofilm sample. Figure 24 shows a plot for principle component 1 vs principle component 2 obtained by applying PCA to 10.5 eV MS data of *E. coli*-yeast multispecies coculture biofilms (as shown is Figure 23). Given that these two microbes showed obvious mass spectral differences for the "pure" regions of each species, it is not surprising that applying PCA to the data also readily distinguished the two species.

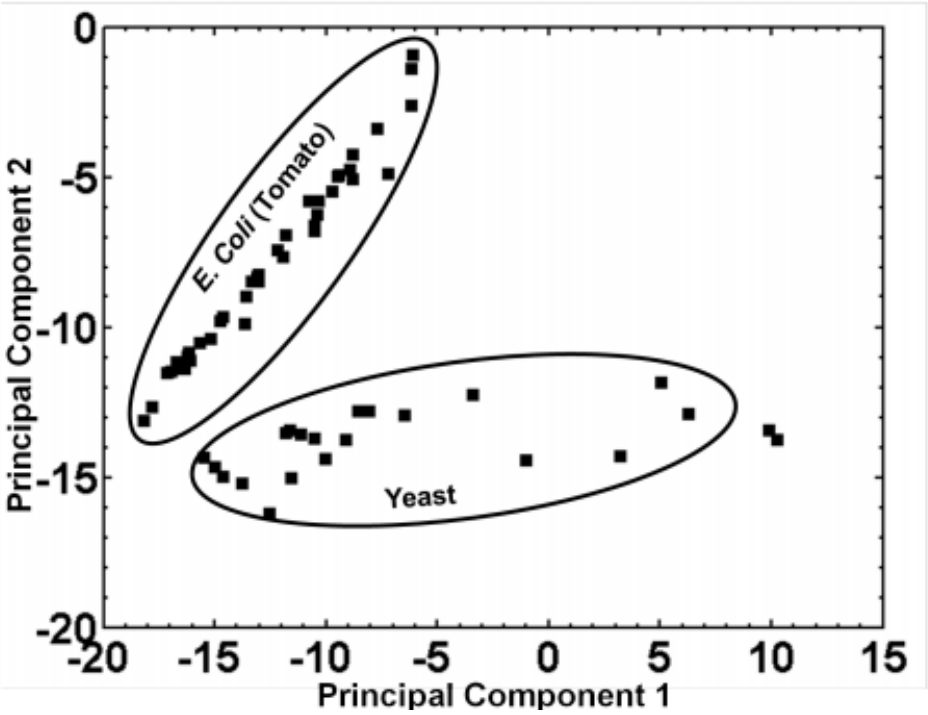

Figure 24 Principal component analysis of 10.5 eV laser LDPI-MS of *E. coli* (tomato strain) and yeast coculture biofilm (m/z 50 to 700). Compared the regions of each biofilm that were far from the mixed region that defines the boundary between the two (referred to as "pure" in text).

The optimized PCA protocol was then applied to a more challenging system wherein a multistrain *E. coli* biofilm was examined. Both 7.87 eV and 10.5 eV laser LDPI-MS data of the genetically similar *E. coli* tomato and citrine coculture biofilms were collected as shown in Figure 11 and 12 in Chapter 3.

5.3.3 PCA of LDPI-MS for Strain Differentiation

Figures 25 shows a plot of principal component 1 vs. principal component 2 for the 7.87 eV laser LDPI-MS data. While the mass spectra of the two strains in coculture samples showed only minor visual differences in the peak pattern (Figure 12), PCA treatment of the "pure" regions of the sample resulted in grouping the two strains separately. Furthermore, the mixed region was clearly distinguished from the two "pure" regions suggesting metabolic interactions resulted in altered physiologies. Figure 25b is a scree plot[152] which shows the variance of the entire data set with respect to the principal components. The scree plot indicates that ~75% of the variance for the data is represented by its first two principal components. In addition, hierarchical cluster analysis (HCA) was performed to the aforementioned 7.87 eV mass spectral data. Figure 26 shows the HCA result for 7.87 eV data. The y-axis in the figure shows the distance between the data sets for each strain and x-axis list the MS trials for each strain. In general, higher distance between trials indicates less correlated data. As shown in Figure 26, the distance on y-axis is lower for MS trials within a strain compared to the distance for trials between different strains. Consequently, trials for a strain are clustered together and away from the cluster for the other strain. Moreover, the data points for the "mixed" region are clustered outside of the two "pure" strain regions, which corresponds to the clustering of the strains obtained by PCA.

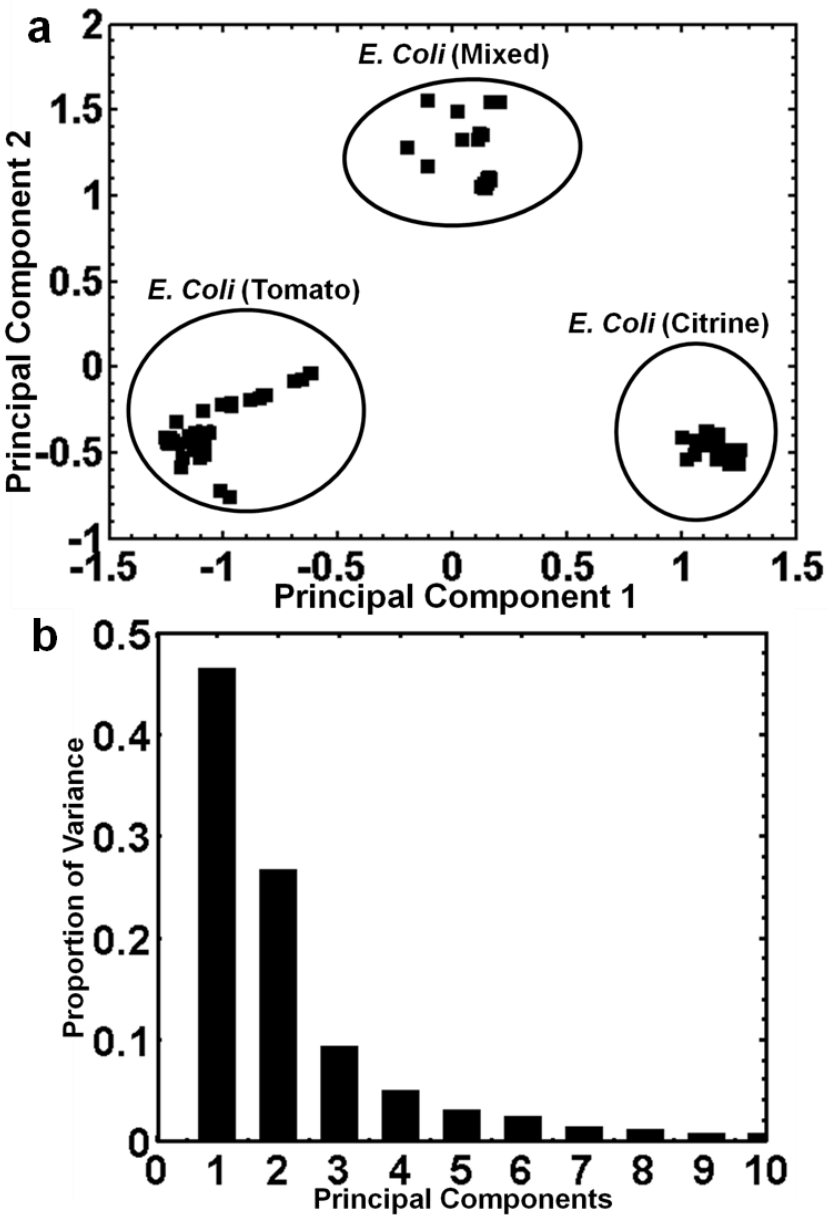

Figure 25 a) Principal component analysis of 7.87 eV laser LDPI-MS of the three different regions of a coculture *E. coli* (tomato and citrine strains) membrane biofilm (m/z 50 to 700). b) Scree plot showing variance of the entire data set with respect to the principal components.

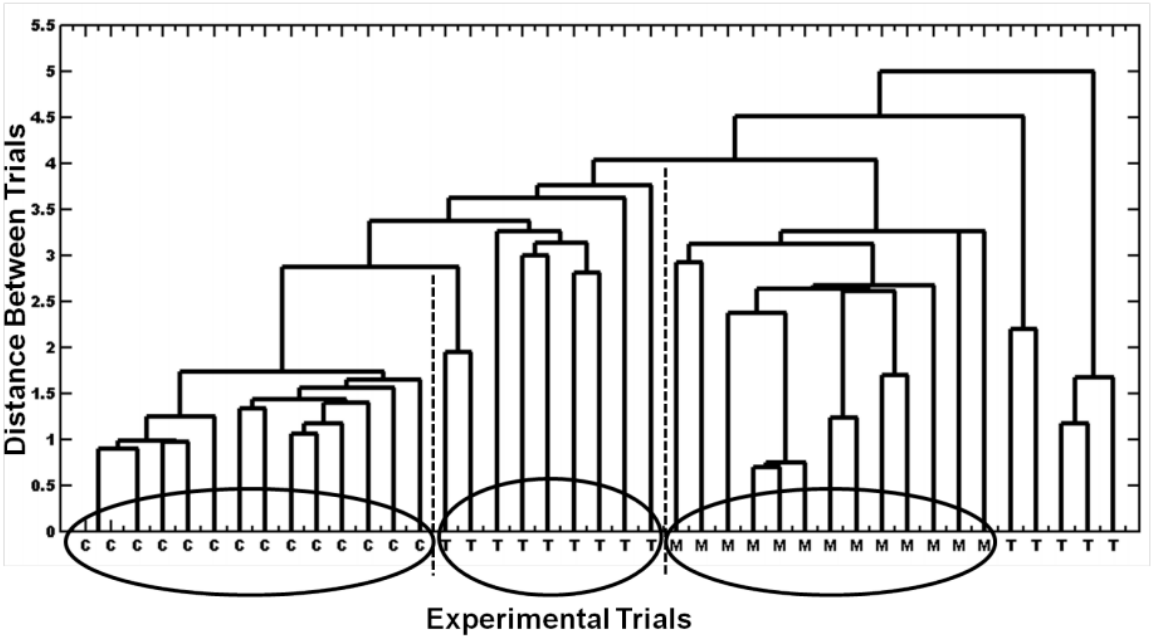

Figure 26 Hierarchical cluster analysis for 7.87 eV LDPI-MS data. The figure shows clustering of mixed region outside of the two pure strains. The y-axis shows the distance between the connected data sets and x-axis list the MS trials for each strain. In general, higher distance between trials indicates less correlated data.

Similarly, PCA was performed on the corresponding 10.5 eV MS data. Figure 27 shows the principal component 1 vs principle component 2 for the 10.5 eV LDPI-MS data of *E. coli* coculture biofilm. 10.5 eV analysis also distinguished the two "pure" regions of the biofilm, albeit with most variance along the first principal component as shown in the scree plot in Figure 27b. PCA for the mixed region of the coculture did not provide consistent reproducible result and is not included here. One probable reason for such an observation is that 10.5 eV photon energy is sufficiently high to ionize a wide range of compounds thereby making the data much more

convoluted. A more sophisticated statistical analysis method may be applied, however no such attempt is made here.

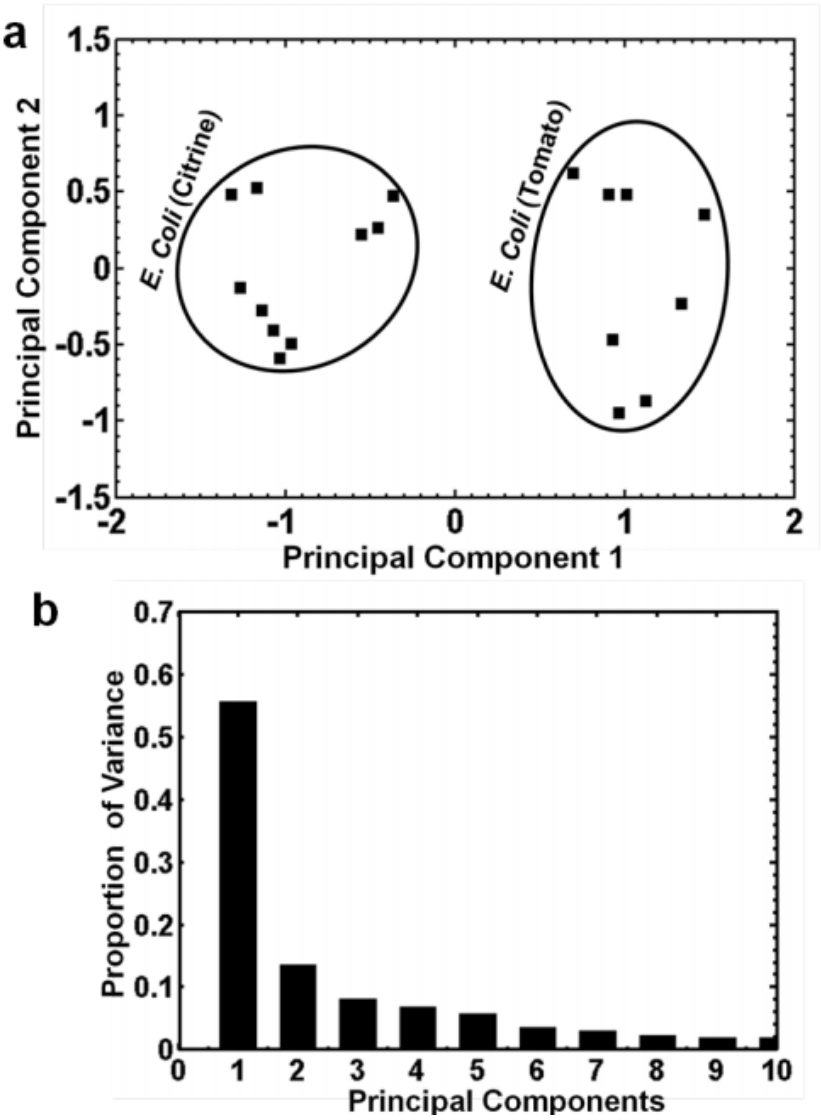

Figure 27 a) Principal component analysis of 10.5 eV laser LDPI-MS of a coculture tomato and citrine *E. coli* membrane biofilm (m/z 50 to 700). b) Scree plot showing the variance of the data with respect to the principal components.

5.3.4 Correlation of MS peaks to strain separation

Figure 28 is the principal component 2 loadings plot, correlating which peaks in the mass spectra are most responsible for the differences seen by PCA between the mixed region and the two "pure" regions of the 7.87 eV laser LDPI-MS. In general, peaks with positive loadings along a given PC axis will show a higher relative intensity in samples with positive scores along the same PC axis (and negative loadings are similarly correlated with negative scores).[154] Figure 25a shows that the *E. coli* mixed region has a positive score while the two pure regions have negative scores along principal component 2. Therefore, positive peaks in Figure 28 loadings plot for PC 2 correspond with the peaks that are more abundant in the mixed region (Figure 25a). Figure 28 indicates that the mass spectral peaks that contributed the most to the separation of the mixed region from the two pure regions were m/z 54, 55, 59, 60, 67, 79, 84, 89, 105, 128 and 133. Similar analysis of the 7.87 eV data for the two pure regions indicated that peaks at m/z 55, 56, 67, 71, 78, 80, 88, 90, 104, 106, 127 and 129 contributed to the separation of the two strains along the first principal component.

Similar plot was drawn for PCA of 10.5 eV laser LDPI-MS data. Figure 29 shows the loading plot along principle component 1 for 10.5 eV data. The result indicated that peaks at m/z 53, 65, 75, 77, 79, 81, 92, 94, 108, 216, 258 and 285 contributed to the separation of the two strains. However, it cannot be determined in these experiments which of these peaks are due to precursor vs. fragment ions.

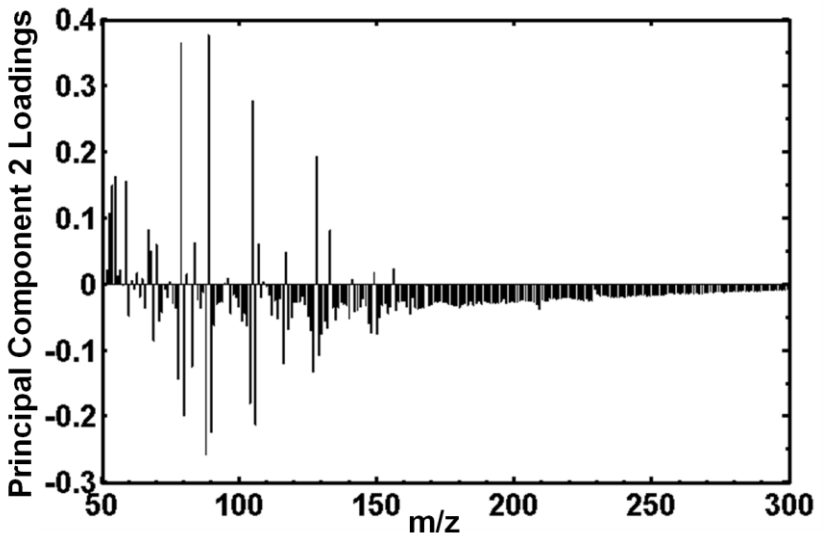

Figure 28 Principal component 2 loadings plot for the 7.87 eV laser LDPI-MS data set of the coculture *E. coli* biofilm analyzed in Figure 25.

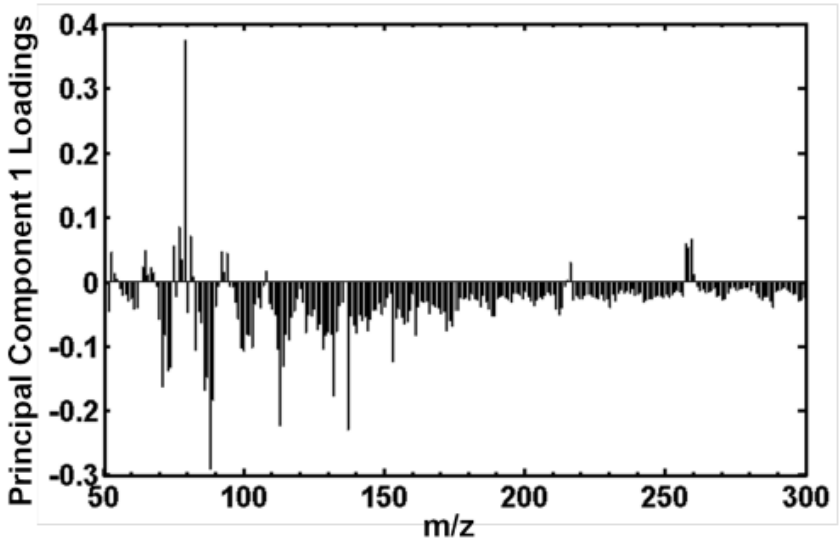

Figure 29 Principle component 1 loadings plot from 10.5 eV laser LDPI-MS data for coculture *E. coli* biofilm analyzed in Figure 27.

5.3.5 Correlation of MS peaks to endogenous species

The principal component loadings plot for the 7.87 eV and 10.5 eV laser LDPI-MS data (Figure 28 & 29) revealed several mass spectral peaks that contributed the most to the separation of the strains. Exact mass measurements and or tandem MS are required to conclusively assign peaks to any compound, so such assignments are generally not attempted here. Nevertheless, hypotheses are made regarding a few of the peaks contributing to the separation of the strains. For example, in case of the principle component 2 loadings plot for 7.87 eV data the m/z 60 peak showed a higher relative intensity in the mixed region (Figure 25 & 28) and contributed to the separation of the mixed region from the "pure" regions. This peak might have arisen from the molecular ion of acetate which is a common *E. coli* metabolic byproduct of glucose metabolism which can be cross-fed to the tomato scavenger strain as a substrate.[7] Similarly, the principal component 1 loadings plot of the 10.5 eV laser LDPI-MS showed that m/z 285 contributed to the difference between the two *E. coli* strains. M/z 285 could be attributed to the stearic acid precursor ion, which is a common constituent of the *E. coli* cell walls and membranes.[142] It is proposed that the two strains' metabolisms create locally different chemical microenvironments that influence biofilm composition.

5.4 Conclusion

Different species as well as separate strains and interfacial regions of coculture biofilms were distinguished by LDPI-MS detection of endogenous species followed by discrimination of the data by PCA. Additionally, hierarchical cluster analysis of the data showed that the strains and metabolic states of coculture biofilms clustered separately, with the results corresponding with those for PCA. This is especially remarkable for the multistrain system because the strains differed

from the wild type K-12 strain by no more than four gene deletions each out of approximately 2000 genes[7] and visual examination of the mass spectral data showed barely any differences.[142]

PCA treatment of 7.87 eV LDPI-MS data separated the strains into three distinct groups (see Figure 25): two "pure" groups and a mixed region. Furthermore, the "pure" regions of the cocultures showed greater variance by PCA when analyzed by 7.87 eV photon energies than by 10.5 eV radiation. It is noteworthy that the *E. coli* mixed region (Figure 25a) had a positive score along principal component 2 which resulted in a grouping outside of the pure tomato and citrine regions.

These results indicate that the mixed region of the multistrain system constituted a different collective metabolic profile than a simple summation of the pure metabolisms, possibly due to inter-strain interactions via metabolite or quorum sensing-like exchange. Use of multiple trials supports the claim of a distinct metabolic state in the mixed region that is not due to contaminants or other matrix effects. In particular, salt gradients are not expected within the multistrain biofilms. Furthermore, salt effects are minimized by the detection of desorbed neutrals in LDPI-MS. LDPI-MS was also able to distinguish the bacteria from the yeast studied here both without and with the application of PCA, both significant accomplishments. These results establish LDPI-MS as another MS tool available to probe local metabolic states and metabolite exchange in microbial systems.[149]

Comparison of the 7.87 and 10.5 eV data is consistent with the expectation that the lower photon energy selects a subset of low ionization energy analytes while 10.5 eV is more inclusive, detecting across a wider range of analytes. These two VUV photon energies therefore give different spreads via PCA and they constitute an additional experimental parameter to differentiate

strains and species. Many metabolites which participate in crossfeeding or quorum sensing between interacting strains and species have relatively low molecular weights, so their molecular ions will be found in the low mass region. The lower mass region is of particular note in the 7.87 eV LDPI-MS of the *E. coli* cocultures.

PCA was also applied to the synchrotron LDPI-MS data, but no coherent results could be obtained from the analysis. One limitation of the synchrotron LDPI-MS data analysis was simply that too few spectra had been collected for a useful data matrix, a problem that could be overcome by further experiments.

6. SECONDARY ION MASS SPECTROMETRIC STUDY OF COCULTURE BIOFILMS

6.1 Introduction

Secondary ion mass spectrometry (SIMS) is a highly sensitive surface analysis technique which is capable detecting both organic and inorganic compounds at submicron resolution. As is briefly described in Chapter 1: SIMS ionization occurs when a sample surface is bombarded with a focused beam of high energy primary ions resulting in sputtering of the sample surface which in turn results in secondary ions or analyte ions. [19] SIMS can be obtained at both positive and negative modes resulting in analyte cations and anions respectively. The ionization is a highly energetic process and often leads to extensive fragmentation of the precursor ions. Traditionally, dynamic SIMS limits the mass range for detectable ions to about m/z 500. However, with the development of novel cluster ion sources the detection mass limit may be stretched up to m/z>1500. SIMS is often coupled to a time of flight mass analyzer (ToF-SIMS) and is often used for the analysis of solid samples and elemental analysis at trace levels. ToF-SIMS has also been successfully applied for biomolecular/natural product analysis.[17, 111, 112]

SIMS is capable of the highest spatial resolution, possible with any current MS technique but it also causes fragmentation at these resolutions. As the primary ion beams can be focused to less than 0.05 μm, SIMS is capable of subcellular resolution.[111] This distinct advantage of high spatial resolution and high sensitivity in the low mass region makes SIMS useful for studying metabolites and other small endogenous species in biological samples such as biofilms. The present study describes SIMS analysis of coculture biofilms in both positive and negative ion

modes. MS data for the two strains and the "mixed" region (region where the two strains overlap) were acquired under identical experimental conditions.

SIMS analysis is often limited by the requirement of flat samples on highly conductive substrates. The present study demonstrates successful SIMS application to relatively thick biofilm samples which were intact on insulating polycarbonate membrane substrate. Biofilms grown on these membranes were ~ 0.5-1 mm thick and had topographic features that could hinder analysis with some of the other more popular MS techniques. However, these biofilm samples intact on insulating membranes were successfully analyzed using SIMS. Consequently, the samples did not require much pretreatment and could be studied in native form however, they needed to be vacuum compatible (in this case dry).

6.2 Experimental

6.2.1 MS Instrumentation

SIMS instrument (TOF.SIMS 5, ION-TOF Inc., Munster, Germany) at the Advanced light Source (Lawrence Berkeley National Laboratory, Berkeley, CA) with 25 keV Bi_3^+ primary ions was used of the study presented here. The details of the instruments have been reported previously.[29, 124] SIMS analysis was performed in both positive and negative ion modes. Each dataset presented here was reproduced using at least two sample replicates. Each spectrum is an average of 100 scans.

6.2.2 Biofilm samples

Coculture biofilms consisted of *Escherichia coli* K-12 strains: tomato and citrine were used for the study. See Chapter 2 for details of the biofilm growth procedure and sample preparation.

SIMS analysis was carried out on biofilms which were intact on polycarbonate membrane substrate. As described in Chapter 2, the membranes were adhered to a stainless steel sample plate with double sided copper tape and were dried under vacuum before analysis.

6.3 Results and discussion

6.3.1 SIMS analysis in positive ion mode

Similar to LDPI-MS study, SIMS data was also collected on three regions of the coculture biofilm: the two regions at the outer edges of the coculture sample which consisted predominantly of one type of microbe ("pure" region) and the center of the sample where the two species overlap ("mixed" region). Figure 30 shows the SIMS spectra obtained for an *E. coli* coculture biofilm. The three traces in the figure show the three regions on the sample: tomato and citrine "pure" strain regions and "mixed" represents the region of overlap of the two strains. The mass intensities for region m/z 250- 1000 has been magnified 100 times to allow for a better visual examination of the mass spectral differences in the spectrum for each region. Moreover, in order to highlight the MS peak differences in the low mass region (m/z < 240 in Figure 30) a separate spectrum showing the mass region m/z 20-240 for the *E. coli* coculture biofilm was plotted in Figure 31.

Figure 30 and 31 show that unlike the LDPI-MS data where mass spectral peak differences were not significant and in most cases the strains differed only in signal intensity, SIMS analysis showed obvious peak differences between strains. For examples, peaks with an asterix "*" on them represent peaks which were unique to either tomato or citrine strain and were not observed in the other strain. Overall, tomato strain showed fewer peaks than citrine in the positive SIMS analysis. Moreover, mixed region showed similar mass spectrum as citrine albeit with varying signal intensity.

Some of the peaks which were present only in citrine region of the coculture were observed at m/z 63.9, 79.2, 85.9, 97.3, 104.3, 108.6, 132.4, 156.3, 186.2, 201.9, 254.9, 269.2, 283.5, 343.4, 414.8, 430.1, 491.4, 533.9, 660.4, 675.7, 719.8, 747.1, 760.6 and 804.9. By contrast fewer peaks were observed in tomato region only and these peaks were at m/z 56.3, 59.3, 60.3, 70.4 and 84.1. It is noteworthy that some of the peaks listed above have been identified to contribute in the separation of the three region of an *E.coli* tomato-citrine coculture biofilm using LDPI-MS followed by PCA. For example peaks at m/z 56.3, 59.3, 60.3, 79.2 and 104.3 contributed to separation of citrine, tomato or the mixed region in PCA treatment of LDPI-MS data (Chapter 5).

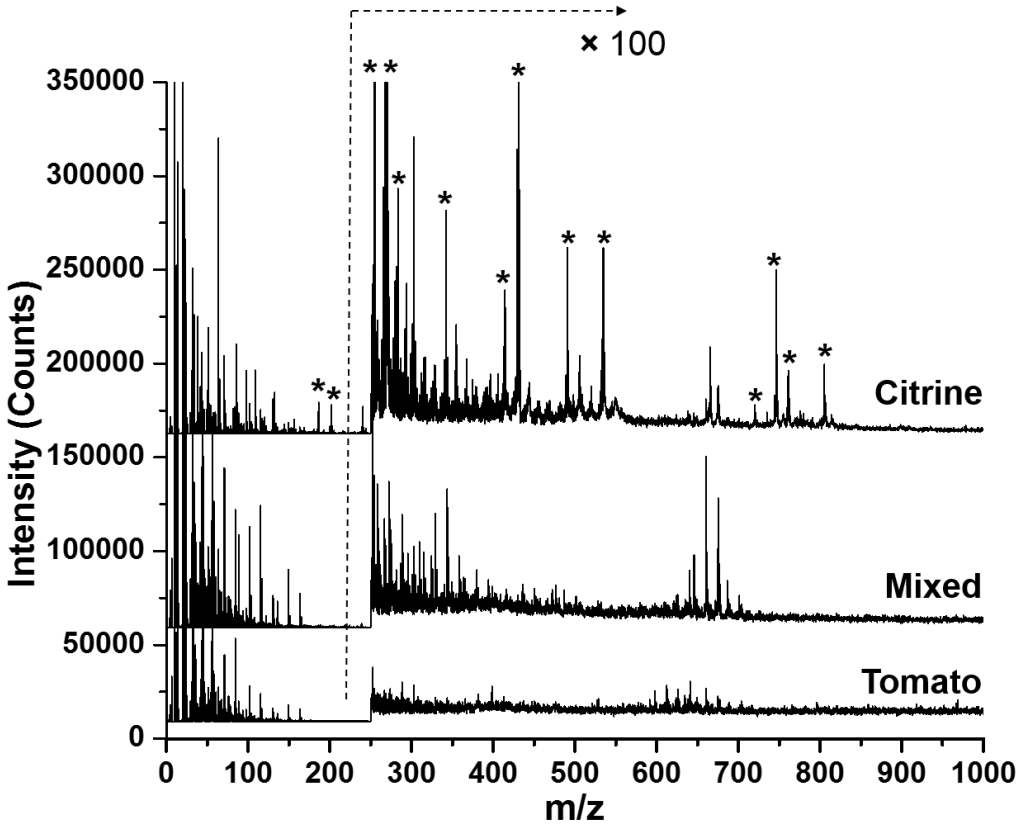

Figure 30 Secondary ion mass spectrometry data in the positive mode for three regions of *E. coli* (citrine and tomato) coculture membrane biofilm. Including the "Mixed" overlapping region. The asterix "*" show peaks which are observed in only one strain.

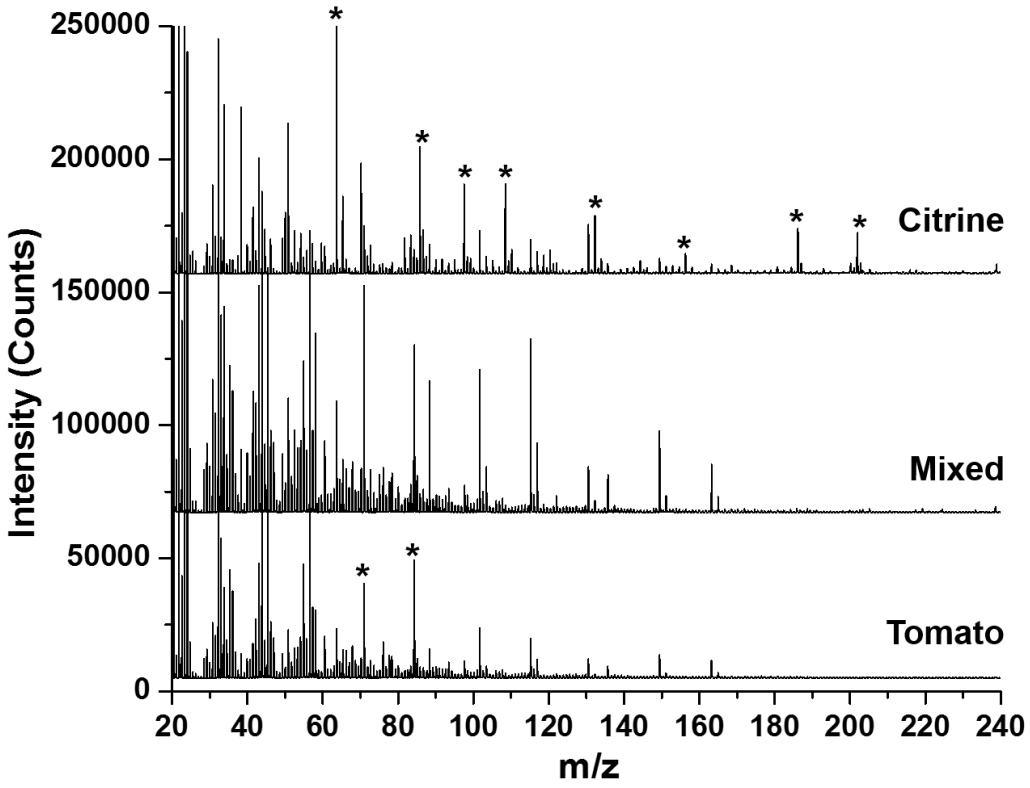

Figure 31 Positive ion mode secondary ion mass spectrometry data of three regions of *E. coli* (citrine and tomato) coculture membrane biofilm highlighting the low mass region. The asterix "*" show peaks which are observed only in one strain.

6.3.2 SIMS analysis in negative ion mode

Figure 32 shows the SIMS spectra for an *E. coli* coculture biofilm in the negative ion mode. The mass region m/z 300- 1000 for all three spectrum were multiplied by a factor of 100 for examining the mass spectral peaks. Similar to the positive SIMS data, the low mass region (m/z < 240 in Figure 32) was plotted as a separate spectra in Figure 33 showing the mass region m/z 20-240. Again, SIMS analysis in the negative mode showed obvious peak differences between strains. Peaks marked with "*" in Figure 32 and 33 represent peaks which were unique to a strain. Unlike

the positive SIMS, for the negative mode, tomato strain showed more peaks than citrine overall. Moreover, the mixed region showed mass spectrum similar to that of tomato.

Mass spectral peaks at m/z 42.5, 50.5, 80.7, 114.2, 215.1, 328.4, 344.6, 461.7, 478.5, 579.2, 591.6, 659.1, 672.4, 693.9 710.5 and 725.3 were some of the peaks which were uniquely observed only in tomato strain of the coculture biofilms and were not present in citrine or in the mixed region. In contrast, peaks at m/z 538.8 and 552.8 were observed only for citrine and mixed region and were not present in tomato.

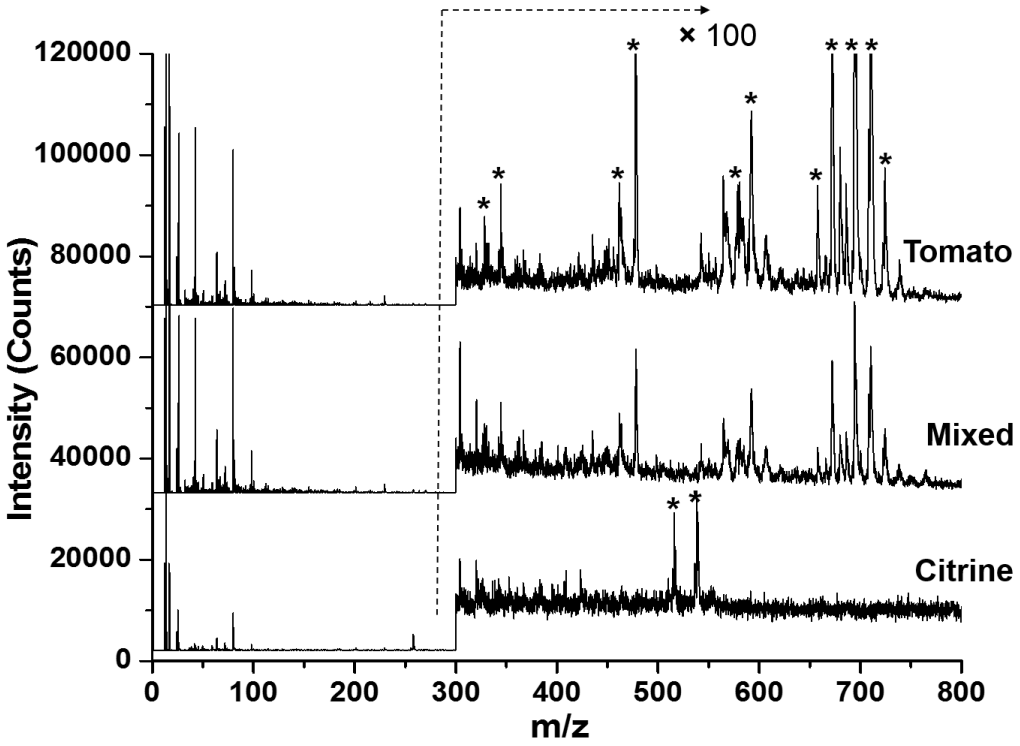

Figure 32 Secondary ion mass spectrometry data in negative mode for three regions of *E. coli* (citrine and tomato) coculture membrane biofilm. Including the "Mixed" overlapping region. The asterix "*" show peaks which are unique to a strain.

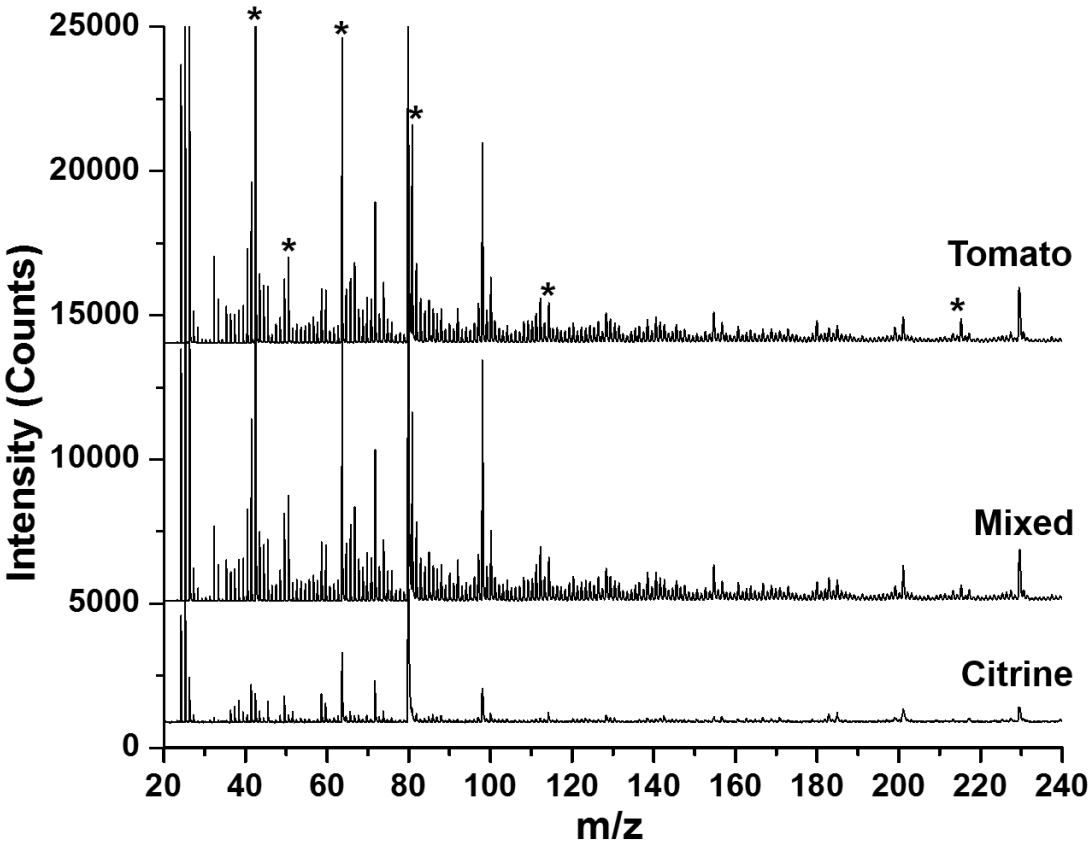

Figure 33 Negative ion mode secondary ion mass spectrometry data of three regions of *E. coli* (citrine and tomato) coculture membrane biofilm highlighting the low mass region. The asterix "*" show peaks which are unique to a strain.

6.4 Conclusion

SIMS analysis often requires thin uniformly flat samples on a highly conductive surfaces, which may limit the analysis of many biological samples in their native form. The work presented here demonstrated that biofilm samples in intact form could be studied with minimal sample preparation. Moreover, the samples were intact on their insulating polycarbonate membrane substrate.

SIMS data for two closely related *E. coli* strains: citrine and tomato showed significant spectral differences both in the positive, as well as negative ion modes. Some of these peaks corresponded with the results found from the PCA study of the LDPI-MS data.

It is noteworthy that for the LDPI-MS study, the two strains did not show much difference in the MS peaks for the three regions and an additional analysis technique i.e.; PCA was utilized to determine peaks contributing to the separation of the strain. On the contrary, SIMS analysis showed unique peaks to each strain and therefore provided an additional dimension of analysis for multi member biofilm system.

However, like LDPI-MS, peaks from the SIMS analysis could not be assigned to any metabolites or other endogenous species because SIMS being a highly energetic desorption/ionization technique causes a multitude of compounds to ablate and ionize. Therefore accurate peak assignments cannot be made without performing additional experiments such as control experiments involving neat compounds, extraction of target analyte followed by SIMS analysis for direct comparison etc. Such experiments were beyond the scope of the work presented here.

In conclusion, it is fair to state that both LDPI-MS and SIMS due to their different desorption/ionization mechanisms provided complementary chemical information for the biofilm systems.

7. CONCLUSIONS

The heterogeneity and spatial localization of microbial structure and interaction within a biofilm makes its comprehensive study a challenge. An attempt was made in this thesis to understand such interactions and syntrophic dependencies of microbial members in biofilms using LDPI-MS. The biofilms used for the study were synthetically engineered models which were ideal for developing MS imaging techniques and for demonstrating spatial portioning of microbes based on small molecule metabolite analysis.

The work presented in this thesis showed 7.87 eV and 10.5 eV LDPI-MS analysis of endogenous species and metabolites in intact biofilms. It also demonstrated that 7.87 and 10.5 eV LDPI-MS possess several advantages for small molecule imaging compared to other MS methods such as MALDI-MS. [16, 23] For example, the ability to collect spectra without addition of desorption-enhancing matrix avoids signal fluctuation due to ion suppression, matrix inhomogeneity, and other quantification-inhibiting effects. Additionally, the single photon ionization mechanism of LDPI-MS is complementary to the protonation that dominates MALDI and LAESI. This complementary ionization indicates the three methods are likely to sample different molecular fractions from intact biological samples.

Although, the LDPI-MS data was acquired under optimized experimental conditions, the effect of varying the delay time between desorption and ionization processes was not explored in this study. However, prior work had showed that sensitivity and resolution can be optimized in LDPI-MS at different mass ranges by varying delay times and other ion optical parameters, with more high mass peaks detected at longer delay times.

The MS data was acquired using two different LDPI-MS instruments: synchrotron and laser LDPI-MS respectively. The synchrotron setup allowed for exploring the effect of increasing photon energies on mass spectral profiles. One the other hand, laser LDPI-MS allowed for in house data analysis and optimization as well as examination of electrically insulating samples such as membrane biofilms. The synchrotron LDPI-MS showed overall higher signal intensity and with appropriate sample preparation should allow for high resolution imaging of biological systems. However, the 7.87 eV fluorine laser and the 10.5 eV laser-based sources are both sufficiently robust that either could be implemented on commercial instrumentation such as vacuum source-based MALDI-MS instruments, converting them into LDPI-MS instruments.

PCA analysis of LDPI-MS data from coculture biofilms resulted in differentiation of individual *E. coli* strains as well the region of "mixed" growth. This was significant, as these strains differed from the wild type K-12 strain by no more than four gene deletions, each out of approximately 2000 genes (Chapter 5). Moreover, the two photon energies gave different spreads via PCA and their respective use in LDPI-MS constitute an additional experimental parameter to differentiate strains and species.

SIMS studies showed distinct mass spectral peaks for the two *E. coli* strains (Chapter 6). Some of these peaks corresponded with the results obtained by LDPI-MS and PCA study. Thereby indicating that SIMS could provide complementary chemical information to the LDPI-MS analysis.

There are several limitations associated with the MS study of biofilms presented in this thesis. For instance, lack of tandem mass capabilities of the LDPI-MS instrument prevented the identification of endogenous compounds. Additionally, the low mass and spatial resolution achieved by the instrument limited the analysis to qualitative exploration of biofilms.

Quantitative analysis of endogenous species may not be readily conceivable as it requires that the instrument to have tandem mass capability and have higher resolution which could be achieved partially by focusing the desorption laser to a smaller spot. Nonetheless, recently the feasibility of quantification capabilities with LDPI-MS has been reported.[151]

Quantitative analysis, albeit of environmental samples was explored in a separate MS work which was performed during a research participation program at a federal laboratory. The work involved study of environmental matrices such as river water effluents and influents, soil, sludge and biosolids for the quantification of persistent harmful contaminants using liquid chromatography mass spectrometry (LC-MS/MS). The analysis was performed on commercial instruments and required extensive sample pretreatment. The choice of extraction and clean-up procedures was governed by the target analyte and the matrix being analyzed. Analytes from water samples were extracted using solid phase extraction whereas for solid matrices such as biosolids, solvent extraction under elevated temperatures and pressures was required. The extracts were then analyzed by LC-MS/MS. Due to the tandem mass capabilities of the instrument, the target compounds were identified by comparing the selected sample precursor/fragment transition to the known standard precursor/fragment transition. Quantification was obtained using the transitions of the target compounds utilizing external calibration.

Similar procedure may be utilized for the quantitative study of biological samples such as biofilms. As mentioned above, LC-MS/MS quantitative analysis of endogenous compounds will require sample purification and extraction steps to concentrate the target analyte and to remove interference from complex biological matrices. The cleanup steps will however, result in the loss of valuable spatial information of intact systems and may not be an ideal choice for studying biofilms.

Commercial LC-MS/MS is ideal for high throughput, trace analysis of compounds where the matrix containing the compound is of limited significance. For biofilm samples where matrix often plays an important role imaging MS techniques such as MALDI-MS, SIMS and LDPI-MS with tandem mass capabilities will be more advantageous.

Overall, a variety of potential applications are foreseen with the LDPI-MS instrument beyond metabolite analysis within intact biofilms. The detection of antibiotics and possible cell wall degradation products within intact biofilms by ≤10.5 eV LDPI-MS [122] indicates the additional potential for pharmacological studies in animal tissue. 10.5 eV LDPI-MS has been used to detect cholesterol and other small molecules within intact animal tissue, complementing peptide analysis by MALDI-MS.[92] Lignin monomers and other important biomass components should be detectable by LDPI-MS since they have been measured using ion sputtered rather than laser desorption.[141, 145]

In the end, to paraphrase a recent comparison of MS methods for crude oil analysis, "*there is no single method or ionization technique that allows for the accurate characterization of all the components present*"[44] in a biological sample, either in its intact form or following extensive sample pretreatment. The overlapping capabilities of different MS techniques indicate that many MS methods can often be used to detect the same species, albeit with significant operational differences. Moreover, different MS analysis often results in complementary information which is essential for complete understanding of a system.

CITED LITERATURE

1. Costerton, J.W., P.S. Stewart, and E.P. Greenberg, *Bacterial biofilms: a common cause of persistent infections.* Science, 1999. **284**: p. 1318-1322.

2. Ghannoum, M. and G.A. O'Toole, eds. *Microbial Biofilms*. 2004, ASM Press: Washington, D.C.

3. Lopez, D., H. Vlamakis, and R. Kolter, *Biofilms.* Cold Spring Harbor Perspectives in Biology, 2010. **2**: p. a000398.

4. Hatt, J.K. and P.N. Rather, *Role of Bacterial Biofilms in Urinary Tract Infections.* Current Topics in Microbiology and Immunology, 2008. **322**: p. 163-192.

5. Stewart, P.S. and M.J. Franklin, *Physiological heterogeneity in biofilms.* Nature Reviews Microbiology, 2008. **6**: p. 199-210.

6. Straight, P.D. and R. Kolter, *Interspecies chemical communication in bacterial development.* Annual Review of Microbiology, 2009. **63**: p. 99-118.

7. Bernstein, H.C., S.D. Paulson, and R.P. Carlson, *Synthetic Escherichia coli consortia engineered for syntrophy demonstrate enhanced biomass productivity.* Journal of Biotechnology, 2012. **157**: p. 159-166.

8. Bernstein, H. and R.P. Carlson, *Microbial Consortia Engineering for Cellular Factories: in vitro to in silico.* Computational and Structural Biotechnology Journal, 2012. **3**(4): p. e201210017.

9. Kersten, R.D. and P.C. Dorrestein, *Secondary metabolomics: natural products mass spectrometry goes global.* ACS Chem Biol, 2009. **4**(8): p. 599-601.

10. Cheng, K.W., C.C. Wong, M. Wang, Q.Y. He, and F. Chen, *Identification and characterization of molecular targets of natural products by mass spectrometry.* Mass Spectrom Rev, 2010. **29**(1): p. 126-55.

11. Watrous, J., N. Hendricks, M. Meehan, and P.C. Dorrestein, *Capturing Bacterial Metabolic Exchange Using Thin Film Desorption Electrospray Ionization-Imaging Mass Spectrometry.* Analytical Chemistry, 2010. **82**(5): p. 1598.

12. Steinmann, D. and M. Ganzera, *Recent advances on HPLC/MS in medicinal plant analysis.* Journal of Pharmaceutical and Biomedical Analysis, 2011. **55**(4): p. 744-57.

13. Kai, M., I. González, O. Genilloud, S.B. Singh, and A. Svatoš, *Direct mass spectrometric screening of antibiotics from bacterial surfaces using liquid extraction surface analysis.* Rapid Communications in Mass Spectrometry, 2012. **26**(20): p. 2477-2482.

14. Amstalden van Hove, E.R., D.F. Smith, and R.M.A. Heeren, *A concise review of mass spectrometry imaging.* Journal of Chromatography A, 2010. **1217**(25): p. 3946.

15. Akhmetov, A., J.F. Moore, G.L. Gasper, P.J. Koin, and L. Hanley, *Laser desorption postionization for imaging MS of biological material.* Journal of Mass Spectrometry, 2010. **45**: p. 137-145.

16. Watrous, J.D. and P.C. Dorrestein, *Imaging mass spectrometry in microbiology.* Nature Reviews Microbiology, 2011. **9**(9): p. 683-94.

17. Trouillon, R., M.K. Passarelli, J. Wang, M.E. Kurczy, and A.G. Ewing, *Chemical Analysis of Single Cells.* Analytical Chemistry, 2012. **85**(2): p. 522-542.

18. Vertes, A., V. Hitchins, and K.S. Phillips, *Analytical Challenges of Microbial Biofilms on Medical Devices.* Analytical Chemistry, 2012. **84**: p. 3858-3866.

19. Fletcher, J.S. and J.C. Vickerman, *Secondary Ion Mass Spectrometry: Characterizing Complex Samples in Two and Three Dimensions.* Analytical Chemistry, 2013. **85**(2): p. 610-639.

20. Wu, C., A.L. Dill, L.S. Eberlin, R.G. Cooks, and D.R. Ifa, *Mass spectrometry imaging under ambient conditions.* Mass Spectrometry Reviews, 2013. **32**(3): p. 218-243.

21. Vekey, K., *Internal energy effects in mass spectrometry.* Journal of Mass Spectrometry, 1996. **31**: p. 445-463.

22. Watrous, J.D., T. Alexandrov, and P.C. Dorrestein, *The evolving field of imaging mass spectrometry and its impact on future biological research.* Journal of Mass Spectrometry, 2011. **46**(2): p. 209-222.

23. Blaze M.T., M., B. Aydin, R.P. Carlson, and L. Hanley, *Identification and imaging of peptides and proteins on Enterococcus faecalis biofilms by matrix assisted laser desorption ionization mass spectrometry.* Analyst, 2012. **137**: p. 5018-5025.

24. McLafferty, F.W. and F. Turecek, *Interpretation of Mass Spectra*. 4th ed. 1993, Mill Valley: University Science Books.

25. Stein, S., *Mass Spectral Reference Libraries: An Ever-Expanding Resource for Chemical Identification.* Analytical Chemistry, 2012. **84**(17): p. 7274-7282.

26. Amirav, A., A. Gordin, M. Poliak, T. Alon, and A.B. Fialkov, *Gas Chromatography Mass Spectrometry with Supersonic Molecular Beams.* Journal of Mass Spectrometry, 2008. **43**: p. 141-163.

27. Hanley, L. and R. Zimmermann, *Light and Molecular Ions: The Emergence of Vacuum UV Single-Photon Ionization in MS.* Analytical Chemistry, 2009. **81**(11): p. 4174-4182.

28. Zimmermann, R., *Photo ionisation in mass spectrometry: light, selectivity and molecular ions.* Analytical and Bioanalytical Chemistry, 2013. **405**(22): p. 6901-6905.

29. Blaze M.T., M., L.K. Takahashi, J. Zhou, M. Ahmed, G.L. Gasper, F.D. Pleticha, and L. Hanley, *Brominated tyrosine and polyelectrolyte multilayer analysis by laser desorption VUV postionization and secondary ion mass spectrometry.* Analytical Chemistry, 2011. **83**: p. 4962-4969.

30. Hertz-Schünemann, R., T. Streibel, S. Ehlert, and R. Zimmermann, *Looking into individual coffee beans during the roasting process: direct micro-probe sampling on-line photo-ionisation mass spectrometric analysis of coffee roasting gases.* Analytical and Bioanalytical Chemistry, 2013. **405**(22): p. 7083-7096.

31. Adam, T. and R. Zimmermann, *Determination of single photon ionization cross sections for quantitative analysis of complex organic mixtures.* Analytical and Bioanalytical Chemistry, 2007. **389**(6): p. 1941-1951.

32. Isaacman, G., K.R. Wilson, A.W.H. Chan, D.R. Worton, J.R. Kimmel, T. Nah, T. Hohaus, M. Gonin, J.H. Kroll, D.R. Worsnop, and A.H. Goldstein, *Improved Resolution of Hydrocarbon Structures and Constitutional Isomers in Complex Mixtures Using Gas Chromatography-Vacuum Ultraviolet-Mass Spectrometry.* Analytical Chemistry, 2012. **84**(5): p. 2335-2342.

33. Mysak, E.R., K.R. Wilson, M. Jimenez-Cruz, M. Ahmed, and T. Baer, *Synchrotron radiation based aerosol time-of-flight mass spectrometry for organic constituents.* Analytical Chemistry, 2005. **77**: p. 5953-5960.

34. Li, Y. and F. Qi, *Recent Applications of Synchrotron VUV Photoionization Mass Spectrometry: Insight into Combustion Chemistry.* Accounts of Chemical Research, 2009. **43**(1): p. 68.

35. Lopez-Avila, V., J. Cooley, R. Urdahl, and M. Thevis, *Determination of stimulants using gas chromatography/high-resolution time-of-flight mass spectrometry and a soft ionization source.* Rapid Communications in Mass Spectrometry, 2012. **26**(23): p. 2714-2724.

36. Harrison, A.G., *Chemical ionization mass spectrometry*. 1992, Boca Raton: CRC Press.

37. Blake, R.S., P.S. Monks, and A.M. Ellis, *Proton-Transfer Reaction Mass Spectrometry.* Chemical Reviews, 2009. **109**: p. 861-896.

38. Covey, T.R., B.A. Thomson, and B.B. Schneider, *Atmospheric pressure ion sources.* Mass Spectrometry Reviews, 2009. **28**(6): p. 870-897.

39. Kauppila, T.J., T. Kuuranne, E.C. Meurer, M.N. Eberlin, T. Kotiaho, and R. Kostiainen, *Atmospheric Pressure Photoionization Mass Spectrometry. Ionization Mechanism and the Effect of Solvent on the Ionization of Naphthalenes.* Analytical Chemistry, 2002. **74**: p. 5470-5479.

40. Syage, J.A., *Mechanism of $[M+H]^+$ formation in photoionization mass spectrometry.* journal of the American Society of Mass Spectrometry, 2004. **15**: p. 1521-1533.

41. Kauppila, T.J., P. Östman, S. Marttila, R.A. Ketola, T. Kotiaho, S. Franssila, and R. Kostiainen, *Atmospheric Pressure Photoionization-Mass Spectrometry with a Microchip Heated Nebulizer.* Analytical Chemistry, 2004. **76**(22): p. 6797-6801.

42. Marchi, I., S. Rudaz, and J. Veuthey, *Atmospheric pressure photoionization for coupling liquid-chromatography to mass spectrometry: A review.* Talanta, 2009. **78**: p. 1–18.

43. Klee, S., S. Albrecht, V. Derpmann, H. Kersten, and T. Benter, *Generation of ion-bound solvent clusters as reactant ions in dopant-assisted APPI and APLI.* Analytical and Bioanalytical Chemistry, 2013. **405**(22): p. 6933-6951.

44. Panda, S.K., K.-J. Brockmann, T. Benter, and W. Schrader, *Atmospheric pressure laser ionization (APLI) coupled with Fourier transform ion cyclotron resonance mass spectrometry applied to petroleum samples analysis: comparison with electrospray ionization and atmospheric pressure photoionization methods.* Rapid Communications in Mass Spectrometry, 2011. **25**(16): p. 2317-2326.

45. Haapala, M., J. Pol, V. Saarela, V. Arvola, T. Kotiaho, R.A. Ketola, S. Franssila, T.J. Kauppila, and R. Kostiainen, *Desorption atmospheric pressure photoionization.* Analytical Chemistry, 2007. **79**: p. 7867-7872.

46. Kersten, H., V. Derpmann, I. Barnes, K.J. Brockmann, R. O'Brien, and T. Benter, *A novel APPI-MS setup for in situ degradation product studies of atmospherically relevant compounds: Capillary atmospheric pressure photo ionization (cAPPI).* Journal of the American Society of Mass Spectrometry, 2011. **22**: p. 2070-2081.

47. Haapala, M., T. Suominen, and R. Kostiainen, *Capillary Photoionization: A High Sensitivity Ionization Method for Mass Spectrometry.* Analytical Chemistry, 2013. **85**(12): p. 5715-5719.

48. Cody, R.B., *Observation of Molecular Ions and Analysis of Nonpolar Compounds with the Direct Analysis in Real Time Ion Source.* Analytical Chemistry, 2009. **81**(3): p. 1101-1107.

49. Ifa, D.R., C. Wu, Z. Ouyang, and R.G. Cooks, *Desorption electrospray ionization and other ambient ionization methods: current progress and preview.* Analyst, 2010. **135**: p. 669-681.

50. Yu, S., E. Crawford, J. Tice, B. Musselman, and J.-T. Wu, *Bioanalysis without Sample Cleanup or Chromatography: The Evaluation and Initial Implementation of Direct Analysis in Real Time Ionization Mass Spectrometry for the Quantification of Drugs in Biological Matrixes.* Analytical Chemistry, 2009. **81**(1): p. 193-202.

51. Musah, R.A., M.A. Domin, M.A. Walling, and J.R.E. Shepard, *Rapid identification of synthetic cannabinoids in herbal samples via direct analysis in real time mass spectrometry.* Rapid Communications in Mass Spectrometry, 2012. **26**(9): p. 1109-1114.

52. Albert, A. and C. Engelhard, *Characteristics of Low-Temperature Plasma Ionization for Ambient Mass Spectrometry Compared to Electrospray Ionization and Atmospheric Pressure Chemical Ionization.* Analytical Chemistry, 2012. **84**(24): p. 10657-10664.

53. Pappas, D., *Status and potential of atmospheric plasma processing of materials.* Journal of Vacuum Science & Technology A, 2011. **29**: p. 020801.

54. Oehrlein, G.S., R.J. Phaneuf, and D.B. Graves, *Plasma-polymer interactions: A review of progress in understanding polymer resist mask durability during plasma etching for nanoscale fabrication.* Journal of Vacuum Science & Technology A, 2011. **29**: p. 010801.

55. Wissdorf, W., M. Lorenz, T. Pöhler, H. Hönen, and T. Benter, *Atmospheric Pressure Ion Source Development: Experimental Validation of Simulated Ion Trajectories within Complex Flow and Electrical Fields.* Journal of the American Society of Mass Spectrometry, 2013. **24**: p. 1456-1466.

56. Hanley, L. and S.B. Sinnott, *The growth and modification of materials via ion-surface processing.* Surface Science, 2002. **500**: p. 500-522.

57. Kebarle, P. and U.H. Verkerk, *Electrospray: From ions in solution to ions in the gas phase, what we know now.* Mass Spectrometry Reviews, 2009. **28**(6): p. 898-917.

58. Konermann, L., E. Ahadi, A.D. Rodriguez, and S. Vahidi, *Unraveling the Mechanism of Electrospray Ionization.* Analytical Chemistry, 2012. **85**(1): p. 2-9.

59. Weston, D.J., *Ambient ionization mass spectrometry: current understanding of mechanistic theory; analytical performance and application areas.* Analyst, 2010. **135**: p. 661-668.

60. Laskin, J., B.S. Heath, P.J. Roach, L. Cazares, and O.J. Semmes, *Tissue Imaging Using Nanospray Desorption Electrospray Ionization Mass Spectrometry.* Analytical Chemistry, 2011. **84**(1): p. 141-148.

61. Ovchinnikova, O.S., V. Kertesz, and G.J. Van Berkel, *Molecular Surface Sampling and Chemical Imaging using Proximal Probe Thermal Desorption/Secondary Ionization Mass Spectrometry.* Analytical Chemistry, 2011. **83**(2): p. 598.

62. Hanley, L., O. Kornienko, E.T. Ada, E. Fuoco, and J.L. Trevor, *Surface mass spectrometry of molecular species.* Journal of Mass Spectrometry, 1999. **34**: p. 705-723.

63. Knochenmuss, R., *Ion formation mechanisms in UV-MALDI.* Analyst, 2006. **131**: p. 966-986.

64. Knochenmuss, R. and L.V. Zhigilei, *Molecular dynamics simulations of MALDI: laser fluence and pulse width dependence of plume characteristics and consequences for matrix and analyte ionization.* Journal of Mass Spectrometry, 2010. **45**(4): p. 333-346.

65. Jaskolla, T.W. and M. Karas, *Compelling evidence for lucky survivor and gas phase protonation: The unified MALDI analyte protonation mechanism.* Journal of the American Society of Mass Spectrometry, 2011. **22**: p. 976-988.

66. Musapelo, T. and K.K. Murray, *Particle Formation in Ambient MALDI Plumes.* Analytical Chemistry, 2011. **83**(17): p. 6601-6608.

67. Trimpin, S., B. Wang, E.D. Inutan, J. Li, C.B. Lietz, A. Harron, V.S. Pagnotti, D. Sardelis, and C.N. McEwen, *A mechanism for ionization of nonvolatile compounds in mass spectrometry: Considerations from MALDI and inlet ionization.* Journal of the American Society of Mass Spectrometry, 2012. **23**: p. 1644-1660.

68. Garrett, T.J. and R.A. Yost, *Analysis of intact tissue by intermediate-pressure MALDI on a linear ion trap mass spectrometer.* Analytical Chemistry, 2006. **78**: p. 2465-2469.

69. Laiko, V.V., S.C. Moyer, and R.J. Cotter, *Atmospheric pressure MALDI/ion trap mass spectrometry.* Analytical Chemistry, 2000. **72**: p. 5239-5243.

70. Römpp, A., K. Schäfer, S. Guenther, Z. Wang, M. Köstler, A. Leisner, C. Paschke, T. Schramm, and B. Spengler, *High-resolution atmospheric pressure infrared laser desorption/ionization mass spectrometry imaging of biological tissue.* Analytical and Bioanalytical Chemistry, 2013. **405**(22): p. 6959-6968.

71. Chen, Z. and A. Vertes, *Early plume expansion in atmospheric pressure midinfrared laser ablation of water-rich targets.* Physical Review E, 2008. **77**(3): p. 036316.

72. Pirkl, A., J. Soltwisch, F. Draude, and K. Dreisewerd, *Infrared Matrix-Assisted Laser Desorption/Ionization Orthogonal-Time-of-Flight Mass Spectrometry Employing a Cooling Stage and Water Ice As a Matrix.* Analytical Chemistry, 2012. **84**(13): p. 5669-5676.

73. Lewis, W.G., Z. Shen, M.G. Finn, and G. Siuzdak, *Desorption/ionization on silicon (DIOS) mass spectrometry: Background and applications.* International Journal of Mass Spectrometry and Ion Processes, 2003. **226**: p. 107-116.

74. McLean, J.A., K.A. Stumpo, and D.H. Russell, *Size-selected (2-10 nm) gold nanoparticles for matrix assisted laser desorption ionization of peptides.* Journal of the American Chemical Society, 2005. **127**: p. 5304-5305.

75. Zhu, Z.J., V.M. Rotello, and R.W. Vachet, *Engineered nanoparticle surfaces for improved mass spectrometric analyses.* Analyst, 2009. **134**: p. 2183-2188.

76. Yanes, O., H.-K. Woo, T.R. Northen, S.R. Oppenheimer, L. Shriver, J. Apon, M.N. Estrada, M.J. Potchoiba, R. Steenwyk, M. Manchester, and G. Siuzdak, *Nanostructure Initiator Mass Spectrometry: Tissue Imaging and Direct Biofluid Analysis.* Analytical Chemistry, 2009. **81**(8): p. 2969.

77. Jun, J.H., Z. Song, Z. Liu, B.J. Nikolau, E.S. Yeung, and Y.J. Lee, *High-Spatial and High-Mass Resolution Imaging of Surface Metabolites of Arabidopsis thaliana by Laser Desorption-Ionization Mass Spectrometry Using Colloidal Silver.* Analytical Chemistry, 2010. **82**(8): p. 3255.

78. Huo, H., M. Shen, S.M. Ebstein, and H. Guthermann, *Surface-assisted laser desorption and ionization mass spectrometry using low-cost matrix-free substrates.* Journal of Mass Spectrometry, 2011. **46**(9): p. 859-864.

79. Kawasaki, H., T. Ozawa, H. Hisatomi, and R. Arakawa, *Platinum vapor deposition surface-assisted laser desorption/ionization for imaging mass spectrometry of small molecules.* Rapid Communications in Mass Spectrometry, 2012. **26**(16): p. 1849-1858.

80. Wu, H.-F., J. Gopal, and M. Manikandan, *Future perspective of nanoparticle interaction-assisted laser desorption/ionization mass spectrometry for rapid, simple, direct and sensitive detection of microorganisms.* Journal of Mass Spectrometry, 2012. **47**(3): p. 355-363.

81. Stolee, J.A., B.N. Walker, V. Zorba, R.E. Russo, and A. Vertes, *Laser-nanostructure interactions for ion production.* Physical Chemistry Chemical Physics, 2012. **14**(24): p. 8453-8471.

82. Inutan, E.D., J. Wager-Miller, K. Mackie, and S. Trimpin, *Laserspray Ionization Imaging of Multiply Charged Ions Using a Commercial Vacuum MALDI Ion Source.* Analytical Chemistry, 2012. **84**(21): p. 9079-9084.

83. Berry, J.I., S. Sun, Y. Dou, A. Wucher, and N. Winograd, *Laser desorption and imaging of proteins from ice via UV femtosecond laser pulses.* Analytical Chemistry, 2003. **75**: p. 5146-5151.

84. Wichmann, J.M., C. Lupulescu, L. Wöste, and A. Lindinger, *Matrix-assisted laser desorption/ionization by using femtosecond laser pulses in the near-infrared wavelength regime.* Rapid Communications in Mass Spectrometry, 2009. **23**(8): p. 1105-1108.

85. Coello, Y., A.D. Jones, T.C. Gunaratne, and M. Dantus, *Atmospheric Pressure Femtosecond Laser Imaging Mass Spectrometry.* Analytical Chemistry, 2010. **82**(7): p. 2753.

86. Cui, Y., C. Bhardwaj, S. Milasinovic, R.P. Carlson, R.J. Gordon, and L. Hanley, *Molecular Imaging and Depth Profiling of Biomaterials Interfaces by Femtosecond Laser Desorption Postionization Mass Spectrometry.* ACS Applied Materials & Interfaces, 2013. **5**: p. 9269-9275.

87. Vogel, A., J. Noack, G. Huttman, and G. Paltauf, *Mechanisms of femtosecond laser nanosurgery of cells and tissues.* Applied Physics B: Lasers and Optics, 2005. **81**: p. 1015-1045.

88. Maxwell, S. and E. Mazur, *Nanoprocessing of subcellular targets using femtosecond laser pulses.* Medical Laser Application, 2005. **20**: p. 193-200.

89. Liu, Y., S. Sun, S. Singha, M.R. Cho, and R.J. Gordon, *3D Femtosecond Laser Patterning of Collagen for Directed Cell Attachment.* Biomaterials, 2005. **26**: p. 4597-4605.

90. Nakamura, H., Y. Liu, T.E. Witt, D.P. Edward, and R.J. Gordon, *Femtosecond laser photodisruption of primate trabecular meshwork: An ex vivo study.* Investigative Ophthalmology & Visual Science, 2009. **50**: p. 1198-1204.

91. Milasinovic, S., Y. Liu, G.L. Gasper, Y. Zhao, J.L. Johnston, R.J. Gordon, and L. Hanley, *Ultrashort pulse laser ablation for depth profiling of bacterial biofilms.* Journal of Vacuum Science & Technology A, 2010. **28**: p. 647-651.

92. Milasinovic, S., Y. Liu, C. Bhardwaj, M. Blaze M.T., R.J. Gordon, and L. Hanley, *Feasibility of depth profiling of animal tissue by ultrashort pulse laser ablation.* Analytical Chemistry, 2012. **84**: p. 3945-3951.

93. Cui, Y., J.F. Moore, S. Milasinovic, Y. Liu, R.J. Gordon, and L. Hanley, *Depth profiling and imaging capabilities of an ultrashort pulse laser ablation time of flight mass spectrometer.* Review of Scientific Instruments, 2012. **83**: p. 093702.

94. Peng, J., N. Puskas, P.B. Corkum, D.M. Rayner, and A.V. Loboda, *High-Pressure Gas Phase Femtosecond Laser Ionization Mass Spectrometry.* Analytical Chemistry, 2012. **84**(13): p. 5633-5640.

95. Shahar, T., S. Dagan, and A. Amirav, *Laser Desorption Fast GC-MS in Supersonic Molecular Beams.* Journal of the American Society of Mass Spectrometry, 1998. **9**: p. 628-637.

96. Sabbah, H., A.L. Morrow, A.E. Pomerantz, and R.N. Zare, *Evidence for Island Structures as the Dominant Architecture of Asphaltenes.* Energy & Fuels, 2011. **25**: p. 1597.

97. Elsila, J.E., N.P. de Leon, and R.N. Zare, *Factors affecting quantitative analysis in laser desorption/laser ionization mass spectrometry.* Analytical Chemistry, 2004. **76**: p. 2430-2437.

98. Getty, S.A., W.B. Brinckerhoff, T. Cornish, S. Ecelberger, and M. Floyd, *Compact two-step laser time-of-flight mass spectrometer for in situ analyses of aromatic organics on planetary missions.* Rapid Communications in Mass Spectrometry, 2012. **26**(23): p. 2786-2790.

99. Pan, Y., H. Yin, T. Zhang, H. Guo, L. Sheng, and F. Qi, *The characterization of selected drugs with infrared laser desorption/tunable synchrotron vacuum ultraviolet photoionization mass spectrometry.* Rapid Communications in Mass Spectrometry, 2008. **22**(16): p. 2515-2520.

100. Nemes, P., A.A. Barton, Y. Li, and A. Vertes, *Ambient Molecular Imaging and Depth Profiling of Live Tissue by Infrared Laser Ablation Electrospray Ionization Mass Spectrometry.* Analytical Chemistry, 2008. **80**(12): p. 4575-4582.

101. Shrestha, B., J.M. Patt, and A. Vertes, *In Situ Cell-by-Cell Imaging and Analysis of Small Cell Populations by Mass Spectrometry.* Analytical Chemistry, 2011. **83**(8): p. 2947-2955.

102. Vaikkinen, A., B. Shrestha, T.J. Kauppila, A. Vertes, and R. Kostiainen, *Infrared Laser Ablation Atmospheric Pressure Photoionization Mass Spectrometry.* Analytical Chemistry, 2012. **84**(3): p. 1630-1636.

103. Galhena, A.S., G.A. Harris, L. Nyadong, K.K. Murray, and F.M. Fernandez, *Small Molecule Ambient Mass Spectrometry Imaging by Infrared Laser Ablation Metastable-Induced Chemical Ionization.* Analytical Chemistry, 2010. **82**(6): p. 2178-2181.

104. Judge, E.J., J.J. Brady, D. Dalton, and R.J. Levis, *Analysis of Pharmaceutical Compounds from Glass, Fabric, Steel, and Wood Surfaces at Atmospheric Pressure Using Spatially Resolved, Nonresonant Femtosecond Laser Vaporization Electrospray Mass Spectrometry.* Analytical Chemistry, 2010. **82**(8): p. 3231.

105. Judge, E.J., J.J. Brady, P.E. Barbano, and R.J. Levis, *Nonresonant Femtosecond Laser Vaporization with Electrospray Postionization for ex vivo Plant Tissue Typing Using Compressive Linear Classification.* Analytical Chemistry, 2011. **83**(6): p. 2145-2151.

106. Zavalin, A., E.M. Todd, P.D. Rawhouser, J. Yang, J.L. Norris, and R.M. Caprioli, *Direct imaging of single cells and tissue at sub-cellular spatial resolution using transmission geometry MALDI MS.* Journal of Mass Spectrometry, 2012. **47**(11): p. 1473-1481.

107. Zinovev, A.V., I.V. Veryovkin, J.F. Moore, and M.J. Pellin, *Laser-driven acoustic desorption of organic molecules from back-irradiated solid foils.* Analytical Chemistry, 2007. **79**: p. 8232-8241.

108. Nyadong, L., J.P. Quinn, C.S. Hsu, C.L. Hendrickson, R.P. Rodgers, and A.G. Marshall, *Atmospheric Pressure Laser-Induced Acoustic Desorption Chemical Ionization Mass Spectrometry for Analysis of Saturated Hydrocarbons.* Analytical Chemistry, 2012. **84**(16): p. 7131-7137.

109. Borton, D.J., L.M. Amundson, M.R. Hurt, A. Dow, J.T. Madden, G.J. Simpson, and H.I. Kenttämaa, *Development of a High-Throughput Laser-Induced Acoustic Desorption Probe and Raster Sampling For Laser-Induced Acoustic Desorption/Atmospheric Pressure Chemical Ionization.* Analytical Chemistry, 2013. **85**(12): p. 5720-5726.

110. Wucher, A., J. Cheng, L. Zheng, and N. Winograd, *Three-dimensional depth profiling of molecular structures.* Analytical and Bioanalytical Chemistry, 2009. **393**: p. 1835-1842.

111. Malm, J., D. Giannaras, M.O. Riehle, N. Gadegaard, and P. SjoÌˆvall, *Fixation and Drying Protocols for the Preparation of Cell Samples for Time-of-Flight Secondary Ion Mass Spectrometry Analysis.* Analytical Chemistry, 2009. **81**(17): p. 7197.

112. Passarelli, M.K., A.G. Ewing, and N. Winograd, *Single-Cell Lipidomics: Characterizing and Imaging Lipids on the Surface of Individual Aplysia californica Neurons with Cluster Secondary Ion Mass Spectrometry.* Analytical Chemistry, 2013. **85**(4): p. 2231-2238.

113. Altelaar, A.F.M., I. Klinkert, K. Jalink, R.P.J. de Lange, R.A.H. Adan, R.M.A. Heeren, and S.R. Piersma, *Gold-enhanced biomolecular surface imaging of cells and tissue by SIMS and MALDI mass spectrometry.* Analytical Chemistry, 2006. **78**: p. 734-742.

114. Fitzgerald, J.J.D., P. Kunnath, and A.V. Walker, *Matrix-Enhanced Secondary Ion Mass Spectrometry (ME SIMS) Using Room Temperature Ionic Liquid Matrices.* Analytical Chemistry, 2010. **82**(11): p. 4413.

115. Fernandez-Lima, F.A., J. Post, J.D. DeBord, M.J. Eller, S.V. Verkhoturov, S. Della-Negra, A.S. Woods, and E.A. Schweikert, *Analysis of Native Biological Surfaces Using a 100 kV Massive Gold Cluster Source.* Analytical Chemistry, 2011. **83**(22): p. 8448-8453.

116. Shard, A.G., R. Havelund, M.P. Seah, S.J. Spencer, I.S. Gilmore, N. Winograd, D. Mao, T. Miyayama, E. Niehuis, D. Rading, and R. Moellers, *Argon Cluster Ion Beams for Organic Depth Profiling: Results from a VAMAS Interlaboratory Study.* Analytical Chemistry, 2012. **84**(18): p. 7865-7873.

117. Aoyagi, S., J.S. Fletcher, S. Sheraz, T. Kawashima, I. Berrueta Razo, A. Henderson, N.P. Lockyer, and J.C. Vickerman, *Peptide structural analysis using continuous Ar cluster and C60 ion beams.* Analytical and Bioanalytical Chemistry, 2013. **405**(21): p. 6621-6628.

118. Jede, R., O. Ganschow, and U. Kaiser, *Sputtered neutral mass spectrometry (SNMS)*, in *Practical Surface Analysis*, D. Briggs and M.P. Seah, Editors. 1992, John Wiley & Sons Ltd.: Chichester. p. 425-506.

119. Zhou, J., L.K. Takahashi, K.R. Wilson, S.R. Leone, and M. Ahmed, *Internal Energies of Ion-Sputtered Neutral Tryptophan and Thymine Molecules Determined by Vacuum Ultraviolet Photoionization.* Analytical Chemistry, 2010. **82**(9): p. 3905.

120. Haase, A., H.F. Arlinghaus, J. Tentschert, H. Jungnickel, P. Graf, A. Mantion, F. Draude, S. Galla, J. Plendl, M.E. Goetz, A. Masic, W. Meier, A.F. Thünemann, A. Taubert, and A. Luch, *Application of Laser Postionization Secondary Neutral Mass Spectrometry/Time-of-*

Flight Secondary Ion Mass Spectrometry in Nanotoxicology: Visualization of Nanosilver in Human Macrophages and Cellular Responses. ACS Nano, 2011. **5**(4): p. 3059-3068.

121. Gasper, G.L., R. Carlson, A. Akhmetov, J.F. Moore, and L. Hanley, *Laser desorption 7.87 eV postionization mass spectrometry of antibiotics in Staphylococcus epidermidis bacterial biofilms.* Proteomics, 2008. **8**: p. 3816-3821.

122. Gasper, G.L., L.K. Takahashi, J. Zhou, M. Ahmed, J.F. Moore, and L. Hanley, *Laser Desorption Postionization Mass Spectrometry of Antibiotic-Treated Bacterial Biofilms using Tunable Vacuum Ultraviolet Radiation* Analytical Chemistry, 2010. **82**: p. 7472-7478.

123. Gasper, G.L., *MS Imaging of Antibiotics with Staph. Epidermidis Bacterial Biofilms by Laser Desorption Postionization*, in *Chemistry*. 2011, University of Illinois at Chicago: Chicago.

124. Takahashi, L.K., J. Zhou, K.R. Wilson, S.R. Leone, and M. Ahmed, *Imaging with Mass Spectrometry: A Secondary Ion and VUV-Photoionization Study of Ion-Sputtered Atoms and Clusters from GaAs and Au.* The Journal of Physical Chemistry A, 2009. **113**(16): p. 4035-4044.

125. Arps, J.H., C.H. Chen, M.P. McCann, and I. Datskou, *Ionization of organic molecules using coherent vacuum utraviolet light.* Applied Spectroscopy, 1989. **43**: p. 1211-1214.

126. Van Bramer, S.E. and M.V. Johnston, *10.5 eV photoionization mass spectrometry of aliphatic compounds.* Journal of the American Society of Mass Spectrometry, 1990. **1**: p. 419-426.

127. Oktem, B., M.P. Tolocka, and M.V. Johnston, *On-line analysis of organic components in fine and ultrafine particles by photoionization aerosol mass spectrometry.* Analytical Chemistry, 2004. **76**: p. 253-261.

128. Miller, J.H., *Experiments in Molecular Genetics*. 1972, New York: Cold Spring Harbor Laboratory.

129. Shin, M.H., D.Y. Lee, K.-H. Liu, O. Fiehn, and K.H. Kim, *Evaluation of Sampling and Extraction Methodologies for the Global Metabolic Profiling of Saccharophagus degradans.* Analytical Chemistry, 2010. **82**(15): p. 6660.

130. Nemes, P., A.S. Woods, and A. Vertes, *Simultaneous Imaging of Small Metabolites and Lipids in Rat Brain Tissues at Atmospheric Pressure by Laser Ablation Electrospray Ionization Mass Spectrometry.* Analytical Chemistry, 2010. **82**(3): p. 982-988.

131. Gasper, G.L., L.K. Takahashi, J. Zhou, M. Ahmed, J.F. Moore, and L. Hanley, *Comparing vacuum and extreme ultraviolet radiation for postionization of laser desorbed neutrals from bacterial biofilms and organic fullerenes.* Nuclear Instruments and Methods in Physics Research, Section A, 2011. **649**: p. 222-224.

132. Heller, D.N., C. Fenselau, R.J. Cotter, P. Demirev, J.K. Olthoff, J. Honovich, T. Tanaka, and Y. Kishimoto, *Mass spectral analysis of complex lipids desorbed directly from lyophilized membranes and cells.* Biochemical and Biophysical Research Communications, 1987. **142**: p. 194-199.

133. Goodacre, R., J.K. Heald, and D.B. Kell, *Characterization of intact microorganism using electrospray ionization mass spectrometry.* FEMS Microbiology Letters, 1999. **176**: p. 17-24.

134. Oursel, D., C. Loutelier-Bourhis, N. Orange, S. Chevalier, V. Norris, and C.M. Lange, *Identification and relative quantification of fatty acids in Escherichia coli membranes by gas chromatography/mass spectrometry.* Rapid Communications in Mass Spectrometry, 2007. **21**: p. 3229-3233.

135. Lias, S.G., J.E. Bartmess, J.F. Liebman, J.L. Holmes, R.D. Levin, and W.G. Mallard, *Gas-Phase Ion and Neutral Thermochemistry.* Journal of Physical and Chemical Reference Data, 1988. **17**(Suppl. No. 1): p. 18-25.

136. Pachuta, S.J. and P.R. Vlasak, *Postacquisition Mass Resolution Improvement in Time-of-Flight Secondary Ion Mass Spectrometry.* Analytical Chemistry, 2012. **84**(3): p. 1744-1753.

137. Green, F.M., I.S. Gilmore, and M.P. Seah, *Mass Spectrometry and Informatics: Distribution of Molecules in the PubChem Database and General Requirements for Mass Accuracy in Surface Analysis.* Analytical Chemistry, 2011. **83**(9): p. 3239-3243.

138. Baran, R., B.P. Bowen, N.J. Bouskill, E.L. Brodie, S.M. Yannone, and T.R. Northen, *Metabolite Identification in Synechococcus sp. PCC 7002 Using Untargeted Stable Isotope Assisted Metabolite Profiling.* Analytical Chemistry, 2010. **82**(21): p. 9034-9042.

139. Perera, S., A. Berthod, E. Dodbiba, and D.W. Armstrong, *Coupling solid-phase microextraction and laser desorption ionization for rapid identification of biological material.* Rapid Communications in Mass Spectrometry, 2012. **26**(7): p. 853-862.

140. Gamez, G., L. Zhu, T.A. Schmitz, and R. Zenobi, *Photoelectron Emission as an Alternative Electron Impact Ionization Source for Ion Trap Mass Spectrometry.* Anal. Chem., 2008. **80**(17): p. 6791-6795.

141. Kostko, O., L.K. Takahashi, and M. Ahmed, *Desorption dynamics, internal energies and imaging of organic molecules from surfaces with laser desorption and vacuum ultraviolet (VUV) photoionization.* Chemistry, An Asian Journal, 2011. **6**: p. 3066-3076.

142. Bhardwaj, C., J.F. Moore, Y. Cui, G.L. Gasper, H.C. Bernstein, R.P. Carlson, and L. Hanley, *Laser desorption VUV postionization MS imaging of a cocultured biofilm.* Analytical Bioanalytical Chemistry, 2013. **405**: p. 6969-6977.

143. Guo, A.C., T. Jewison, M. Wilson, Y. Liu, C. Knox, Y. Djoumbou, P. Lo, R. Mandal, R. Krishnamurthy, and D.S. Wishart, *E. coli metabolite database.* Nucleic Acids Research, 2013. **41**: p. D625-D630.

144. Jewison, T., V. Neveu, J. Lee, C. Knox, P. Liu, R. Mandal, R.K. Murthy, I. Sinelnikov, A.C. Guo, M. Wilson, Y. Djoumbou, and D.S. Wishart, *S. cervisiae metabolite database.* Nucleic Acids Research, 2012. **40**: p. D815-D820.

145. Takahashi, L.K., J. Zhou, O. Kostko, A. Golan, S.R. Leone, and M. Ahmed, *Vacuum-Ultraviolet Photoionization and Mass Spectrometric Characterization of Lignin Monomers Coniferyl and Sinapyl Alcohols.* Journal of Physical Chemistry A, 2011. **115**: p. 3279-3290.

146. Nobile, C.J., H.A. Schneider, J.E. Nett, D.C. Sheppard, S.G. Filler, D.R. Andes, and A.P. Mitchell, *Complementary Adhesin Function in C. albicans Biofilm Formation.* Current Biology, 2008. **18**(14): p. 1017-1024.

147. Brenner, K., L. You, and F.H. Arnold, *Engineering microbial consortia: a new frontier in synthetic biology.* Trends in Biotechnology, 2008. **26**(9): p. 483-489.

148. Carlsson, J., *Bacterial Metabolism in Dental Biofilms.* Advances in Dental Research, 1997. **11**(1): p. 75-80.

149. Phelan, V.V., W.T. Liu, K. Pogliano, and P.C. Dorrestein, *Microbial metabolic exchange--the chemotype-to-phenotype link.* Nature Chemical Biology, 2012. **8**(1): p. 26-35.

150. Momeni, B., K.A. Brileya, M.W. Fields, and W. Shou, *Strong inter-population cooperation leads to partner intermixing in microbial communities.* eLife Sciences, 2013. **2**.

151. Blaze M.T., M., A. Akhmetov, B. Aydin, P.D. Edirisinghe, G. Uygur, and L. Hanley, *Quantification of antibiotic in biofilm-inhibiting multilayers by 7.87 eV laser desorption postionization MS imaging.* Analytical Chemistry, 2012. **84**: p. 9410-9415.

152. Otto, M., *Chemometrics: Statistics and Computer Application in Analytical Chemistry*. 2007, New York: Wiley-VCH.

153. Tyler, B.J., G. Rayal, and D.G. Castner, *Multivariate analysis strategies for processing ToF-SIMS images of biomaterials.* Biomaterials, 2007. **28**(15): p. 2412-2423.

154. Graham, D.J. and D.G. Castner, *Multivariate Analysis of ToF-SIMS Data from Multicomponent Systems: The Why, When, and How.* Biointerphases, 2012. **7**: p. 49.

155. Tyler, B.J., S. Rangaranjan, J. Möller, A. Beumer, and H.F. Arlinghaus, *TOF-SIMS imaging of chlorhexidine-digluconate transport in frozen hydrated biofilms of the fungus Candida albicans.* Applied Surface Science, 2006. **252**: p. 6712-6715.

156. Chen, P., Y. Lu, and P.B. Harrington, *Biomarker profiling and reproducibility study of MALDI-MS measurements of Escherichia coli by analysis of variance - principal component analysis.* Analytical Chemistry, 2008. **80**: p. 1474-1481.

157. Qian, J., J.E. Cutler, R.B. Cole, and Y. Cai, *MALDI-TOF mass signatures for differentiation of yeast species, strain grouping and monitoring of morphogenesis markers.* Analytical Bioanalytical Chemistry, 2008. **392**: p. 439-449.

158. Timmins, É.M., S.A. Howell, B.K. Alsberg, W.C. Noble, and R. Goodacre, *Rapid Differentiation of Closely RelatedCandida Species and Strains by Pyrolysis-Mass Spectrometry and Fourier Transform-Infrared Spectroscopy.* Journal of Clinical Microbiology, 1998. **36**(2): p. 367-374.

APPENDIX

Permission for reproduction of published work is attached here. Following articles have been used either in parts or in full in this thesis work.

[Chhavi Bhardwaj, Jerry F. Moore, Yang Cui, Gerald L. Gasper, Hans C. Bernstein, Ross P. Carlson & Luke Hanley. Laser desorption VUV postionization MS imaging of a cocultured biofilm. Analytical Bioanalytical Chemistry (2013) 405 (22), 6969-6977 DOI:10.1007/s00216-012-6454-0]- Reproduced by permission of The Royal Society of Chemistry. See Appendix A.

[Chhavi Bhardwaj & Luke Hanley. Ion sources for the mass spectrometric identification of natural products. Natural Product Reports (2014) DOI: 10.1039/C3NP70094A] Reproduced by permission of The Royal Society of Chemistry. See Appendix A.

[Chhavi Bhardwaj, Yang Cui, Theresa Hofstetter, Suet Liu, Hans C. Bernstein, Ross P. Carlson, Musahid Ahmed & Luke Hanley. Differentiation of Microbial Species and Strains in Coculture Biofilms by Multivariate Analysis of Laser Desorption Postionization Mass Spectra. Analyst (2013) 138 (22), 6844-6851 DOI: 10.1039/C3AN01389H]- Reproduced by permission of The Royal Society of Chemistry. See Appendix A.

SPRINGER LICENSE
TERMS AND CONDITIONS

Mar 14, 2014

This is a License Agreement between University of Illinois at Chicago ("You") and Springer ("Springer") provided by Copyright Clearance Center ("CCC"). The license consists of your order details, the terms and conditions provided by Springer, and the payment terms and conditions.

All payments must be made in full to CCC. For payment instructions, please see information listed at the bottom of this form.

License Number	3345031340397
License date	Mar 09, 2014
Licensed content publisher	Springer
Licensed content publication	Analytical and Bioanalytical Chemistry
Licensed content title	Laser desorption VUV postionization MS imaging of a cocultured biofilm
Licensed content author	Chhavi Bhardwaj
Licensed content date	Jan 1, 2012
Volume number	405
Issue number	22
Type of Use	Thesis/Dissertation
Portion	Full text
Number of copies	1
Author of this Springer article	Yes and you are the sole author of the new work
Order reference number	
Title of your thesis / dissertation	Laser Desorption Postionization Mass Spectrometric Analysis of Multispecies Coculture Biofilms
Expected completion date	Jun 2014
Estimated size(pages)	150
Total	0.00 USD
Terms and Conditions	

Introduction

The publisher for this copyrighted material is Springer Science + Business Media. By clicking "accept" in connection with completing this licensing transaction, you agree that the following terms and conditions apply to this transaction (along with the Billing and Payment terms and conditions established by Copyright Clearance Center, Inc. ("CCC"), at the time that you opened your Rightslink account and that are available at any time at http://myaccount.copyright.com).

Limited License

With reference to your request to reprint in your thesis material on which Springer Science and Business Media control the copyright, permission is granted, free of charge, for the use indicated in your enquiry.

Licenses are for one-time use only with a maximum distribution equal to the number that you identified in the licensing process.

This License includes use in an electronic form, provided its password protected or on the university's intranet or repository, including UMI (according to the definition at the Sherpa website: http://www.sherpa.ac.uk/romeo/). For any other electronic use, please contact Springer at (permissions.dordrecht@springer.com or permissions.heidelberg@springer.com).

The material can only be used for the purpose of defending your thesis, and with a maximum of 100 extra copies in paper.

Although Springer holds copyright to the material and is entitled to negotiate on rights, this license is only valid, subject to a courtesy information to the author (address is given with the article/chapter) and provided it concerns original material which does not carry references to other sources (if material in question appears with credit to another source, authorization from that source is required as well).

Permission free of charge on this occasion does not prejudice any rights we might have to charge for reproduction of our copyrighted material in the future.

Altering/Modifying Material: Not Permitted

You may not alter or modify the material in any manner. Abbreviations, additions, deletions and/or any other alterations shall be made only with prior written authorization of the author(s) and/or Springer Science + Business Media. (Please contact Springer at (permissions.dordrecht@springer.com or permissions.heidelberg@springer.com)

Reservation of Rights

Springer Science + Business Media reserves all rights not specifically granted in the combination of (i) the license details provided by you and accepted in the course of this licensing transaction, (ii) these terms and conditions and (iii) CCC's Billing and Payment terms and conditions.

Copyright Notice:Disclaimer

You must include the following copyright and permission notice in connection with any reproduction of the licensed material: "Springer and the original publisher /journal title, volume, year of publication, page, chapter/article title, name(s) of author(s), figure number(s), original copyright notice) is given to the publication in which the material was originally published, by adding; with kind permission from Springer Science and Business Media"

Warranties: None

Example 1: Springer Science + Business Media makes no representations or warranties with respect to the licensed material.

Example 2: Springer Science + Business Media makes no representations or warranties with respect to the licensed material and adopts on its own behalf the limitations and disclaimers established by CCC on its behalf in its Billing and Payment terms and conditions for this licensing transaction.

Indemnity
You hereby indemnify and agree to hold harmless Springer Science + Business Media and CCC, and their respective officers, directors, employees and agents, from and against any and all claims arising out of your use of the licensed material other than as specifically authorized pursuant to this license.

No Transfer of License
This license is personal to you and may not be sublicensed, assigned, or transferred by you to any other person without Springer Science + Business Media's written permission.

No Amendment Except in Writing
This license may not be amended except in a writing signed by both parties (or, in the case of Springer Science + Business Media, by CCC on Springer Science + Business Media's behalf).

Objection to Contrary Terms
Springer Science + Business Media hereby objects to any terms contained in any purchase order, acknowledgment, check endorsement or other writing prepared by you, which terms are inconsistent with these terms and conditions or CCC's Billing and Payment terms and conditions. These terms and conditions, together with CCC's Billing and Payment terms and conditions (which are incorporated herein), comprise the entire agreement between you and Springer Science + Business Media (and CCC) concerning this licensing transaction. In the event of any conflict between your obligations established by these terms and conditions and those established by CCC's Billing and Payment terms and conditions, these terms and conditions shall control.

Jurisdiction
All disputes that may arise in connection with this present License, or the breach thereof, shall be settled exclusively by arbitration, to be held in The Netherlands, in accordance with Dutch law, and to be conducted under the Rules of the 'Netherlands Arbitrage Instituut' (Netherlands Institute of Arbitration).*OR:*

All disputes that may arise in connection with this present License, or the breach thereof, shall be settled exclusively by arbitration, to be held in the Federal Republic of Germany, in accordance with German law.

Other terms and conditions:

v1.3

If you would like to pay for this license now, please remit this license along with your payment made payable to "COPYRIGHT CLEARANCE CENTER" otherwise you will be invoiced within 48 hours of the license date. Payment should be in the form of a check or money order referencing your account number and this invoice number RLNK501246062. Once you receive your invoice for this order, you may pay your invoice by credit card.

Please follow instructions provided at that time.

Make Payment To:
Copyright Clearance Center
Dept 001
P.O. Box 843006
Boston, MA 02284-3006

For suggestions or comments regarding this order, contact RightsLink Customer Support: customercare@copyright.com or +1-877-622-5543 (toll free in the US) or +1-978-646-2777.

Gratis licenses (referencing $0 in the Total field) are free. Please retain this printable license for your reference. No payment is required.

SPRINGER LICENSE
TERMS AND CONDITIONS

Mar 14, 2014

This is a License Agreement between University of Illinois at Chicago ("You") and Springer ("Springer") provided by Copyright Clearance Center ("CCC"). The license consists of your order details, the terms and conditions provided by Springer, and the payment terms and conditions.

All payments must be made in full to CCC. For payment instructions, please see information listed at the bottom of this form.

License Number	3347820304078
License date	Mar 14, 2014
Licensed content publisher	Springer
Licensed content publication	Analytical and Bioanalytical Chemistry
Licensed content title	Laser desorption VUV postionization MS imaging of a cocultured biofilm
Licensed content author	Chhavi Bhardwaj
Licensed content date	Jan 1, 2012
Volume number	405
Issue number	22
Type of Use	Thesis/Dissertation
Portion	Figures
Author of this Springer article	Yes and you are the sole author of the new work
Order reference number	
Original figure numbers	Figures 1,2,3,4,5,6
Title of your thesis / dissertation	Laser Desorption Postionization Mass Spectrometric Analysis of Multispecies Coculture Biofilms
Expected completion date	Jun 2014
Estimated size(pages)	150
Total	0.00 USD
Terms and Conditions	

Introduction

The publisher for this copyrighted material is Springer Science + Business Media. By clicking "accept" in connection with completing this licensing transaction, you agree that the following terms and conditions apply to this transaction (along with the Billing and Payment terms and conditions established by Copyright Clearance Center, Inc. ("CCC"), at the time that you opened your Rightslink account and that are available at any time at http://myaccount.copyright.com).

Limited License

With reference to your request to reprint in your thesis material on which Springer Science and Business Media control the copyright, permission is granted, free of charge, for the use indicated in your enquiry.

Licenses are for one-time use only with a maximum distribution equal to the number that you identified in the licensing process.

This License includes use in an electronic form, provided its password protected or on the university's intranet or repository, including UMI (according to the definition at the Sherpa website: http://www.sherpa.ac.uk/romeo/). For any other electronic use, please contact Springer at (permissions.dordrecht@springer.com or permissions.heidelberg@springer.com).

The material can only be used for the purpose of defending your thesis, and with a maximum of 100 extra copies in paper.

Although Springer holds copyright to the material and is entitled to negotiate on rights, this license is only valid, subject to a courtesy information to the author (address is given with the article/chapter) and provided it concerns original material which does not carry references to other sources (if material in question appears with credit to another source, authorization from that source is required as well).

Permission free of charge on this occasion does not prejudice any rights we might have to charge for reproduction of our copyrighted material in the future.

Altering/Modifying Material: Not Permitted

You may not alter or modify the material in any manner. Abbreviations, additions, deletions and/or any other alterations shall be made only with prior written authorization of the author(s) and/or Springer Science + Business Media. (Please contact Springer at (permissions.dordrecht@springer.com or permissions.heidelberg@springer.com)

Reservation of Rights

Springer Science + Business Media reserves all rights not specifically granted in the combination of (i) the license details provided by you and accepted in the course of this licensing transaction, (ii) these terms and conditions and (iii) CCC's Billing and Payment terms and conditions.

Copyright Notice:Disclaimer

You must include the following copyright and permission notice in connection with any reproduction of the licensed material: "Springer and the original publisher /journal title, volume, year of publication, page, chapter/article title, name(s) of author(s), figure number(s), original copyright notice) is given to the publication in which the material was originally published, by adding; with kind permission from Springer Science and Business Media"

Warranties: None

Example 1: Springer Science + Business Media makes no representations or warranties with respect to the licensed material.

Example 2: Springer Science + Business Media makes no representations or warranties with respect to the licensed material and adopts on its own behalf the limitations and disclaimers established by CCC on its behalf in its Billing and Payment terms and conditions for this licensing transaction.

Indemnity
You hereby indemnify and agree to hold harmless Springer Science + Business Media and CCC, and their respective officers, directors, employees and agents, from and against any and all claims arising out of your use of the licensed material other than as specifically authorized pursuant to this license.

No Transfer of License
This license is personal to you and may not be sublicensed, assigned, or transferred by you to any other person without Springer Science + Business Media's written permission.

No Amendment Except in Writing
This license may not be amended except in a writing signed by both parties (or, in the case of Springer Science + Business Media, by CCC on Springer Science + Business Media's behalf).

Objection to Contrary Terms
Springer Science + Business Media hereby objects to any terms contained in any purchase order, acknowledgment, check endorsement or other writing prepared by you, which terms are inconsistent with these terms and conditions or CCC's Billing and Payment terms and conditions. These terms and conditions, together with CCC's Billing and Payment terms and conditions (which are incorporated herein), comprise the entire agreement between you and Springer Science + Business Media (and CCC) concerning this licensing transaction. In the event of any conflict between your obligations established by these terms and conditions and those established by CCC's Billing and Payment terms and conditions, these terms and conditions shall control.

Jurisdiction
All disputes that may arise in connection with this present License, or the breach thereof, shall be settled exclusively by arbitration, to be held in The Netherlands, in accordance with Dutch law, and to be conducted under the Rules of the 'Netherlands Arbitrage Instituut' (Netherlands Institute of Arbitration).*OR:*

All disputes that may arise in connection with this present License, or the breach thereof, shall be settled exclusively by arbitration, to be held in the Federal Republic of Germany, in accordance with German law.

Other terms and conditions:

v1.3

If you would like to pay for this license now, please remit this license along with your payment made payable to "COPYRIGHT CLEARANCE CENTER" otherwise you will be invoiced within 48 hours of the license date. Payment should be in the form of a check or money order referencing your account number and this invoice number RLNK501251548. Once you receive your invoice for this order, you may pay your invoice by credit card.

Please follow instructions provided at that time.

Make Payment To:
Copyright Clearance Center
Dept 001
P.O. Box 843006
Boston, MA 02284-3006

For suggestions or comments regarding this order, contact RightsLink Customer Support: customercare@copyright.com or +1-877-622-5543 (toll free in the US) or +1-978-646-2777.

Gratis licenses (referencing $0 in the Total field) are free. Please retain this printable license for your reference. No payment is required.

Author Deposition

The following apply only to authors signing one of the non-Open Access Licence to Publish. For authors who have signed one of the Open Access Licence to Publish, or are thinking of signing one of the Open Access Licence to Publish, please click on the relevant link below.

Deposition of any form of the article is allowed in non-commercial repositories only.

Deposition by the RSC

The RSC shall:

- Deposit the accepted version of the submitted article in non-commercial repository(ies) as deemed appropriate, including but not limited to the author(s)' funding agency repository(ies). There shall be an embargo of making the above deposited material available to the public of 12 months from the date of acceptance.

Allowed Deposition by the author(s)

When the author accepts the exclusive Licence to Publish for a journal article, he/she retains certain rights concerning the deposition of the whole article. He/she may:

- Deposit the accepted version of the submitted article in their institutional repository(ies). There shall be an embargo of making the above deposited material available to the public of 12 months from the date of acceptance. There shall be a link from this article to the PDF of the final published article on the RSC's website once this final version is available.
- Make available the accepted version of the submitted article via the personal website(s) of the author(s) or via the Intranet(s) of the organisation(s) where the author(s) work(s). No embargo period applies.
- Make available the PDF of the final published article via the personal website(s) of the author(s) or via the Intranet(s) of the organisation(s) where the author(s) work(s). No embargo period applies.
- Republish the PDF of the final published article in theses of the author(s) in printed form and may make available this PDF in this theses of author(s) via any website(s) that the university(ies) of the author(s) may have for the deposition of theses. No embargo period applies.

Excluded deposition of any version of the article by any person or organisation

- No deposited article, whether in an Institutional Repository, Funding Body Repository or personal website, may be forwarded to any website collection of research articles without prior agreement from the RSC.
- Deposition of the article on any website acting as a collection of personal articles from multiple scientists is explicitly prohibited. This does not apply to Institutional and Funding Body Repositories.

Open Access Author Deposition

When the author signs an Open Access Licence to Publish for a journal article, he/she retains certain rights where he/she can deposit the article.

Funding Agency Open Access Author Deposition

When the author signs a Funding Agency Open Access Licence to Publish for a journal article, he/she retains certain rights where he/she can deposit the article.

Related Links

SHERPA/RoMEO
Read the SHERPA/RoMEO publisher copyright policies and self-archiving

External links will open in a new browser window

Contact and Further Information

Gill Cockhead

Publishing Contracts & Copyright Executive
Tel: +44(0) 1223 432 134
Email: Gill Cockhead

VITA

CHHAVI BHARDWAJ

Education

Ph.D., Analytical chemistry, University of Illinois at Chicago, 2014

M.S. Chemistry, University of Illinois at Chicago, 2009

M.Sc., Chemistry, University of Delhi, 2005

B.Sc. (Honors), Chemistry, with physics and mathematics (minors), University of Delhi, 2003

Experience

US Environmental Protection Agency, Chicago, IL
Intern through ORISE 7/2013- Present

- Developed and validated methods for trace analysis of environmental contaminants by UPLC-MS/MS
- Performed quantification and limit of detection studies using SRM and MRMs
- Developed and optimized solid/liquid extraction protocols for environmental matrices

University of Illinois at Chicago, Chicago, IL
Research Assistant 1/2009- 06/2013

- Designed and constructed a vacuum ultraviolet ionization laser source for an MS setup
- Developed MS methods for analysis of endogenous metabolites in intact biological systems
- Developed MALDI-MS and LDPI-MS imaging methods for microbial biofilms and mammalian tissues
- Applied chemometric methods to MS data from biological samples for species/strain classification
- Developed SFC-MS methods for separation of racemic mixtures and enantiomeric excess calculations
- Developed toxicity assays and antibiotic inhibition studies for bacterial cells

Lawrence Berkeley National Laboratory, Berkeley, CA
Visiting Researcher 9/2010, 9/2011

- Characterized small molecules in biological systems with tunable VUV and EUV synchrotron radiation
- Tested hybridized systems using SIMS, SNMS, laser desorption and synchrotron radiation ionization.

VITA (CONTINUED)

University of Illinois at Chicago, Chicago, IL
Research Assistant 8/2006- 1/2009

- Developed and optimized methods for solid phase peptide synthesis
- Developed and optimized methods for HPLC purification of peptides
- Analyzed beta amyloid peptides and proteins using NMR
- Developed methods for mammalian cell culture and neurotoxicity assays

Publications

1. **Chhavi Bhardwaj** & Luke Hanley. Ion sources for the mass spectrometric identification of natural products. Natural Product Reports (2014) DOI: 10.1039/C3NP70094A
2. Artem Akhmetov, **Chhavi Bhardwaj** and Luke Hanley. Laser Desorption Postionization Mass Spectrometry Imaging of Biological Targets. Submitted as book chapter in Springer volume on MS Imaging of Small Molecules (2013)
3. **Chhavi Bhardwaj**, Yang Cui, Theresa Hofstetter, Suet Liu, Hans C. Bernstein, Ross P. Carlson, Musahid Ahmed & Luke Hanley. Differentiation of Microbial Species and Strains in Coculture Biofilms by Multivariate Analysis of Laser Desorption Postionization Mass Spectra. Analyst (2013) 138 (22), 6844-6851
4. Yang Cui, **Chhavi Bhardwaj**, Slobodan Milasinovic, Ross P. Carlson, Robert J. Gordon & Luke Hanley. Molecular Imaging and Depth Profiling of Biomaterials Interfaces by Femtosecond Laser Desorption Postionization Mass Spectrometry. ACS Applied Materials & Interfaces (2013) 5 (19), 9269–9275
5. **Chhavi Bhardwaj**, Jerry F. Moore, Yang Cui, Gerald L. Gasper, Hans C. Bernstein, Ross P. Carlson & Luke Hanley. Laser desorption VUV postionization MS imaging of a cocultured biofilm. Analytical Bioanalytical Chemistry (2013) 405 (22), 6969-6977
6. Slobodan Milasinovic, Yaoming Liu, **Chhavi Bhardwaj**, Melvin Blaze M. T., Robert J. Gordon & Luke Hanley. Feasibility of Depth Profiling of Animal Tissue by Ultrashort Pulse Laser Ablation. **Analytical Chemistry** (2012), 84, 3945−3951
7. Nalinda P Wickramasinghe, Sudhakar Parthasarathy, Christopher R Jones, **Chhavi Bhardwaj**, Fei Long, Mrignayani Kotecha, Shahila Mehboob, Leslie W-M Fung, Jaan Past, Ago Samoson & Yoshitaka Ishii. Nanomole-scale protein solid-state NMR by breaking intrinsic 1H T1 boundaries. Nature Methods (2009), 6 (3), 215-218

VITA (CONTINUED)

Presentations

1. Principal Component Analysis of Laser Desorption Postionization Mass Spectrometry Data for Mixed/Coculture Biofilms. **Chhavi Bhardwaj**, Yang Cui, Theresa Hofstetter, Suet Liu, Hans C. Bernstein, Ross P. Carlson, Musahid Ahmed and Luke Hanley, ASMS Conference, Minneapolis, June 2013

2. Small Molecules Detection with an Ultrashort Pulsed Laser Ablation VUV Postionization TOF-MS. Yang Cui, Chhavi Bhardwaj, Slobodan Milasinovic, Robert Gordon & Luke Hanley, ASMS Conference, Minneapolis, June 2013

3. Detection of Small Molecules on Intact Biofilms using Femtosecond Laser Desorption Postionization Mass Spectrometry. Yang Cui, Chhavi Bhardwaj, Slobodan Milasinovic, Robert Gordon & Luke Hanley, AVS 60th International Symposium and Exhibition, Long Beach, October 2013

4. Old & New Strategies in Mass Spectrometric (MS) Imaging of Biomaterials. Chhavi Bhardwaj, Yang Cui, Melvin Blaze M.T., Slobodan Milasinovic, Ross P. Carlson, Musahid Ahmed, Robert Gordon & Luke Hanley, National meeting of ACS, New Orleans, April 2013

5. Differentiation of Microbial Species and Strains in Cocultured Biofilms using Laser Desorption Postionization Mass Spectrometry & Multivariate Analysis. **Chhavi Bhardwaj**, Yang Cui, Theresa Hofstetter, Suet Liu, Hans C. Bernstein, Ross P. Carlson, Musahid Ahmed and Luke Hanley, Oral Presentation, Pittcon Conference, Philadelphia March 2013

6. 7.87 eV Laser Desorption Postionization MS Imaging to Quantify Small Molecule Antibiotics on Intact Colony Biofilms. Melvin Blaze M.T., Chhavi Bhardwaj and Luke Hanley, ASMS Conference, Vancouver, May 2012

7. Imaging Bacterial Biofilms using Laser Desorption Postionization Mass Spectrometry: Comparing 10.5 eV to 7.87 eV photoionization. **Chhavi Bhardwaj**, Jerry F. Moore, Gerald Gasper, Yang Cui, Hans Bernstein, Ross P. carlson and Luke Hanley, Poster Presentation, ASMS Conference, Denver, June 2011

8. MALDI vs. Laser Desorption Vacuum Ultraviolet Postionization MS for Imaging of Bacterial Biofilms. Berdan Aydin Sevinc, Melvin Blaze M.T., Peter J. Koin, Chhavi Bhardwaj, Artem Akhmetov, Gerald L. Gasper, Jerry F. Moore, and Luke Hanley, ASMS Conference, Salt Lake City, May 2010

9. Multidimensional Solid Sate NMR Analysis of Amyloid Fibrils for NAC (8-18) & A-beta(1-42). Christopher Jones, **Chhavi Bhardwaj**, Nalinda Wickramasinghe, Nancy Rios and Yoshitaka Ishii, ENC Conference, Asilomar, March 2008